A Study of Iterative and Adaptive Control Methods for Mechanical Systems with Parametric Uncertainties

March 2008

NILKHAMHANG, Itthisek

DISSERTATION

Submitted to the School of Integrated Design Engineering, Keio University, in partial fulfullment of the requirements for the degree of Doctor of Philosophy

To my family and dear friends

Abstract

In industrial applications, system engineers often encounter the daunting task of designing controllers for unknown or uncertain systems. The complexity of this process can be greatly increased by the magnitude of the system and the presence of nonlinear dynamics. Adaptive and iterative control theories have emerged as a powerful tool to design efficient and robust controllers, despite this lack of information. They have been successfully applied throughout a wide range of engineering discipline to achieve desired performance and provide information about parametrically uncertain systems.

As a vital component of most industrial processes, the control of mechanical systems has generated immense research interest. While adaptive and iterative control algorithms have been used to resolve many issues, there remain to this day countless topics that must be addressed by a diligent and knowledgeable system engineer. It is therefore the objective of this thesis to explore the various issues involved with adaptive and iterative control of parametrically uncertain mechanical systems. The focus of this study is narrowed by considering three specific applications, each representing different aspects of the general control problem: iterative control of an unknown multi-mass motor system; adaptive control of vehicular suspension systems; and robust adaptive friction compensation.

Chapter 1 begins with an introduction to the control problem of parametrically uncertain mechanical systems. This is elaborated in Chapter 2, which provides a literature review of existing control methods for multi-mass torsional motors, vehicular suspension systems and friction compensation, along with mathematical preliminaries that are utilized throughout the thesis. The motivation of this research is presented in detail.

The results of this study are presented in Chapter 3 to 5. First, a linear, two-mass torsional motor system with parametric uncertainties is considered in Chapter 3. A novel iterative feedback tuning method is proposed that yields an optimal controller, while simultaneously

identifying unknown system parameters and reducing the number of required experiments per iteration. Chapter 4 investigates the semi-active vibration control of an unknown vehicular suspension system with magnetorheological damper. A total adaptive control algorithm that combines an inverse controller with linear-parameterization and a suitable reference feedback controller is proposed. Stability and robustness conditions for the total system consisting of the two adaptation algorithms are clarified. Chapter 5 extends the use of a linearly-parameterized approximation function to the friction compensation problem. The newly proposed generalized Maxwell-slip model is employed to describe friction effects. The result is a robust adaptive friction compensator that greatly reduces positional and velocity tracking error in the presence of friction. Finally, Chapter 6 summarizes the main results of this study and concludes with suggestions for future research.

Acknowledgements

As this long and arduous journey comes to a close, it is time to look back over the years and consider all the paths and opportunities that have led to this junction. One cannot do so without a sense of humility and appreciation for the contributions made by numerous individuals.

The author would like to express his sincerest gratitude to Professor Akira Sano of Keio University. His patience, guidance and support have been crucial in the completion of this thesis. Through the outstanding teachings and examples of Professor Sano, the author has gained a sincere appreciation for the field of control engineering, as both a powerful tool for analytical studies and an essential component of industrial design. Most importantly, Professor Sano has instilled a sense of wonder and excitement in the author that will be invaluable in his future development as an academic, a researcher, and a human being.

This thesis would be also be remiss without acknowledging the enormous contributions of Associate Professor Waree Kongprawechon of Thammasat University. The author was first introduced to the field of control engineering through the words and teachings of Dr. Kongprawechon, whose engaging lectures and insightful comments provided the initial motivation for this undertaking. Her efforts and kindness throughout the years are the main reasons that the author was given this opportunity to come to Japan and realize his potential.

The author would also like to thank the committee members, Professor Nozomu Hamada, Professor Hiromitsu Ohmori, and Professor Toshiyuki Murakami, for their patience and recommendations. In addition, the author is indebted to Professor Sawasd Tantaratana and Associate Professor Issarachai Ngamroo of Thammasat University for their guidance.

It is also important to remember that not all support is of an academic nature. The author therefore would like to thank the numerous friends and acquaintances over the years who have provided unceasing comfort and solace in times of hardship, and a smile when most greatly appreciated. In particular, the author would like to mention his fellow students of

Sano-Ohmori Laboratory, Dr. Shohei Kikuchi and Dr. Yuanming Ding, the Thai community in Japan, and his classmates from Thammasat University. Other notable individuals are Dr. Sasiporn Usanavasin, Dr. Montian Tianprateep, Ms. Saranyupa Chaiprasithikul, Ms. Sayo Sasaki, and Ms. Numjai Lurngnateetape.

Lastly, the author would like to reserve his deepest gratitude for his family, who are the true inspiration and motivation behind this thesis. Their love and faith in the author has helped him to overcome the countless obstacles and challenges that have arisen throughout the years. The author therefore dedicates this thesis to his parents and brother, in recognition of their eternal support and kindness, and to other friends and companions that have joined him on this long, winding road.

Contents

Abbreviations

The technical terms listed below will be expressed by their abbreviations in this thesis. Other abbreviations will be defined at their first occurrence.

LS	Least Square
LMS	Least Mean Square
RLS	Recursive Least Square
MSE	Mean-Square Error
RMSE	Root Mean-Square Error
LQ	Linear Quadratic
SAC	Simple Adaptive Control
CGT	Command Generator Tracking
IFT	Iterative Feedback Tuning
MR	Magnetorheological
GMS	Generalized Maxwll-Slip
PSO	Particle Swarm Optimization
SPR	Strictly Positive Real
ASPR	Almost Strictly Positive Real
PE	Persistently Exciting
ASCS	Active Suspension Control System

Chapter 1

Introduction

In industrial applications, system engineers often encounter the daunting task of designing controllers for unknown or uncertain systems. Not only must they guarantee that certain performance criterions are met, but it is expected that information about the system be identified, often in an online manner. The complexity of this process can be greatly increased by the magnitude of the system and the presence of nonlinear dynamics.

Adaptive and iterative control theories have emerged as a powerful tool to design efficient and robust controllers, despite this lack of information. They have been successfully applied throughout a wide range of engineering discipline to achieve desired performance and provide information about parametrically uncertain systems. This includes an astounding mix of applications, such as electrical power grids, biological systems, geo-mechanics, and even economics and other social studies.

As a vital component of most industrial processes, the control of mechanical systems have generated immense research interest, with particular emphasis on parametrical uncertainties and robustness. While adaptive and iterative control algorithms have been used to resolve many issues, there remain to this day countless topics that must be addressed by a diligent and knowledgeable system engineer.

It is therefore the objective of this thesis to explore the various issues involved with adaptive and iterative control of parametrically uncertain mechanical systems. The focus of this study is narrowed by considering three specific applications, each representing different aspects of the general control problem. In particular, the iterative control of an unknown multi-mass torsional motor system, adaptive control of vehicular suspension systems, and robust adaptive friction

compensation are considered.

1.1 Multi-mass Torsional Motor System

Torsional motor systems are an integral part of many industrial and mechanical processes. However, velocity control of such multi-mass systems when physical parameters are uncertain or unknown is a complicated task. It is therefore desirable to develop an effective and easily implemented method for achieving control performance of an uncertain system.

A commonly employed approach for controller design is iterative feedback tuning (IFT) [18,19]. The IFT algorithm involves the minimization of a performance function by a gradient-based tuning method. However, the tuning process is greatly hindered when system knowledge is lacking or incomplete. Without an accurate mathematical description of the system, it is not possible to analytically calculate the gradient of the output error with respect to the controller parameters. In such a situation, IFT requires determining the system transfer function using separate identification techniques or performing additional experiments for gradient estimation. However, prohibitive experimental conditions, such as cost, stability issues, and closed-loop identifiability, mean that these are not always viable solutions.

This thesis addresses the iterative tuning problem for an unknown two-mass motor system. It has been demonstrated that a direct relationship exists between the physical parameters of a two-mass system and the linear gains of a feedforward controller [27] that was constructed using the command generator tracking (CGT) theory [9, 22]. The feedforward controller includes a suitable reference model that generates signals necessary for establishing this relationship [17, 27]. This concept was further developed by investigating the feasibility of using IFT to determine the feedforward and feedback controller parameters as the error is minimized [33, 34]. However, a system identification method called output oversampling [52] was required to determine the system transfer function, which is necessary for iterative tuning.

Therefore, one of the purposes of this thesis is to propose a novel iterative tuning algorithm for the feedforward and feedback controllers. The structure of the feedforward and feedback controllers is chosen to establish a clear relationship between physical model parameters of the two-mass motor system and the feedforward controller based on CGT theory [9]. From this relationship, the controller can be tuned directly by estimates of the physical model parameters to minimize tracking error. In addition, an estimated system transfer function can be

analytically obtained from the estimated model parameters at each iteration. This estimated transfer function allows for the direct calculation of the output error gradients with respect to the feedforward and feedback controller parameters that are required to conduct IFT.

The proposed algorithm is an efficient integration of IFT [18, 19] and the feedforward controller designed using CGT [27,33,34]. In utilizing system information provided by the feedforward controller to construct an estimated system transfer function, the additional experiments for gradient estimation, required by ordinary IFT in the case of an unknown system, become unnecessary. This reduction in the number of experiments performed per iteration is beneficial in terms of efficiency and cost. Likewise, a separate system identification process is no longer required. The proposed tuning algorithm is self-sufficient in minimizing the output error, as the system transfer function can be estimated directly from the relationship with the feedforward controller parameters. It also has the additional benefit of identifying the physical parameters of the system as the output error is improved.

The resulting, unified algorithm provides a powerful tool for achieving trajectory tracking of a completely unknown two-mass system. The validity and efficiency of the method is demonstrated by velocity control experiments. It is noted that no prior knowledge of system parameters or transfer function is required to implement this algorithm.

1.2 Adaptive Damper Control of Suspension System

Magnetorheological (MR) damper is a promising semi-active device in areas of vibration isolation for suspension systems and civil structures. The viscosity of MR fluid is controllable depending on input voltage or current. The MR damper inherently has hysteresis characteristics in nonlinear friction mechanism, and many efforts have been devoted to the modeling of nonlinear behavior from static and dynamic points of view [49, 58]. Static or quasi-static models include no dynamics but can express a nonlinear mapping from velocity to damping force [13, 40, 58]. It is not easy to identify the hysteresis curve by using a small number of model parameters from actual road surface excitation data. To model the hysteresis dynamics explicitly, the Bouc-Wen model and its variations have also been investigated, in which the input-output relation is expressed by a set of nonlinear differential equations [49, 58]. Hammerstein class of nonlinear model was also investigated [48]. These models can simulate the nonlinear behavior of the MR damper, however it includes too many nonlinear model parame-

ters to be identified in a real-time manner. Alternative modeling is based on the LuGre friction model [41] which was originally developed to describe nonlinear friction phenomena [11]. It has a relatively simple structure and the number of model parameters can also be reduced. However, it is not adequate for real-time design of an inverse controller. Thus, an MR damper model based on the LuGre model and an analytical method for adaptive inverse controller design has been explored [42, 54].

It is desired that the input to MR damper be determined so that the specified damping force is produced to attenuate vibrations of the suspension system. The necessary damping force can be calculated to minimize the linear quadratic (LQ) or linear quadratic gaussian (LQG) performance when the linear dynamic equation is given for the controlled structure. A clipped-optimal control algorithm has also been applied [15], in which a linear optimal controller is combined with a force feedback loop designed to adjust the input voltage. Its modification was also considered in [28, 59]. These approaches did not use any inversion dynamics of MR damper. By regarding the total system including the MR damper and structure as a nonlinear controlled system, nonlinear control design methods can also be applied, such as neuro-control approach [12], sliding mode control [28], adaptive skyhook control [60], gain scheduled control [38], bilinear H_∞ control [46] and others.

The purpose of this research is to provide a new fully adaptive control approach which can deal with uncertainties in both models of MR damper and suspension mechanism. The proposed approach consists of two adaptive controllers. The first is an adaptive inverse control for compensating the nonlinear hysteresis dynamics of the MR damper, which can be realized by identifying a forward model of the MR damper and then calculating the input voltage to MR damper to generate a reference damping force. It can also be realized by directly updating the inverse model of MR damper without identification of the forward model, which works as an adaptive inverse controller. The other is an adaptive reference control based on an adaptive skyhook approach [60], which gives the desired damping force to match the seat dynamics to a specified reference dynamics even in the presence of uncertainties in the suspension structure. Another purpose of this study is to clarify stability condition for the total system consisting of the two adaptation algorithms. Validity of the proposed algorithm is also examined in simulation studies.

1.3 Adaptive Friction Compensation

It is widely recognized that most mechanical systems involving two or more contact surfaces with relative motion, would experience to varying degrees some form of frictional effects. The presence of dynamic friction in such industrial applications as robotic manipulators, hydraulic systems, precision engineering, and so forth, can lead to significant tracking error, or even instability. Passive friction compensation techniques, such as lubrication, present only a partial solution to the problem, and should be complemented by an effective control scheme [6]. However, the task of controller design is greatly complicated by nonlinearities of the surface contact mechanics, structural and parametric uncertainties.

The demand for an accurate and efficient friction compensation method has led to immense research efforts from control engineers. Most notably, the works of Armstrong-Hélouvry [4,5], in which important contributions from tribology, lubrication, and physics literatures are restated in a control framework, have generated considerable interest in the friction problem. A comprehensive overview and survey of friction characteristics and classical compensation methods can be found in the references [4, 5, 39]. Traditionally, the friction process is characterized by two regimes: the so-called presliding or micro-slip regime; and the gross sliding regime. Important properties of friction that have been observed include presliding hysteresis, stick-slip limit cycling, non-local memory, non-drifting property, viscosity, the nonlinear Stribeck effect, static and Coulomb friction. A generic friction model based upon these physical considerations and experimental data has been proposed [1]. Though the generic friction model is highly accurate and captures all the important properties of friction, its mathematical complexity renders it an invalid choice for controller design. However, the generic friction model remains a powerful tool for analyzing the fidelity and accuracy of other friction models, which are classified by their static and dynamic characteristics.

Currently, friction compensation schemes are divided into non-model and model-based methods. Studies have shown that simple PD or PID controllers suffer significant performance degradation due to the nonlinear characteristics of friction, which can lead to hunting behaviors and instability [5]. Several observer-based nonlinear friction compensation scheme have been proposed [20]. Black-box methods employing neural networks or fuzzy logic for friction compensation have also been widely researched [25, 26, 44]. In comparison, the potential of model-based adaptive friction compensation has been demonstrated by several researchers. These efforts in-

clude the modeling and compensation of Coulomb friction [3,16], a control scheme for dynamic, linear friction [30], and nonlinear static mapping of the Stribeck effect [31]. These methods provide powerful arguments for the use of adaptive control in friction compensation, but do not combine it with a sufficiently complex and accurate dynamic friction model.

To this end, several dynamic friction models have been developed [7,14], the most popular of which is the LuGre model [11]. Due to its relative simplicity, extensive literature exists regarding the use of the LuGre friction model in various compensation schemes [10, 32, 43]. However, it has been pointed out that the LuGre model compromises fidelity in favor of simplicity. Most notably, the LuGre model does not explicitly account for friction lag characteristics, and its hysteresis-like behavior fails to exhibit non-drifting and non-local memory properties [53].

Therefore, this thesis develops a robust adaptive compensation scheme using the generalized Maxwell-slip (GMS) friction model, which has been proposed as a more accurate representation of the friction phenomenon than the LuGre model [2, 29]. The GMS model consists of parallel elementary blocks, and separates frictional mechanism into two regimes: sticking and slipping. This results in a hybrid system, with two separate models. Maxwell-slip functions are utilized to describe the hysteresis behavior in the sticking regime. For the slipping regime, a state rate law is employed that includes the Stribeck effect and an explicit term for describing frictional lag characteristics. The GMS model yields results that correspond to experimental observation, while maintaining a simpler structure than the generic friction model [1]. Offline identification algorithms of the GMS model using Nelder-Mead simplex [55] and particle swarm optimization (PSO) [23, 24, 37] have been presented. However, designing an adaptive controller using the GMS model can be difficult due to its switching nature and also the nonlinear Stribeck effect.

The main novelty of this study is the proposal of a polynomial Stribeck function that is readily applicable to the GMS friction model. The validity of using a polynomial approximation function to describe the Stribeck effect has been investigated in previous works [8,21,35,36,56]. By using the polynomial approximation function, the development of adaptive control laws are simplified, as friction models can be linearly-parameterized. For the reasons outlined above, the GMS friction model is chosen for the model-based adaptive controller. Previous investigations [35,36] suggest that issues of robustness may occur due to unmodeled dynamics, which include dynamic perturbations, switching uncertainties, and the approximation error of the polynomial equation. Therefore, this study specifically addresses the issue by introducing a sliding-mode based smooth adaptive robustifying term into the control law [47]. Stability analysis is presented

to show the robustness of the algorithm, provided that a bound on the unmodeled terms is known to exist. The validity of the proposed robust adaptive control algorithm based upon the GMS friction model is demonstrated by simulation results.

1.4 Outline and Contributions

As stated above, the main purpose of this thesis is the study of iterative and adaptive algorithms for identification and control of mechanical systems involving parametric uncertainties. This section gives an overview of the thesis and a summary of the contributions chapter by chapter.

Chapter 2

Chapter 2 gives a short introduction to the various mechanical systems that are dealt with in this thesis, and the associated control problems. This chapter gives the motivation that prompted the start of this study, and the overall direction of this thesis.

Chapter 3

Chapter 3 explores the issue of using iterative methods to design efficient controllers for parametrically uncertain torsional motor systems. A 2DOF control structure is proposed, and a direct relationship between controller parameters and physical model parameters is established by employing the CGT concept. This is utilized to estimate system parameters at each iteration, which then allows the analytical calculation of error gradients necessary for iterative tuning.

Chapter 4

Chapter 4 continues the exploration of parametrically uncertain mechanical systems by considering the adaptive control design of a vehicle suspension system via a semi-active MR damper. The control structure consists of a reference feedback controller, responsible for generating an active damping force that guarantees desirable performances, and an inverse controller, whose main purpose is the linearization of the MR damper so that almost active damping force can be achieved. Robust LQ design and adaptive skyhook method are employed to construct the

reference feedback controller for the case where the suspension system parameters are known and unknown, respectively. Forward modeling and inverse model via polynomial approximation is considered for design of the adaptive inverse controller.

Chapter 5

This chapter extends the study to friction compensation schemes. A robust adaptive feedforward control algorithm is developed from the GMS friction model, and applied to the velocity and position control of a system with unknown mass. Procedures are outlined for identifying the GMS model using PSO, and simulations are conducted to verify the validity of the proposed controller design.

Chapter 6

The final chapter of this thesis gives concluding remarks and some suggestions for future research.

Chapter 2

Literature Review

Parametric uncertainty in mechanical systems greatly hinders the controller design process. Whether caused by incomplete system knowledge or varying operational conditions, these uncertainties prevent the formulation of effective control schemes with guaranteed robustness and performance. The motivation of this research is the examination of various adaptive and iterative methods to overcome this obstacle. Specifically, it examines three applications in which parametric uncertainties play an important role: multi-mass torsional motor systems; semi-active control of suspension systems; and friction compensation of parametrically uncertain systems.

This chapter introduces the main issues involving parametric uncertainties of mechanical systems. It presents fundamental knowledge and theories regarding the various systems that will be dealt with by this thesis, as well as an overview of existing control techniques. As such, it clarifies the problem settings of Chapter 3 to 5 and provides the motivation behind this research.

2.1 Multi-mass Torsional Motor Systems

Torsional motor systems form an integral part of many industrial and mechanical processes. When the system involves multiple masses and connecting shafts, this can lead to complicated controller design. Multi-mass linear systems also require greater knowledge about system parameters that are not always available or are uncertain.

The control of an uncertain multi-mass torsional motor system may be approached from

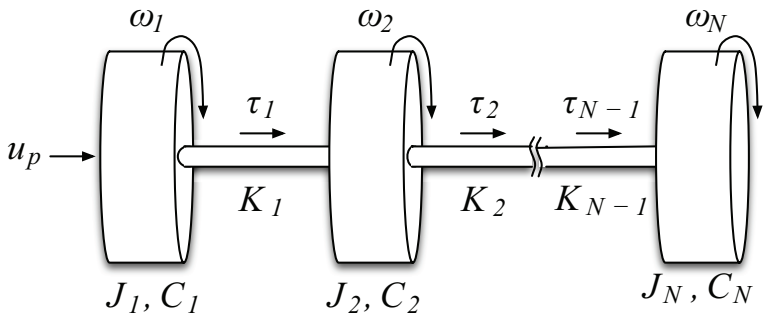

Figure 2.1: N-mass torsional system.

either an adaptive or iterative framework. Adaptive methods are powerful tools for dealing with parametrically uncertain systems. However, they can involve complex adaptation laws which may prove cumbersome when dealing with large amounts of parameters.

In contrast, iterative tuning methods exist to determine optimal controller parameters, and are especially suited to systems that under go repetitive action. Iterative methods often yield greater assurances regarding the stability of the overall algorithm. As most torsional motor systems in industrial applications fall into this repetitive category, an iterative tuning approach is taken by this study for controller design.

This section clarifies the mathematical preliminaries necessary for developing iterative control schemes of multi-mass torsional motor systems. It begins with a general description of the multi-mass system, and follows with an overview of the command generator tracking (CGT) theory that will form the basis of the controller employed in this research. A brief explanation of existing iterative tuning methods, as well as an analysis of their short-comings, is presented. Finally, the motivation of this research is discussed.

2.1.1 System Description

A multi-mass torsional motor system is depicted in Figure 2.1, and consists of a number of inertial masses connected to a motor by a system of shafts or belts. The relevant physical parameters include the masses or inertial moments of the motor and loads, as well as the spring and damping constants of each shaft or belt. For the N-mass system depicted in Figure 2.1,

the mathematical expression is given as follows:

$$\dot{\boldsymbol{x}}_p(t) = \boldsymbol{A}_p \boldsymbol{x}_p(t) + \boldsymbol{b}_p u_p(t) \tag{2.1}$$

$$y_p(t) = \boldsymbol{c}_p^T \boldsymbol{x}_p(t) \tag{2.2}$$

where:

$$\boldsymbol{x}_p(t) = \begin{bmatrix} \omega_1(t) & \tau_1(t) & \omega_2(t) & \tau_2(t) & \dots & \omega_{N-1}(t) & \tau_{N-1}(t) & \omega_N(t) \end{bmatrix}^T$$

$$\boldsymbol{A}_p = \begin{bmatrix} -C_1/J_1 & -1/J_1 & 0 & 0 & \dots & 0 & 0 & 0 \\ 1/K_1 & 0 & -1/K_1 & 0 & \dots & 0 & 0 & 0 \\ 0 & 1/J_2 & -C_2/J_2 & -1/J_2 & \dots & 0 & 0 & 0 \\ \vdots & \vdots & \vdots & \vdots & \ddots & \vdots & \vdots & \vdots \\ 0 & 0 & 0 & 0 & \dots & 1/K_{N-1} & 0 & -1/K_{N-1} \\ 0 & 0 & 0 & 0 & \dots & 0 & 1/J_N & -C_N/J_N \end{bmatrix}$$

$$\boldsymbol{b}_p = \begin{bmatrix} 1/J_1 & 0 & \dots & 0 \end{bmatrix}^T$$

$$\boldsymbol{c}_p = \begin{bmatrix} 1 & 0 & \dots & 0 \end{bmatrix}^T$$

Here, J_i and C_i are the inertial moment and viscous damping constant of each mass, respectively, and K_i is the spring constant of each shaft. Also, $\omega_i(t)$ is the velocity of each mass, while $\tau_i(t)$ is the torque in each shaft. Mass 1 is assumed to be driving motor that will be subjected to an input torque, while masses 2 to N represent loads. The output of the system is given by the velocity of the driving motor, and the control objective is the design of an input torque $u_p(t)$ such that $y_p(t)$ tracks a given trajectory $y_m(t)$ to a pre-determined degree of accuracy.

2.1.2 Command Generator Tracking Theory

The control objective can be restated in a manner such that it represents a CGT problem. Let the reference model of a given system be defined according to:

$$\dot{\boldsymbol{x}}_m(t) = \boldsymbol{A}_m \boldsymbol{x}_m(t) + \boldsymbol{b}_m u_m(t) \tag{2.3}$$

$$y_m(t) = \boldsymbol{c}_m^T \boldsymbol{x}_m(t) \tag{2.4}$$

Here, $u_m(t)$ is a reference signal that has a derivative up to the N^{th} degree. The main result of the CGT principle is summarized in the following theorem.

THEOREM 2.1 *(Command Generator Tracking) There exist ideal states and input when perfect tracking is achieved. These ideal states and input are expressable as a linear combination of the states of the reference model, the reference input, and all of the derivatives of the input:*

$$\begin{bmatrix} \boldsymbol{x}_p^*(t) \\ u_p^*(t) \end{bmatrix} = \begin{bmatrix} \boldsymbol{S}_{11} & s_{12} & s_{13} & \dots & s_{1(N+2)} \\ \boldsymbol{s}_{21}^T & s_{22} & s_{23} & \dots & s_{2(N+2)} \end{bmatrix} \begin{bmatrix} \boldsymbol{x}_m(t) \\ u_m(t) \\ \dot{u}_m(t) \\ \vdots \\ u_m^{(N)}(t) \end{bmatrix} \tag{2.5}$$

The perfect tracking problem becomes one of determining solvable expressions for all elements of the $\boldsymbol{S}$ matrix, where:

$$\boldsymbol{S} = \begin{bmatrix} \boldsymbol{S}_{11} & s_{12} & s_{13} & \dots & s_{1(N+2)} \\ \boldsymbol{s}_{21}^T & s_{22} & s_{23} & \dots & s_{2(N+2)} \end{bmatrix} \tag{2.6}$$

By examining the above theorem, it is noted that the ideal input to the plant, $u_p^*(t)$, is determined as:

$$u_p^*(t) = \boldsymbol{s}_{21}^T \boldsymbol{x}_m(t) + s_{22} u_m(t) + s_{23} \dot{u}_m(t) + \ldots + s_{2(N+2)} u_m^{(N)}(t) \tag{2.7}$$

The method for determining the $\boldsymbol{S}$ matrix will be given in this thesis for the case of a 2-mass torsional motor system.

2.1.3 Iterative Feedback Tuning

In many industrial applications which involve repetitive motions, iterative feedback tuning (IFT) can be considered as a viable alternative to adaptive control. A brief discussion of the conventional IFT method is considered [18, 19]. Assume an unknown system whose discrete transfer function is described by $G_o(z)$, and a general 2DOF controller $C(z, \boldsymbol{k})$. Here, $C(z, \boldsymbol{k}) = \{C_r(z, \boldsymbol{k})\ C_y(z, \boldsymbol{k})\}$ are the discrete feedforward and feedback controllers defined by the gain vector $\boldsymbol{k} = [K_1, K_2, \ldots, K_M]$, where M is the length of $\boldsymbol{k}$. This configuration is shown in Figure 2.2. The control objective is the tracking of the desired response y_m. The controller is parameterized at iteration i by the gain vector $\boldsymbol{k}^{(i)}$. In this paper, the performance criterion is chosen as a quadratic function based upon N measured, discrete-time, error signals given as:

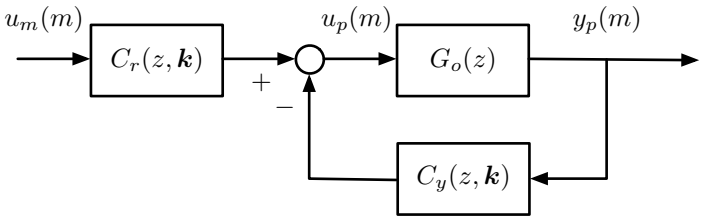

Figure 2.2: A general 2DOF discrete-time controller.

$$J(\boldsymbol{k}^{(i)}) = \frac{1}{2N}\sum_{m=1}^{N}(L_y\tilde{y}(m, \boldsymbol{k}^{(i)}))^2 \tag{2.8}$$

In (2.8), the notation $\tilde{y}(m, \boldsymbol{k}^{(i)})$ signifies the error signal at sampling instant mT_s, with the controller $C(z, \boldsymbol{k}^{(i)})$ operating in the closed loop. For the sake of simplicity, the frequency weighted filter L_y is taken to be 1. The optimal controller parameter $\boldsymbol{k}^*$ is defined by:

$$\boldsymbol{k}^* = \arg\min_{\boldsymbol{k}} J(\boldsymbol{k}) \tag{2.9}$$

This can be obtained by the following iterative algorithm:

$$\boldsymbol{k}^{(i+1)} = \boldsymbol{k}^{(i)} - \gamma^{(i)}\boldsymbol{R}(\boldsymbol{k}^{(i)})^{-1}\frac{\partial J(\boldsymbol{k}^{(i)})}{\partial \boldsymbol{k}} \tag{2.10}$$

$$\frac{\partial J(\boldsymbol{k}^{(i)})}{\partial \boldsymbol{k}} = \frac{1}{N}\sum_{m=1}^{N}\left(\tilde{y}(m, \boldsymbol{k}^{(i)})\frac{\partial \tilde{y}(m, \boldsymbol{k}^{(i)})}{\partial \boldsymbol{k}}\right) \tag{2.11}$$

Here, $\gamma^{(i)}$ is a sequence of positive real numbers that determines the step-size, and $\boldsymbol{R}(\boldsymbol{k}^{(i)})$ is a sequence of positive definite matrices. This study defines $\boldsymbol{R}(\boldsymbol{k}^{(i)})$ as:

$$\boldsymbol{R}(\boldsymbol{k}^{(i)}) = \frac{1}{N}\sum_{m=1}^{N}\mathrm{diag}\left(\left(\frac{\partial \tilde{y}(m, \boldsymbol{k}^{(i)})}{\partial K_1}\right)^2, \ldots, \left(\frac{\partial \tilde{y}(m, \boldsymbol{k}^{(i)})}{\partial K_M}\right)^2\right) \tag{2.12}$$

Notice that the solution of (2.11) requires the gradient of the output with respect to each controller parameter in $\boldsymbol{k}^{(i)}$. For the discrete-time, closed-loop system, the gradient is given as:

$$\frac{\partial \tilde{y}(m, \boldsymbol{k}^{(i)})}{\partial \boldsymbol{k}} = T_o(z, \boldsymbol{k}^{(i)})\left(\frac{\partial C_r(z, \boldsymbol{k}^{(i)})}{\partial \boldsymbol{k}}u_m(m) - \frac{\partial C_y(z, \boldsymbol{k}^{(i)})}{\partial \boldsymbol{k}}y_p(m, \boldsymbol{k}^{(i)})\right) \tag{2.13}$$

where:

$$T_o(z, \boldsymbol{k}^{(i)}) = \frac{G_o(z)}{1 + C_y(z, \boldsymbol{k}^{(i)}) G_o(z)}$$

To calculate the error gradient in (2.13), it is obvious that the transfer function $G_o(z)$ is necessary. Without this information, conventional IFT requires additional experiments to be performed in order to obtain a suitable estimate of the gradient, or the use of separate system identification procedures. Instead, a novel iterative algorithm will be presented by this study that can simplify the tuning process by eliminating these extra procedures.

2.1.4 Research Motivation

Torsional motor systems form an integral part of many industrial and mechanical processes. When the system involves multiple masses and connecting shafts, this can lead to complicated controller design. Multi-mass linear systems also require greater knowledge about system parameters which are not always available or are uncertain.

As outlined in the previous sections, the control of an uncertain multi-mass torsional motor system may be approached from either an adaptive or iterative framework. Adaptive methods are powerful tools for dealing with parametrically uncertain systems. However, they can involve complex adaptation laws which may prove cumbersome when dealing with large amounts of parameters.

In contrast, iterative tuning methods exist to determine optimal controller parameters and are especially suited to systems that under go repetitive action. Iterative control typically signifies greater assurances regarding the stability of the overall algorithm. As most torsional motor systems in industrial applications fall into this repetitive category, an iterative tuning approach is taken by this study for controller design.

Most iterative methods are gradient-based and requires precise knowledge about system parameters. An alternative approach is the iterative feedback tuning (IFT) method, developed by [18, 19]. This algorithm substitutes *a priori* information about the system with additional experiments per iteration to estimate the error gradient. The number of required additional experiments is related to the size of the controller. Obviously, this is an impractical approach when dealing with systems that involves high operational cost or is time-sensitive.

Thus, this study formulates a novel iterative tuning algorithm based upon IFT that would eliminate the need for these additional experiments. It explores the relationship between phys-

ical model parameters and the gains of a feedforward controller designed by using CGT theory. This is utilized to construct an estimated system transfer function at each iteration, which is then used to estimate the error gradient required for iterative tuning. In this manner, the performance objective can be realized, while allowing the simultaneous identification of system parameters. The proposed algorithm is, to the author's knowledge, currently the only existing method for identifying all the physical parameters of a two-mass motor system in an online manner while achieving trajectory tracking objectives.

2.2 Vibration and Suspension Systems

The second topic of this thesis continues the investigation of control methods for applications in vibration and suspension systems involving parametric uncertainties. Vibration suppression is an important field for structural and mechanical engineers. It is inherently related to the integrity of the system and other performance criterions. In particular, this thesis will focus on uncertain vehicle suspension systems installed with a magnetorheological (MR) damper.

Vehicle suspension system is a critical component in ensuring ride comfort, safety, road damage minimization, and overall vehicle performance. Numerous researches by mechanical engineers and the automotive industry have led to passive, semi-active, and active control solutions. Of these, passive control is the simplest but suffers from a narrow range of operational frequency and is highly susceptible to parametric uncertainties. Active control provides ideal performance over a wide range of frequency and is able to adapt to changing environmental conditions. However, it consumes a large amount of power and thus should be avoided. In recent years, semi-active controls via electrorheological (ER) and MR dampers have emerged as an efficient and economically feasible alternative to active actuator control of suspension systems.

In the following section, a basic description of a vehicle suspension system consisting of the car chassis and wheel assembly is presented. This is followed by a discussion of active damping controller via conventional and robust linear quadratic (LQ) designs for the case of known system parameters. This is extended to the uncertain case by application of the adaptive skyhook method. The issue of semi-active damping using MR damper is then considered, with an overview of existing MR damper models and control techniques. Finally, the motivation of this research and its direction is presented.

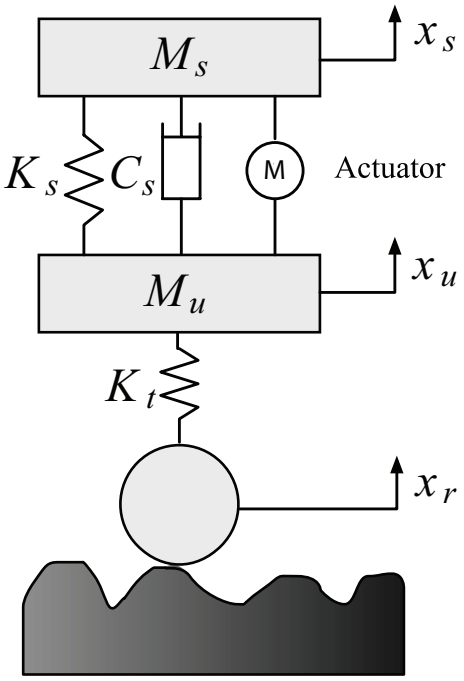

Figure 2.3: Suspension system with actuator damping.

2.2.1 System Description

The structure of a suspension system is presented in Figure 2.3. Mathematically, the dynamical equation is given as:

$$M_s\ddot{x}_s + C_s(\dot{x}_s - \dot{x}_u) + K_s(x_s - x_u) = -u_p \tag{2.14}$$

$$M_u\ddot{x}_u + C_s(\dot{x}_u - \dot{x}_s) + K_s(x_u - x_s) + K_t(x_u - x_r) = u_p \tag{2.15}$$

$$x = x_s - x_u \tag{2.16}$$

where x is the relative displacement between the car chassis and the wheel assembly; M_s is the sprung mass, which represents the car chassis; M_u is the unsprung mass, which represents the wheel assembly; C_s and K_s are damping and stiffness of the uncontrolled suspension system, respectively; K_t serves to model the compressibility of the pneumatic tire. x_s and x_u are the displacements of the sprung and unsprung mass, respectively; x_r is the road displacement input; u_p is the damping force supplied to the system. This can be represented in the state-space form

as:

$$\dot{\boldsymbol{x}}_p = \boldsymbol{A}\boldsymbol{x}_p + \boldsymbol{b}u_p + \boldsymbol{e}\dot{x}_r \tag{2.17}$$

where:

$$\boldsymbol{x}_p = \begin{bmatrix} x_s - x_u & x_u - x_r & \dot{x}_s & \dot{x}_u \end{bmatrix}^T$$

$$\boldsymbol{A} = \begin{bmatrix} 0 & 0 & 1 & -1 \\ 0 & 0 & 0 & 1 \\ -K_s/M_s & 0 & -C_s/M_s & C_s/M_s \\ K_s/M_u & -K_t/M_u & C_s/M_u & -C_s/M_u \end{bmatrix}$$

$$\boldsymbol{b} = \begin{bmatrix} 0 & 0 & -1/M_s & 1/M_u \end{bmatrix}^T$$

$$\boldsymbol{e} = \begin{bmatrix} 0 & -1 & 0 & 0 \end{bmatrix}^T$$

2.2.2 Active Damping Control

Active damping control via actuators has been extensively explored in the literature. Assuming a sufficiently large power supply, an arbitrary damping force may be injected as the input signal $u_p = F_A$. The question of active damping control thus becomes the design of this input signal. Traditionally, this is accomplished for the case of known and constant suspension parameters by using conventional linear quadratic control. However, system parameters are often unavailable or uncertain. This has inspired the development of adaptive methods such as the skyhook method in order to generate an appropriate active damping force. These methods are presented in the following section.

Conventional LQ Control

Linear quadratic (LQ) design of the active damping force is possible when exact information exists regarding the physical parameters of the suspension system. LQ controller design is a well-established discipline and numerous papers exist regarding the methodology. This section presents the preliminary mathematical background of optimal LQ control.

Consider the suspension system given in the previous discussion. Assuming that information about the suspension system parameters is available, the following performance function is

defined:

$$J_2 = \int_0^\infty \begin{bmatrix} \boldsymbol{x}_p^T & F_A \end{bmatrix} \begin{bmatrix} \boldsymbol{Q} & \boldsymbol{0} \\ \boldsymbol{0}^T & r \end{bmatrix} \begin{bmatrix} \boldsymbol{x}_p \\ F_A \end{bmatrix} dt$$
$$= \int_0^\infty \left(\boldsymbol{x}_p^T \boldsymbol{Q} \boldsymbol{x}_p + r F_A^2 \right) dt \tag{2.18}$$

where $\boldsymbol{Q} = q\boldsymbol{I}$, while $q > 0$ and $r > 0$. Assuming that the road perturbation $\dot{x}_r$ is a random signal with zero mean, the active control force is given by:

$$F_A = -\boldsymbol{k}^T \boldsymbol{x}_p \tag{2.19}$$
$$\boldsymbol{k} = \frac{\boldsymbol{P}\boldsymbol{b}}{r} \tag{2.20}$$

and $\boldsymbol{P}$ is the solution of the corresponding Riccati equation:

$$\boldsymbol{Q} + \boldsymbol{P}\boldsymbol{A} + \boldsymbol{A}^T \boldsymbol{P} - r\boldsymbol{k}\boldsymbol{k}^T = \boldsymbol{0} \tag{2.21}$$

If all of the states are not available, an observer can be designed from the sensor data, for instance $x_s - x_u$ and $\ddot{x}_s$, and an output controller is implemented.

Adaptive Skyhook Method

LQ control design is effective only in the case when the physical parameters of the suspension system are available. However, when the system involves parametric uncertainties, the Riccati equation cannot be solved. In this case, it becomes necessary to apply adaptive control methods. While several adaptive schemes have been proposed for active damping control of uncertain systems, this thesis employs an adaptive reference feedback controller constructed from the skyhook method. The adaptive reference feedback control can match the chassis dynamical response to a desired reference dynamics even when the suspension system involves parametric uncertainty.

Following the adaptive scheme [60], the desired reference dynamics is specified by:

$$\ddot{x}_s + 2\zeta\omega\dot{x}_s + \omega^2(x_s - x_u) = 0 \tag{2.22}$$

where ω is the natural frequency, ζ is a damping constant, and s is the Laplace operator. Then, the control error ξ is given by:

$$\xi = \dot{x}_s + (s + 2\zeta\omega)^{-1}\omega^2(x_s - x_u) \tag{2.23}$$

Define the parameter vector as:

$$\boldsymbol{\theta}_S = \begin{bmatrix} M_s & C_s & K_s \end{bmatrix}^T \tag{2.24}$$

Now the active damper force is given as:

$$F_A = \kappa\xi - \hat{\boldsymbol{\theta}}_S^T \boldsymbol{\varphi}_S \tag{2.25}$$

where $\kappa > 0$ is a design constant, and:

$$\hat{\boldsymbol{\theta}}_S = \begin{bmatrix} \hat{M}_s & \hat{C}_s & \hat{K}_s \end{bmatrix}^T \tag{2.26}$$

$$\boldsymbol{\varphi}_S = \begin{bmatrix} -\frac{\omega^2 s(x_s - x_u)}{(s+2\zeta\omega)} & \dot{x}_s - \dot{x}_u & x_s - x_u \end{bmatrix}^T \tag{2.27}$$

Here, $\hat{\boldsymbol{\theta}}_S$ is the parameter estimates of $\boldsymbol{\theta}_S$ given by the following adaptive law:

$$\dot{\hat{\boldsymbol{\theta}}}_S = \dot{\tilde{\boldsymbol{\theta}}}_S = -\boldsymbol{\Gamma}_S \boldsymbol{\varphi}_S \xi - \sigma_S \boldsymbol{\Gamma}_S \hat{\boldsymbol{\theta}}_S \tag{2.28}$$

where $\tilde{\boldsymbol{\theta}}_S = \hat{\boldsymbol{\theta}}_S - \boldsymbol{\theta}_S$. $\boldsymbol{\Gamma}_S$ is a positive-definite matrix, and σ_S is a positive design constant. For practical implementation, $\boldsymbol{\Gamma}_S$ is chosen constant. The main stability result for the adaptive reference feedback controller is presented in the following theorem.

THEOREM 2.2 *Assume $\kappa > 0$ is satisfied. Then the control law (2.25), along with the adaptive law (2.28), guarantees that the control error signal ξ and the parameter estimation errors $\tilde{\boldsymbol{\theta}}_S$ remain bounded and converge to a small neighborhood of the origin.*

Proof: Consider a candidate of the Lyapunov function as:

$$V_S = \frac{1}{2} M_s \xi^2 + \frac{1}{2} \tilde{\boldsymbol{\theta}}_S^T \boldsymbol{\Gamma}_S^{-1} \tilde{\boldsymbol{\theta}}_S \tag{2.29}$$

Taking the time-derivative of V_S and using the control law (2.25):

$$\begin{aligned} \dot{V}_S &= M_s \xi \dot{\xi} + \tilde{\boldsymbol{\theta}}_S^T \boldsymbol{\Gamma}_S^{-1} \dot{\tilde{\boldsymbol{\theta}}}_S \\ &= \xi \left(M_s \ddot{x}_s + M_s (s + 2\zeta\omega)^{-1} \omega^2 s (x_s - x_u) \right) + \tilde{\boldsymbol{\theta}}_S^T \boldsymbol{\Gamma}_S^{-1} \dot{\tilde{\boldsymbol{\theta}}}_S \\ &= \xi \left(-\boldsymbol{\theta}_S^T \boldsymbol{\varphi}_S - F_A \right) + \tilde{\boldsymbol{\theta}}_S^T \boldsymbol{\Gamma}_S^{-1} \dot{\tilde{\boldsymbol{\theta}}}_S \\ &= \xi \left(-\kappa\xi + \tilde{\boldsymbol{\theta}}_S^T \boldsymbol{\varphi}_S \right) + \tilde{\boldsymbol{\theta}}_S^T \boldsymbol{\Gamma}_S^{-1} \dot{\tilde{\boldsymbol{\theta}}}_S \end{aligned} \tag{2.30}$$

Now using the adaptive law (2.28):

$$\begin{aligned}\dot{V}_S &= -\kappa\xi^2 - \sigma_S \tilde{\boldsymbol{\theta}}_S^T \hat{\boldsymbol{\theta}}_S \\ &\leq -\kappa\xi^2 - \frac{\sigma_S}{2}\tilde{\boldsymbol{\theta}}_S^T \tilde{\boldsymbol{\theta}}_S + \frac{\sigma_S}{2}\boldsymbol{\theta}_S^T \boldsymbol{\theta}_S \end{aligned} \tag{2.31}$$

Thus:

$$\dot{V}_S \leq -c_S V_S + \lambda_S \tag{2.32}$$

where:

$$c_S = \min\left\{2\kappa, \frac{\sigma_S}{\lambda_{\max}(\boldsymbol{\Gamma}_S^{-1})}\right\} \tag{2.33}$$

$$\lambda_S = \frac{\sigma_S}{2}\boldsymbol{\theta}_S^T \boldsymbol{\theta}_S \tag{2.34}$$

Since κ and σ_S are positive design constants, $\lambda_S/c_S > 0$ and the following result is obtained:

$$0 \leq V_S(t) \leq \lambda_S/c_S + (V_S(0) - \lambda_S/c_S)\, e^{-c_S t} \tag{2.35}$$

Thus, the control error ξ and the parameter estimation errors $\tilde{\boldsymbol{\theta}}_S$ are uniformly bounded and converge to a small neighborhood of the origin. It is also noted that if the σ-modification term is set to zero, then asymptotic convergence of ξ is guaranteed. □

2.2.3 Semi-active Control via MR Damper

While active control of suspension systems provide ideal performance over a wide range of frequency, it suffers from the requirement of a sufficiently large power supply. In reality, this is a severe limitation that must be avoided. In recent years, this has led to increased research activities in semi-active control via ER or MR dampers.

Semi-active dampers produce variable damping force dependent upon applied voltage or current. This thesis considers the application of the MR damper for vibration suppression of vehicle suspension systems. The following section presents an overview of the MR damper mechanics and existing semi-active control methods.

Magnetorheological Damper

MR damper is a semi-active device in which the viscosity of the fluid is controllable by the input voltage or current. It can be installed in place of the actuator between the chassis and

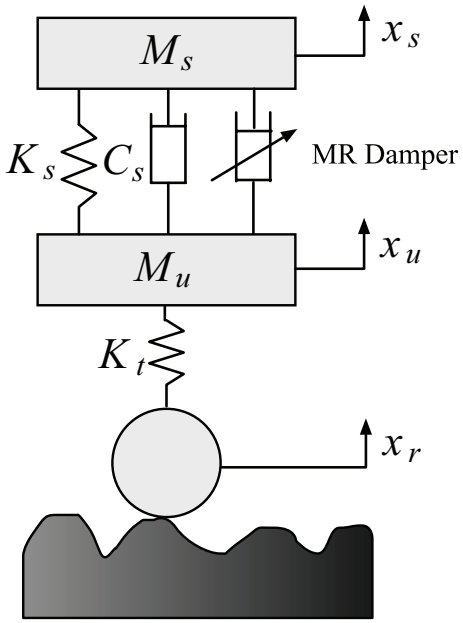

Figure 2.4: Suspension system with MR damper.

the wheel assembly, as shown in Figure 2.4. A cross sectional diagram of a typical MR damper is shown in Figures 2.5 and 2.6. A variety of approaches have been taken to modeling of the nonlinear hysteresis behavior of the MR damper.

The stress-strain behavior of the Bingham viscoplastic model [45] is often used to describe the behavior of MR fluids. In this model, the plastic viscosity is defined as the slope of the measured shear stress versus shear strain rate data. Thus, for positive values of the shear rate, $\dot{\gamma}$, the total stress is given by:

$$\tau = \tau_y + \eta\dot{\gamma} \tag{2.36}$$

where τ_y is the yield stress induced by the magnetic field and η is the viscosity of the fluid.

Based on this model of the rheological behavior of ER and MR fluids, [50, 51] proposed an idealized mechanical model, denoted the Bingham model, for the behavior of an ER damper. The Bingham model consists of a Coulomb friction element placed in parallel with a viscous damper. In this model, for nonzero piston velocity, $\dot{x}$, the force generated by the device is given as:

$$F_{MR} = F_C sgn(\dot{x}) + c_0\dot{x} + F_0 \tag{2.37}$$

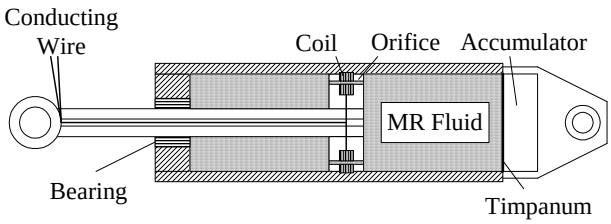

Figure 2.5: Cross-sectional diagram of a typical MR damper.

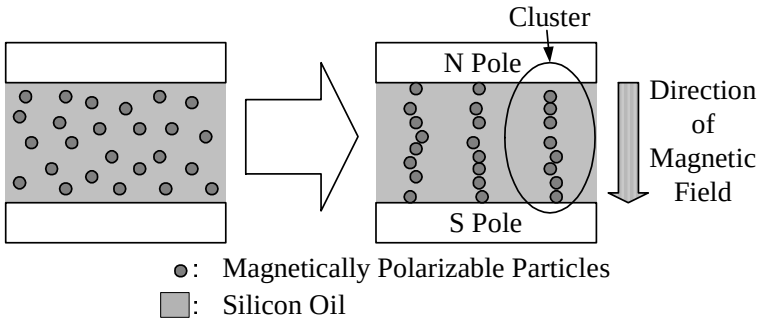

Figure 2.6: MR damper fluid when subjected to a magnetic field.

where c_0 is the damping coefficient and F_C is the frictional force, which is related to the fluid yield stress. An offset F_0 is included to account for the nonzero mean observed in the measured force due to the presence of the accumulator.

One model that is numerically tractable and has been used extensively for modeling hysteretic systems is the Bouc-Wen model [57]. The Bouc-Wen model is extremely versatile and can exhibit a wide variety of hysteretic behavior. A schematic of this model is shown in Figure 2.7. The force in this system is given by:

$$F_{MR} = c_0\dot{x} + k_0\left(x - x_0\right) + \alpha z \tag{2.38}$$

$$\dot{z} = -\gamma|\dot{x}||z|^{n-1}z - \beta\dot{x}|z|^n + A\dot{x} \tag{2.39}$$

where z is an internal state variable. By adjusting the parameters of the model γ, β and A, one can control the linearity in the unloading and the smoothness of the transition from the pre-yield to the post-yield region. In addition, the force F_0 due to the accumulator can be directly incorporated into this model as an initial deflection x_0 of the linear spring k_0.

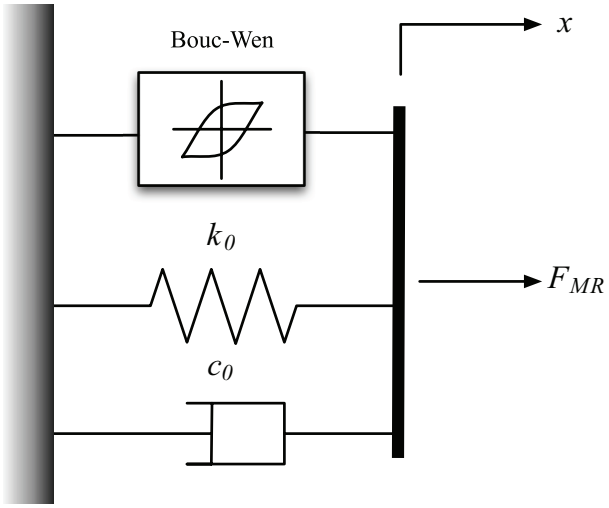

Figure 2.7: Bouc-Wen Model of the MR damper.

The Bouc-Wen model was generalized to describe the MR damper by introducing fluctuating magnetic fields [49, 58]. The proposed model is shown in Figure 2.8, and the applied force is given by:

$$F_{MR} = c_0 (\dot{x} - \dot{y}) + k_0 (x - y) + k_1 (x - x_0) + \alpha z \tag{2.40}$$

or equivalently:

$$F_{MR} = c_1 \dot{y} + k_1 (x - x_0) \tag{2.41}$$

where the evolutionary variable z is determined by:

$$\dot{z} = -\gamma |\dot{x} - \dot{y}| |z|^{n-1} z - \beta (\dot{x} - \dot{y}) |z|^n + A (\dot{x} - \dot{y}) \tag{2.42}$$

and:

$$\dot{y} = \frac{1}{(c_0 + c_1)} (c_0 \dot{x} + k_0 (x - y)) \tag{2.43}$$

To construct a valid model, the functional dependence of the parameters on the applied voltage or current must be determined. It was discovered in [49] that the steady state yield level appears to vary linearly with the applied voltage, and have nonzero initial value. The viscous damping

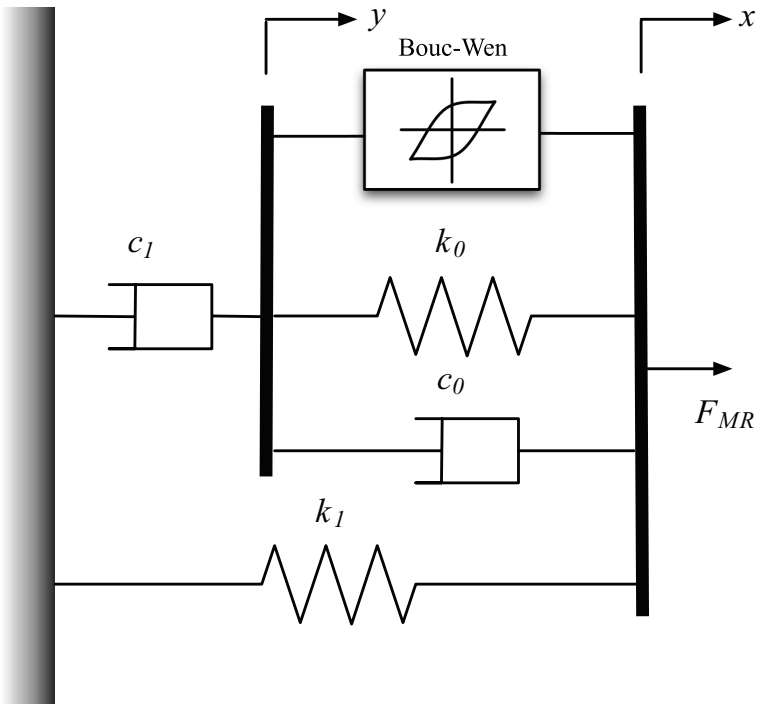

Figure 2.8: Mechanical model of the MR damper.

constants also vary linearly with the applied voltage. Therefore, the following relationships were established:

$$\alpha(u) = \alpha_a + \alpha_b u \tag{2.44}$$

$$c_0(u) = c_{0a} + c_{0b} u \tag{2.45}$$

$$c_1(u) = c_{1a} + c_{1b} u \tag{2.46}$$

$$\dot{u} = -\eta\,(u - v) \tag{2.47}$$

where v is the applied voltage. In this model, a total of 14 parameters is required to describe the MR damper.

Compared to the Bouc-Wen model [49, 58], the LuGre model has a simpler structure and smaller number of parameters is needed for expression of its behavior [41]. The LuGre model may also be modified so that a necessary input voltage can be analytically calculated to produce the specified command damping force F_A [42]. Therefore, this research will employ the LuGre model to describe the MR damper.

Clipped-Optimal Control

The MR damper is a semi-active device, and therefore does not have the ability to generate arbitrary damping force as would an active actuator. The response of the MR damper is dependent on the relative displacement and velocity at the point of attachment. Clipped-optimal control was proposed as an algorithm for the control of a semi-active MR damper [15], in which a linear optimal controller is combined with a force feedback loop designed to adjust the input voltage. Its modification was also considered in [28, 59].

In the clipped-optimal control scheme, the MR damper will only be turned on by a fixed positive voltage, or turned off by applying zero voltage. No intermediate voltage is used. If the magnitude of the force produced by the damper is smaller than the desired force and the two forces have the same sign, the voltage applied to the damper is increased to the maximum level so as to increase the force produced by the damper in order to match the desired control force. Otherwise, the command voltage is set to zero. The algorithm for selecting the voltage signal is mathematically stated as [15]:

$$v = V_{\max} H\left(\left(F_A - F_{MR}\right) F_{MR}\right) \tag{2.48}$$

where $V_{\max}$ is the maximum permissible voltage and F_A is the desired control force produced by an active control scheme, such as the LQ controller or the skyhook method described in the previous section. $H(\cdot)$ is the Heaviside step function. A graphical representation of the algorithm is given in Figure 2.9.

Robust LQ Control with Dissipativity

In the active damping control section, conventional LQ design was presented as a viable method for achieving vibration suppression. However, the semi-active constraint of the MR damper signifies that $F_{MR} \neq F_A$ and therefore it is necessary to define the following disturbance term:

$$\delta_{MR} = F_{MR} - F_A \tag{2.49}$$

which is assumed to be bounded by:

$$\|\delta_{MR}\|_2 \leq \Delta_{MR} \tag{2.50}$$

Restating (2.17) in terms of F_A and δ_{MR}:

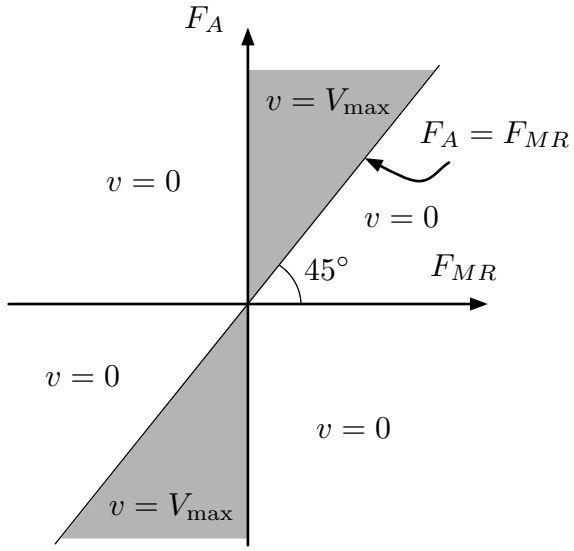

Figure 2.9: Clipped-optimal control algorithm.

$$\dot{\boldsymbol{x}}_p = \boldsymbol{A}\boldsymbol{x}_p + \boldsymbol{b}F_A + \boldsymbol{b}\delta_{MR} + \boldsymbol{e}\dot{x}_r \tag{2.51}$$

The presence of this disturbance term implies that conventional LQ control may not yield a satisfactory control signal. It thus becomes necessary to restate the control objective in an H_∞ framework. The robust control objective with dissipativity becomes:

$$J_\infty = \sup_{\delta_{MR} \in L_2} \frac{\|z\|_2}{\|\delta_{MR}\|_2} < \gamma \tag{2.52}$$

where:

$$z = \begin{bmatrix} \left(\boldsymbol{Q} - r^{-1}\boldsymbol{s}\boldsymbol{s}^T\right)^{\frac{1}{2}} & \boldsymbol{0} \\ r^{-\frac{1}{2}}\boldsymbol{s}^T & r^{\frac{1}{2}} \end{bmatrix} \begin{bmatrix} \boldsymbol{x}_p \\ F_A \end{bmatrix} \tag{2.53}$$

Here, $\boldsymbol{Q} = q\boldsymbol{I}$ and $\boldsymbol{s} = \begin{bmatrix} \boldsymbol{0}^T & s_1 & s_2 \end{bmatrix}^T$, while $q > 0$ and $r > 0$. Therefore:

$$\begin{aligned} \|z\|_2 &= \int_0^\infty \begin{bmatrix} \boldsymbol{x}_p^T & F_A \end{bmatrix} \begin{bmatrix} \boldsymbol{Q} & \boldsymbol{s} \\ \boldsymbol{s}^T & r \end{bmatrix} \begin{bmatrix} \boldsymbol{x}_p \\ F_A \end{bmatrix} dt \\ &= \int_0^\infty \left(\boldsymbol{x}_p^T \boldsymbol{Q}\boldsymbol{x}_p + 2\boldsymbol{x}_p^T \boldsymbol{s}F_A + rF_A^2\right) dt \end{aligned} \tag{2.54}$$

Assuming that the road perturbation $\dot{x}_r$ is a random signal with zero mean, the active control force considering the dissipativity is given by:

$$F_A = -\boldsymbol{k}^T \boldsymbol{x}_p \tag{2.55}$$

$$\boldsymbol{k} = \frac{\boldsymbol{P}\boldsymbol{b} + \boldsymbol{s}}{r} \tag{2.56}$$

and $\boldsymbol{P}$ is the solution of the corresponding Riccati equation:

$$\boldsymbol{Q} + \boldsymbol{P}\boldsymbol{A} + \boldsymbol{A}^T\boldsymbol{P} - \boldsymbol{P}\boldsymbol{b}\left(1 - \gamma^{-2}\right)\boldsymbol{b}^T\boldsymbol{P} = \boldsymbol{0} \tag{2.57}$$

If all of the states are not available, an observer can be designed from the sensor data, for instance $x_s - x_u$ and $\ddot{x}_s$, and an output controller is implemented.

2.2.4 Research Motivation

The motivation of this research was inspired by the inherent uncertainties involved in mechanical suspension systems. Vibration problem is a great concern in structural mechanics and the automotive industries, where systems are commonly subjected to high level of excitation from external sources. The introduction of a damping force, via passive, semi-active, or active methods, is necessary to mitigate these disturbances and ensure structural integrity.

This portion of the thesis focuses primarily on vehicle suspension systems. The essential role of the suspension mechanism is to ensure ride comfort, vehicle safety, road damage minimization, and overall vehicle performance. Conventional passive suspensions have been shown to provide adequate damping only in certain frequency ranges and no online feedback action is utilized. The effectiveness of passive damping solutions is also offset by varying operational parameters, such as the mass of the chassis. Active suspension systems via actuators can circumvent these limitations by providing an arbitrary damping force which can adapt to system variations and guarantee improved performance over a wide range of frequency. Thus, it has been extensively studied and various schemes have been proposed. However, active suspensions suffer from a requirement of a large power supply.

This led to a shift in focus towards semi-active damping design, which is capable of providing significant improvements over passive suspension systems while consuming much less power than active control schemes. The switch to semi-active suspension has been further accelerated by the growing availability and economic feasibility of electrorheological (ER) and magnetorheological (MR) dampers.

The MR damper has been successfully employed in a wide range of vibration suspension systems, such as bridges, helicopter rotors, suspension seats, and seismic reduction. In particular, it has found wide-spread interest in the automotive industry as a method of vehicle suspension. Many control strategies have been developed for the MR damper, such as skyhook, groundhook, hybrid control, H_∞ control, and model-following sliding mode control.

However, practical applications involving the MR damper is considerably limited by its hysteretic and nonlinear characteristics. As outlined in the previous section, modeling of the MR damper is an important component of controller design. A wide range of model exists to describe the MR damper, including the Bouc-Wen hysteresis model, neural network or fuzzy models, nonlinear blackbox model, NARX model, and viscoelastic-plastic model. Recently, a linearized model based upon the LuGre friction formulation has been proposed and investigated. This has allowed the design of an inverse controller so that the MR damper outputs almost active damping force.

This research expands upon the idea of an inverse controller that linearizes the MR damper, thus allowing almost active damping force to be applied to the suspension system. It deals with the inherent hysteretic and nonlinear behaviors of the MR damper, while considering parametric uncertainties. The inverse control is also combined with a reference controller using robust LQ design or the skyhook method to provide a total suspension system. Robustness and stability conditions will be considered in the presence of uncertainties in both the vehicle suspension and MR damper systems.

2.3 Friction Compensation

The final topic explored in this thesis is the control of mechanical systems acting under the influence of friction. It is widely recognized that most mechanical systems involving two or more contact surfaces with relative motion would experience, to varying degrees, some form of frictional effects. The presence of dynamic friction in such industrial applications as robotic manipulators, hydraulic systems, precision engineering, and disc drives, can lead to significant control error, or even instability. A summarized list of friction-induced errors in mechanical systems is given in Table 2.1.

It is a common approach to apply passive compensation techniques, such as lubrication and hardware design, to mitigate frictional effects. However, this is only a partial solution

Table 2.1: Friction-induced errors in mechanical systems.

Task	Error	Main Friction Contributor
Regulator	Steady-state error or hunting	Stiction
Tracking with velocity reversal	Stand-still, lost motion	Stiction
Tracking at low velocities	Stick-slip oscillation	Stribeck effect, stiction
Tracking at high velocities	Large tracking error	Viscosity

to the problem, and should be complemented by an effective control scheme. The necessity for applying control theories to friction compensation results from the nonlinearity of surface contact mechanics, structural and parametric uncertainties. This is further complicated by environmental and operational factors which can greatly impact frictional behaviors.

As a result, the study of friction compensation continues to garner immense research interest from mechanical and control engineers alike. Numerous researches exist in the field of tribology that characterize the important effects of friction. These properties include static and dynamic behaviors, such as hysteresis, the Stribeck effect, frictional lag, and stick-slip mechanics. Various models have been proposed throughout the years that attempt to combine the greatest amount of accuracy in describing these frictional effects while maintaining a mathematical simplicity that facilitates design and control purposes.

In this section, the main frictional properties are presented, especially those with the greatest significance to positional and velocity tracking. A brief survey of popular friction models is then presented, along with a comparison of the benefits and costs of each. A detailed description of the newly proposed generalized Maxwell-slip (GMS) friction model is also given that will form the mathematical preliminaries of this research. Finally, the motivation of this research and its direction is discussed.

2.3.1 Friction Characteristics

Tribology refers to the science and technology of interacting surfaces in relative motion, with particular emphasis on friction, wear and lubrication. Due to the pervasive presence of friction in all mechanical systems where two or more surfaces are in contact, the study of friction has inspired immense research efforts amongst mechanical and control engineers over the years.

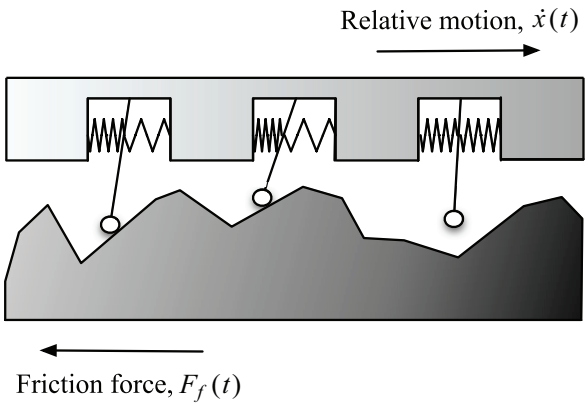

Figure 2.10: Asperity-view of friction mechanism.

This has led to a deep understanding of the complex mechanisms behind the friction process, which manifest themselves as static or dynamic properties, such as hysteresis, the Stribeck effect, frictional lag, and stick-slip mechanics.

In general, the friction mechanism is divided into two regimes: micro-slip or sticking regime; and gross sliding or slipping regime. An asperity-based description, in which the contact surfaces are viewed as a number of asperity or bristles, is often used to describe this phenomenon and is shown in Figure 2.10. The micro-slip regime refers to the effects of friction observed as two contact surfaces begin to experience relative displacement from a stationary position. The individual asperities undergo elastic deformation that results in a proportional, spring-like force opposing the direction of motion. At a certain static level, the asperity force reaches its maximum break-away value, and each asperity enters the gross sliding regime, which is dominated by the Stribeck effect, Coulomb friction, and frictional lag. The switching mechanism between two regimes is referred to as *stiction*, and is a main cause of tracking error in mechanical systems. This asperity-based view of the friction process has resulted in the identification of several key properties.

Stribeck Effect

Immediately after transition into the gross sliding regime, the friction force experiences an initial, negatively sloped decline from its maximum static friction value to a certain Coulomb friction level. This phenomenon is commonly referred to as the Stribeck effect, where the

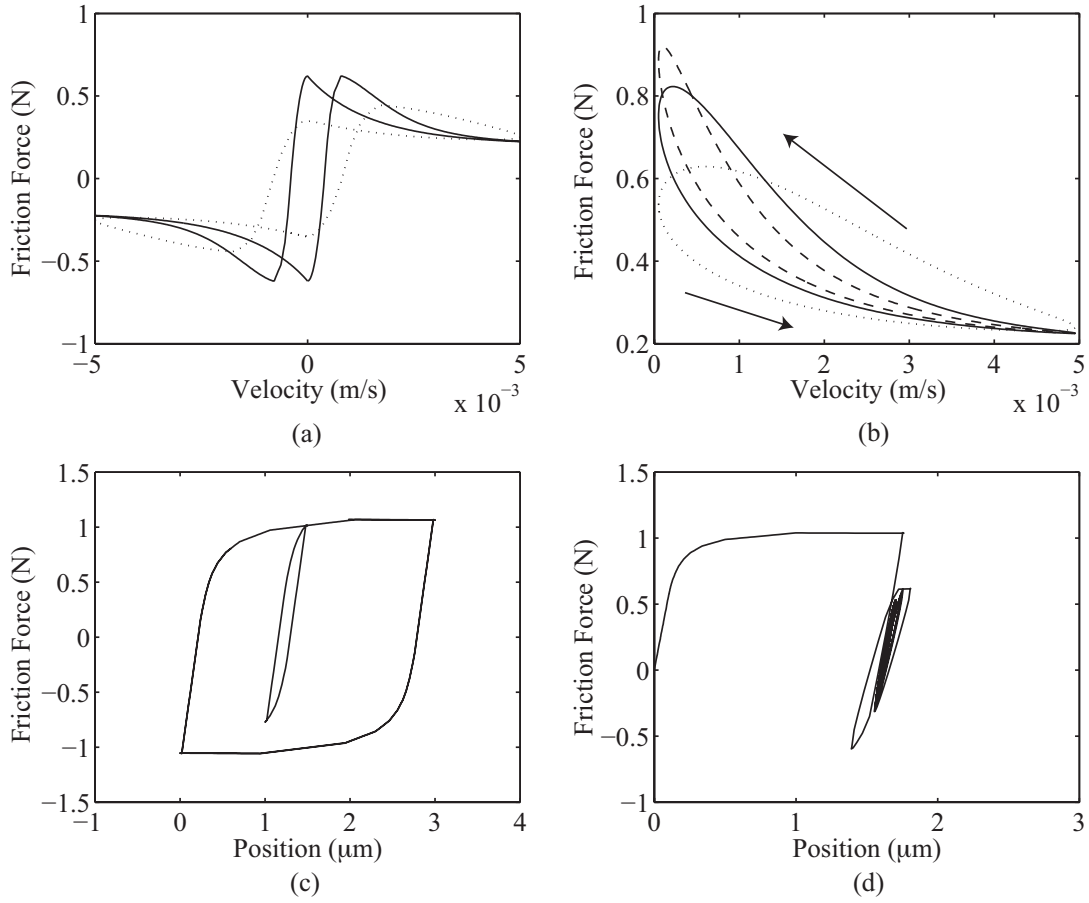

Figure 2.11: (a) Friction force for sinusoidal velocity at 2.5Hz (dotted) and 7.5Hz (solid); (b) frictional lag in 2 quadrant for sinusoidal velocity at 2.5Hz (dotted), 7.5Hz (solid), and 10Hz (dashed); (c) non-local memory in sticking regime; and (d) non-drifting property.

amount and rate of decline is dependent on the materials comprising the contact surfaces and the presence of any lubrication. Upon reaching the Coulomb friction level, the friction behavior is governed by a constant Coulomb force and a certain velocity-dependent viscous term. The Stribeck effect is a nonlinear, static function usually described by the following mathematical expression:

$$s(\dot{x}) = F_C + (F_S - F_C)\, e^{-\left(\frac{|\dot{x}|}{V_S}\right)^{\sigma_S}} \tag{2.58}$$

where F_C is the Coulomb friction parameter, F_S represents static friction, V_S is the Stribeck velocity, and σ_S is a shaping factor. The Stribeck effect is shown in Figures 2.11(a) and 2.11(b).

Frictional Lag

Another important property is frictional lag, which refers to the rate dependency of the friction force in the gross sliding regime. Friction lag is a dynamic behavior that results in a larger friction force for increasing velocities than for decreasing velocities, and becomes more apparent for large acceleration and deceleration. This is illustrated in Figure 2.11(b).

Presliding Hysteresis

In the presliding regime, the mechanics of friction is dominated by the spring-action of the asperity. The interplay between stiction and elastic deformation of each asperity results in a hysteresis behavior. The friction force is a function of the displacement at one time instant, as well as the history of displacement and friction force. Key properties of this hysteretic spring motion are non-local memory and non-drifting properities, which are shown in Figures 2.11(c) and 2.11(d). The hysteresis behavior continues until each asperity reaches its maximum attainable static friction level, after which it moves into the gross sliding regime.

2.3.2 Friction Models

Combining knowledge gleaned from tribological studies about the nature of friction, applied mathematicians and control engineers have developed several models to describe the friction process. This includes both static and dynamic models that varies greatly in terms of complexity and accuracy. This section presents some of the most popular friction models that are relevant from the perspective of control engineers involved with designing mechanical systems.

Static Friction Models

Traditionally, friction was viewed as a rate-independent, static function of velocity and displacement. These static friction models represent the classical framework for friction compensation and analysis. The simplest of these is the Coulomb friction model, named after Charles Augustin de Coulomb, which is independent of contact surface area and is expressible as:

$$F_f = F_C sgn(\dot{x}) \tag{2.59}$$

where F_C is the Coulomb friction parameter, which is proportional to the normal load. The magnitude of F_C varies depending on the material of the contact surface and the presence of

lubrication, as determined by $F_C = \mu F_N$, where μ is the material-dependent friction coefficient and F_N is the normal load. Note that the Coulomb friction does not specify a friction force for zero velocity, which may vary on any value in the interval between $-F_C$ and F_C. The Coulomb friction model has been extensively used for friction compensation as a result of its relative simplicity.

Another important component of a static friction model is viscous friction, a velocity-dependent force that is caused by the viscosity of lubricants. Generally it is stated as:

$$F_f = F_V \dot{x} \tag{2.60}$$

An alternative expression that provides better fit to experimental data is:

$$F_f = F_V |\dot{x}|^{\delta_V} sgn(\dot{x}) \tag{2.61}$$

where δ_V depends on the geometry of the application.

As mentioned in the previous section, stiction force and the Stribeck effect are also significant properties that may be combined with Coulomb and viscous friction to form a unified, static friction model. Generally, this is given as:

$$\begin{aligned} F_f &= F_V \dot{x} + sgn(\dot{x}) \left(F_C + (F_S - F_C)\, e^{-\left(\frac{|\dot{x}|}{V_S}\right)^{\sigma_S}} \right) \\ &= F_V \dot{x} + sgn(\dot{x}) s(\dot{x}) \end{aligned} \tag{2.62}$$

where $s(\dot{x})$ is the Stribeck curve as defined previously. This static model can be obtained by measuring friction force for motion with constant velocity and is sometimes asymmetrical. Various modifications exist of this static friction model, such as the Karnopp and Armstrong models, which are included as references in this thesis.

Dynamic Friction Models

While static friction models have been widely employed for control purposes, they do not conform to certain observable friction behaviors. In particular, they fail to include the hysteresis behavior during presliding motion. In order to describe these properties, the development of dynamic friction model becomes necessary. This is driven both by intellectual curiosity and increasingly stringent demand on precision and accuracy of mechanical systems. The complexity and accuracy of each model varies, as shown in Table 2.2.

Table 2.2: Friction model comparison table.

Property	Static	Dahl	Bliman-Sorine	Lugre	Leuven	GMS
Stribeck	○	-	-	○	○	○
Presliding	-	○	○	○	○	○
Break-away	-	-	○	○	○	○
Friction lag	-	-	-	○	○	○
Non-drifting	-	-	-	-	○	○
Transition	-	-	-	-	-	○

Dynamic friction models were originally developed to describe the hysteresis behavior during presliding motion. The Dahl friction model was proposed as a simple mathematical description of the friction process based upon the stress-strain curve in classical solid mechanics. It models the stress-strain curve by the following differential equation:

$$\frac{dF_f}{dx} = \sigma \left(1 - \frac{F_f}{F_C} sgn(\dot{x})\right)^{\alpha} \tag{2.63}$$

where x is the relative displacement, σ is the stiffness coefficient, and α is a shaping factor of the stress-strain curve. The magnitude of the friction force will never exceed the Coulomb friction value if its initial condition satisfies $|F_f(0)| < F_C$. The Dahl model may also be restated in the time domain as:

$$\frac{dF_f}{dx} = \frac{dF_f}{dt}\frac{dx}{dt} = \sigma\dot{x} - \frac{F_f}{F_C}|\dot{x}| \tag{2.64}$$

where $\alpha = 1$. It is a generalization of ordinary Coulomb friction, and does not account for the Stribeck effect or stiction.

Similar to the Dahl model, the Bliman-Sorine friction models are rate-independent descriptions, in which the magnitude of friction is a function of $sgn(\dot{x})$ and the space variable z defined by:

$$z = \int_{t_0}^{t} |v(\tau)| d\tau \tag{2.65}$$

Bliman-Sorine models vary in complexity, and are expressed as linear systems in the space variable z as:

$$\frac{d\boldsymbol{x}_z}{dz} = \boldsymbol{A}\boldsymbol{x}_z + \boldsymbol{b}sgn(\dot{x}) \tag{2.66}$$

$$F_f = \boldsymbol{c}^T\boldsymbol{x}_z \tag{2.67}$$

The first-order Bliman-Sorine model reduces to the Dahl model and does not describe stiction or the Stribeck effect. To overcome this obstacle, a second-order model is usually employed, which is essentially a parallel connection of a fast and slow Dahl model. The fast model has higher steady-state friction level. The force from the slow model is subtracted from the fast model, resulting in stiction. However, it was observed that the second-order model only approximates the Stribeck effect and does not conform to observed friction characteristics.

A generic friction model based upon physical considerations and experimental data has been proposed [1]. It minutely examines all mechanisms involved in the friction process, resulting in a complex mathematical description. The complexity of the generic friction model renders it impractical for use in controller design, and further discussion is omitted. However, the generic friction model remains a powerful tool for analyzing the fidelity and accuracy of other friction models.

Other dynamical friction models can be found in the literature. However, of particular interest are the LuGre and GMS friction models. These models represent a suitable combination of accuracy and simplicity, and a detailed description will be given in the following section.

LuGre Friction Model

The LuGre friction model was proposed by [11] and effectively combines static and Dahl friction models. As such, it is capable of describing presliding hysteresis and the Stribeck effect. The two regimes are described by a single set of equations that results in a smooth transition between presliding and sliding actions. The friction force is expressed in terms of an internal state variable z as:

$$\frac{dz}{dt} = \dot{x} - \sigma_0\frac{|\dot{x}|}{s(\dot{x})}z \tag{2.68}$$

$$F_f = \sigma_0 z + \sigma_1\dot{z} + \sigma_V\dot{x} \tag{2.69}$$

The LuGre model is based on the asperity concept, and employs a nonlinear differential equation to implicitly describe frictional lag in the sliding regime, hysteresis in the presliding regime,

and a rate-dependent varying break-away force. It is determined by the stiffness parameter σ_0, the micro-viscous friction coefficient σ_1, and gross viscosity coefficent σ_V, in addition to the parameters associated with the Stribeck effect.

It is noted that the steady-state solution of the LuGre friction model reduces to the static friction model:

$$z_{ss} = \frac{1}{\sigma_0} s(\dot{x}) sgn(\dot{x}) \tag{2.70}$$

$$F_{f,ss} = \sigma_0 z_{ss} + \sigma_v \dot{x} = s(\dot{x}) sgn(\dot{x}) + \sigma_V \dot{x} \tag{2.71}$$

Likewise, when $\sigma_0 = 0$, $\sigma_1 = 0$, and $F_S = F_C$, the LuGre model essentially reduces to the Dahl model.

The mathematical simplicity of the LuGre moel has resulted in its popularity for control purposes, in particular identification, dissipativity, and adaptive control considerations. Its main advantage is an integrated friction model without the need of a switching function. However, this comes at a cost to accuracy. Specifically, it is not capable of describing non-local behavior in the presliding regime and does not explicitly account for frictional lag.

GMS Friction Model

The generalized Maxwell-slip (GMS) friction model is an extension of the Leuven model. The Leuven model introduces the concept of an explicit, non-local hysteresis function and is structurally similar to the LuGre model. It also employs an internal state variable z which serves to model the average deflection of the asperity junctions. However, the Leuven model is considerably more complex than the LuGre model, and as such is subjected to implementation problems.

Attempts to improve the Leuven model eventually led the recent formulation of the GMS friction model. The GMS model maintains a simpler structure than the generic model while providing more accuracy than the LuGre model. However it has a switching structure which can result in a complicated controller design process.

The GMS model is an asperity-based description of the friction phenomenon. It consists of parallel connections of elementary blocks, shown in Figure 2.12 and expressed by:

$$F_f = \sum_{i=1}^{N} F_i \tag{2.72}$$

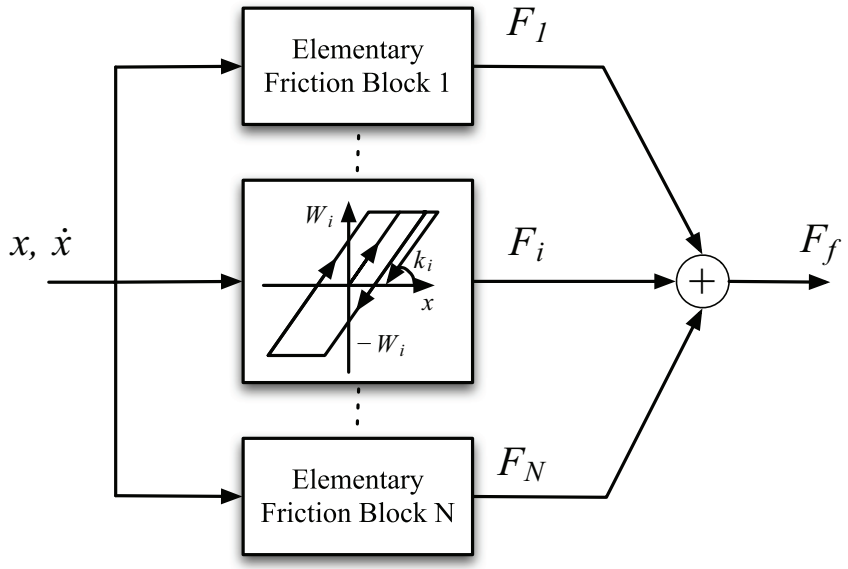

Figure 2.12: Parallel connections of N elementary blocks in the GMS model.

Here, N represents the number of elementary blocks employed by the GMS model, and viscous friction is neglected. Each elementary block is governed by a set of two dynamical equations, depending on whether it is in a sticking or slipping state. The sticking state contains a Maxwell-slip equation to describe hysteresis and other presliding characteristcs. The slipping state equation results in frictional lag and the Stribeck effect. Mathematically, this is expressed as:

- If the elementary block is sticking, the differential equation is given by:

$$\dot{F}_i = k_i \dot{x} \tag{2.73}$$

  and the elementary block remains sticking until $|F_i| > \alpha_i s(\dot{x}) = W_i$.

- If the elementary block is slipping, the differential equation is given by:

$$\dot{F}_i = C\left(\alpha_i sgn(\dot{x}) - \frac{F_i}{s(\dot{x})}\right) \tag{2.74}$$

  and the elementary block remains slipping until the velocity goes through zero.

Here, C is a constant term introduced by the GMS model to directly account for frictional lag dynamics, and $\sum \alpha_i = 1$. Notice the hybrid structure of the GMS model; two separate models are used to represent the sticking and slipping states. From a control perspective, any controller constructed using the GMS model would have to account for this switching structure.

Several offline methods have been proposed to identify the parameters associated with the GMS model. Experimental identification procedures using the Nelder-Mead Simplex algorithm has been presented [55]. Another method is the use of particle swarm optimization (PSO), which is a global minimization technique designed for nonlinear problems that avoids being trapped by local minimums [23, 24]. It is therefore especially suited to the identification of the GMS friction model, which has been explored previously [37].

Considering only the slipping state of friction under constant velocity, the steady-state equation for each elementary block reduces to:

$$F_{i,ss} = \alpha_i sgn(\dot{x}) s(\dot{x}) \tag{2.75}$$

Defining $\delta_{i,D} = F_i - F_{i,ss}$, the frictional force equation in the slipping regime becomes:

$$\begin{aligned} F_i &= F_{i,ss} + \delta_{i,D} \\ &= \alpha_i sgn(\dot{x}) s(\dot{x}) + \delta_{i,D} \end{aligned} \tag{2.76}$$

Analysis of the above equation reveals that the friction force is comprised of two terms: a static term corresponding to the Stribeck effect; and a dynamic term $\delta_{i,D}$ that acts as a perturbation.

2.3.3 Model-Based Friction Compensation Schemes

Friction compensation schemes are commonly categorized as model and non-model based algorithms. This section presents an overview of existing model-based approaches that have been explored in the literature. Most model-based friction compensation schemes have a feedforward structure with an appropriate friction model included in the forward loop of the controller. The role of the friction model is to generate an estimated friction force that would effectively cancel out frictional effects and result in linearization of the closed loop transfer function.

A key component of model-based compensation schemes is the model itself. The choice of friction model is a trade-off between complexity and accuracy. Some of the more popular friction models for control purposes have been outlined in the previous section. Another important consideration for control engineers is the amount of available knowledge regarding system parameters. As friction is a complicated process whose internal mechanisms are difficult or impossible to discern, uncertainty about frictional parameters is a daunting obstacle. This has inspired many research into friction compensation from an adaptive or robust framework.

As stated in previous sections, static friction models and nonlinear mappings are mathematically simple and have thus been employed extensively for friction compensation. Notable works include the modeling and compensation of Coulomb friction by [3, 16]. A more precise approach was taken by [31], which considers nonlinear static mapping of the Stribeck effect. These methods provide powerful arguments for the use of adaptive control in friction compensation, but do not combine it with a sufficiently complex and accurate dynamic friction model.

To this end, several dynamic friction models have been developed [7,14], the most popular of which is the LuGre model [11]. Due to its relative simplicity, extensive literature exists regarding the use of the LuGre friction model in various compensation schemes [10, 32, 43]. However, it has been pointed out that the LuGre model compromises fidelity in favor of simplicity. Most notably, the LuGre model does not explicitly account for friction lag characteristics, and its hysteresis-like behavior fails to exhibit non-drifting and non-local memory properties [53]. As of the beginning of this research, no effective compensation method has been proposed for the Leuven or GMS friction models.

2.3.4 Non-Model-Based Friction Compensation Schemes

A different approach is non-model-based friction compensation. As previously stated, knowledge about the structure and parameters of any model-based approach is subjected to a high degree of uncertainty. This is augmented by variations in environmental and operational conditions. Non-model-based friction compensation attempts to circumvent these obstacles by taking a data- or signal-based control tactic. A common method employed by engineers is the conventional PD or PID controller. The main benefits of the PD/PID controller is its simplicity and intuitive structure. In this case, the control signal is formulated using only the error signal and its respective derivatives. However, studies have shown that simple PD or PID controllers suffer significant performance degradation due to the nonlinear characteristics of friction, which can lead to hunting behaviors and instability [5]. This can be improved with the use of a stiff PD controller. An alternative is observer-based nonlinear friction compensation scheme [20]. Black-box methods employing neural networks or fuzzy logic for friction compensation have also been widely researched [25, 26, 44].

Though non-model-based friction compensation schemes may provide suitable system per-

formance, they do not yield additional knowledge about the friction mechanism. Moreover, changes in physical parameters or operating conditions would necessitate a redesign of the controller. In the interest of specifically addressing this uncertainty issue in mechanical systems, this research thus takes a model-based approach to friction compensation.

2.3.5 Research Motivation

It has been widely established that friction is present in most mechanical systems. However, frictional parameters are highly uncertain and may vary greatly with changes in environmental conditions, such as temperature, wear, material, geometry, and lubrication. This falls directly within the scope of this thesis, which aims to study the application of adaptive and learning control algorithms to uncertain mechanical systems.

The main difficulty in dealing with friction compensation is finding the right balance between modeling precision and complexity. The previous sections have established the major characteristics of friction that a good model should accurately describe and presented some of the more popular models that have been explored in the literature. Particular emphasis was placed in examining the structure of the LuGre model and the GMS friction model. Though the LuGre model has drawn considerable research interest in recent years due to its relatively simple structure that utilizes an integrated equation to describe frictional dynamics, it is noted that it does so at the price of fidelity to observed data. After careful consideration of this fact, this study focuses on developing a friction compensation scheme using the GMS friction model.

The GMS friction model provides a highly accurate description of the friction process. It is an asperity-based model with two separate sets of equations to govern the dynamics in the presliding and sliding regimes. Using a parallel connection of elementary blocks, the Maxwell-slip hysteresis functions capture the relevant presliding behaviors of friction that play a major role in systems involving high precision and multiple zero-velocity crossing. It also introduces a term in the sliding regime dynamics to directly account for frictional lag.

From a control perspective, the GMS model is an attractive candidate for friction compensation. At the time of this research, no effective algorithms have yet been proposed based upon the GMS friction model. However, the main difficulty that must be addressed when utilizing the GMS model is its switching structure and the nonlinearity of the Stribeck effect. The motivation of this research is the development of a comprehensive friction compensation

scheme based upon the GMS friction model which simultaneously addresses these problems while considering uncertainties and other robustness issues involving system parameters.

Chapter 3

Multi-Mass Torsional Motor System

This chapter begins the investigation of adaptive and iterative control methods for parametrically uncertain mechanical systems by considering the velocity control of a linear multi-mass torsional motor system. Torsional motor systems are widely employed in industrial and robotic processes, and are often tasked with performing repetitive movements along a given trajectory. However, system parameters are seldom accurately known or are subjected to changes depending on operating conditions. It is therefore desirable that an iterative tuning method be established that can produce optimal controllers despite these uncertainties, while simultaneously providing as much information about the system as possible.

In the following chapter, an introduction to the velocity control problem of parametrically uncertain torsional motors is given. The mathematical description of a general two-mass motor system will be presented. The proposed 2-degree-of-freedom (2DOF) controller is discussed, which includes a reference model in the feedforward path. The command generator tracking (CGT) theory is then used to establish a clear relationship between the optimal gains of the feedforward controller and the physical model parameters of the two-mass torsional motor system. This relationship is critical to the proposal of a novel algorithm for iterative feedback tuning (IFT) of a completely unknown two-mass torsional motor system. By defining the feedforward controller gains in terms of physical model parameter estimates, the error gradient necessary for iterative tuning becomes analytically calculable, thus eliminating the requirements of additional experiments per iteration as demanded by conventional IFT methods. The effectiveness of the proposed method in achieving trajectory tracking and identification of all physical parameters is demonstrated via experimentation.

3.1 Introduction

Torsional motor systems are an integral part of many industrial and mechanical processes, where they are often employed for repetitive tasks along fixed trajectories. The design of an efficient velocity controller generally requires precise knowledge about system structures and parameters. However, this information is seldom available to control engineers in actual applications, or varies depending on operating conditions. Lacking accurate parametric knowledge about the system can greatly complicate the controller design process. It is therefore necessary for control engineers to develop an effective and easily implementable method to achieve control performance objectives of an uncertain system, while at the same time yielding as much information about the system as possible.

A popular method for controller design of a mechanical system is iterative feedback tuning (IFT) [18, 19]. The IFT algorithm involves the minimization of a performance function by a gradient-based tuning method. However, the tuning process is greatly hindered when system knowledge is lacking or incomplete. Without an accurate mathematical description of the system, it is not possible to analytically calculate the gradient of the output error with respect to the controller parameters. In such a situation, IFT requires determining the system transfer function using separate identification techniques or performing additional experiments for gradient estimation. Prohibitive experimental conditions, such as cost, stability issues, and closed-loop identifiability, mean that these are not always viable solutions.

This study addresses the iterative tuning problem of an unknown two-mass motor system. It has been demonstrated that a direct relationship exists between the physical parameters of a two-mass system and the linear gains of a feedforward controller [27] that was constructed using the CGT theory [9, 22]. The feedforward controller includes a suitable reference model that generates signals necessary for establishing this relationship [17, 27]. This concept was further developed by investigating the feasibility of using IFT to determine the feedforward and feedback controller parameters as the error is minimized [33, 34]. However, a system identification method was required to determine the system transfer function, which is necessary for iterative tuning.

Therefore, one of the purposes of this study is to propose a novel iterative tuning algorithm for the feedforward and feedback controllers. The structure of the feedforward and feedback controllers is chosen to establish a clear relationship between physical model parameters of the

two-mass motor system and the feedforward controller based on CGT theory [9]. From this relationship, the controller can be tuned directly by estimates of the physical model parameters to minimize tracking error. In addition, an estimated system transfer function can be analytically obtained from the estimated model parameters at each iteration. This estimated transfer function allows for the direct calculation of the output error gradients with respect to the feedforward and feedback controller parameters that are required to conduct IFT.

The proposed algorithm is an efficient integration of IFT [18, 19] and the feedforward controller designed using CGT [27, 33, 34]. In utilizing system information provided by the feedforward controller to construct an estimated system transfer function, the additional experiments for gradient estimation, required by ordinary IFT in the case of an unknown system, become unnecessary. This reduction in the number of experiments performed per iteration is beneficial in terms of efficiency and cost. Likewise, a separate system identification process is no longer required. The proposed tuning algorithm is self-sufficient in minimizing the output error, as the system transfer function can be estimated directly from the relationship with the feedforward controller parameters. It also has the additional benefit of identifying the physical parameters of the system as the output error is improved.

The resulting, unified algorithm provides a powerful tool for achieving trajectory tracking of a completely unknown two-mass system. The validity and efficiency of the method is demonstrated by velocity control experiments of a two-mass motor system. It is noted that no prior knowledge of system parameters or transfer function is required to implement this algorithm. The proposed algorithm is, to the author's knowledge, currently the only existing method for identifying all the physical parameters of a two-mass motor system in an online manner while achieving trajectory tracking objectives.

3.2 System Description

A two-mass, torsional motor system is shown in Figure 3.1. The experimental set-up for a two-mass motor system, as depicted in Figure 3.2, is considered. The motor input is given by a continuous-time, torque command input $u_p(t)$. J_1 and J_2 are the inertial moment of the motor and load respectively. C_1 and C_2 are the viscous damping constants of the motor and load respectively. K_1 denotes the shaft time constant and $\tau_1(t)$ is the shaft torque. The motor and load speed are denoted as $\omega_1(t)$ and $\omega_2(t)$. The speed of the motor $\omega_1(t)$ is required to track the

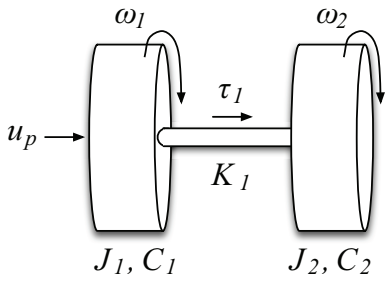

Figure 3.1: Two-mass torsional motor system.

output of a reference model with time constant T_d. The two-mass system can be represented by the following continuous-time state-space model:

$$\dot{\boldsymbol{x}}_p(t) = \boldsymbol{A}_p \boldsymbol{x}_p(t) + \boldsymbol{b}_p u_p(t) \tag{3.1}$$

$$y_p(t) = \boldsymbol{c}_p^T \boldsymbol{x}_p(t) \tag{3.2}$$

where:

$$\boldsymbol{x}_p(t) = \begin{bmatrix} \omega_1(t) & \tau_1(t) & \omega_2(t) \end{bmatrix}^T$$

$$\boldsymbol{A}_p = \begin{bmatrix} -C_1/J_1 & -1/J_1 & 0 \\ 1/K_1 & 0 & -1/K_1 \\ 0 & 1/J_2 & -C_2/J_2 \end{bmatrix}$$

$$\boldsymbol{b}_p = \begin{bmatrix} 1/J_1 & 0 & 0 \end{bmatrix}^T$$

$$\boldsymbol{c}_p = \begin{bmatrix} 1 & 0 & 0 \end{bmatrix}^T$$

The transfer function $G_o(s)$ from $u_p(t)$ to $y_p(t)$ is expressed as:

$$y_p(t) = G_o(s) u_p(t) \tag{3.3}$$

$$G_o(s) = \frac{N_o(s)}{D_o(s)} \tag{3.4}$$

where:

$$N_o(s) = \frac{1}{J_1}\left(s^2 + \frac{C_2}{J_2}s + \frac{1}{K_1 J_2}\right)$$

$$D_o(s) = s^3 + \left(\frac{C_1}{J_1} + \frac{C_2}{J_2}\right)s^2 + \left(\frac{1}{K_1 J_1} + \frac{1}{K_1 J_2} + \frac{C_1 C_2}{J_1 J_2}\right)s + \frac{C_1 + C_2}{K_1 J_1 J_2}$$

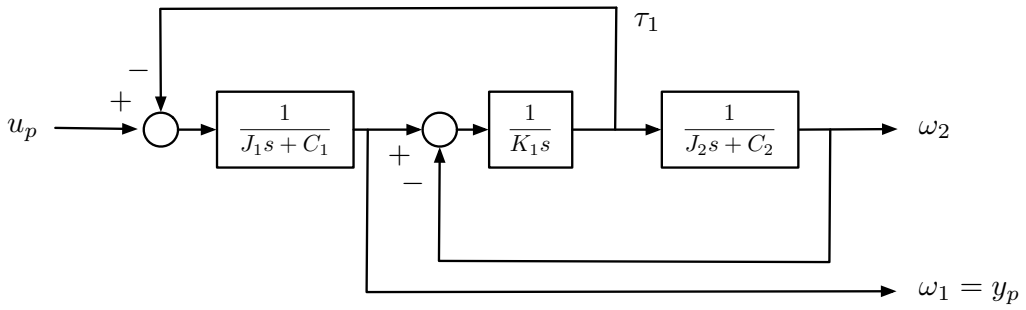

Figure 3.2: Block diagram of two-mass motor system.

It is assumed that all physical model parameters in the above transfer function are unknown and should be determined.

3.3 Proposed Controller Structure

3.3.1 Feedforward and Feedback Controllers

The proposed reference model of the controlled system has the following state-space representation:

$$\dot{\boldsymbol{x}}_m(t) = \boldsymbol{A}_m \boldsymbol{x}_m(t) + \boldsymbol{b}_m u_M(t) \tag{3.5}$$

$$y_m(t) = \boldsymbol{c}_m^T \boldsymbol{x}_m(t) \tag{3.6}$$

where:

$$\boldsymbol{x}_m(t) = \begin{bmatrix} x_{m_1}(t) & x_{m_2}(t) & x_{m_3}(t) \end{bmatrix}^T$$

$$\boldsymbol{A}_m = \begin{bmatrix} 0 & 1 & 0 \\ 0 & 0 & 1 \\ 0 & 0 & 0 \end{bmatrix}$$

$$\boldsymbol{b}_m = \begin{bmatrix} 0 & 0 & 1 \end{bmatrix}^T$$

$$\boldsymbol{c}_m = \begin{bmatrix} 1 & 0 & 0 \end{bmatrix}^T$$

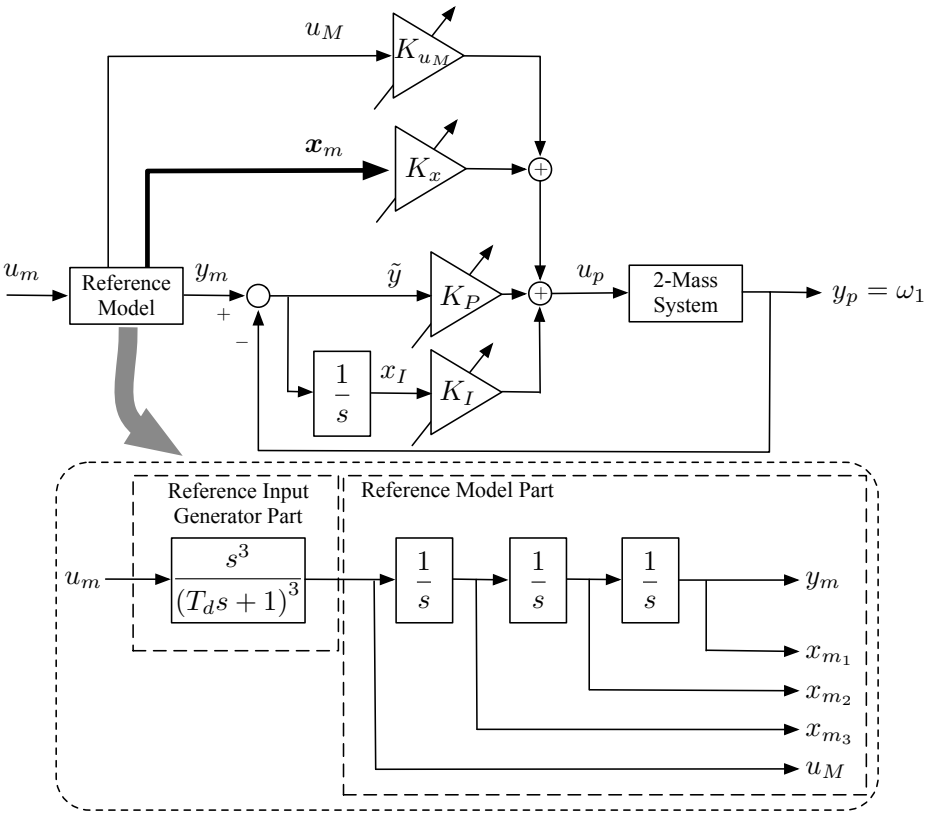

Figure 3.3: CGT-based 2DOF controller.

The reference model and an input generator with a desired time constant T_d are incorporated directly into the feedforward path of a simple adaptive controller (SAC) [17, 22], as shown in Figure 3.3. This formulates the CGT-based controller. Unlike the SAC theory, this study proposes the inclusion of the reference model and input generator so that a clear relationship between the feedforward controller and the physical model estimates can be established using the CGT theory. The command input is formally defined as:

$$u_p(t) = \boldsymbol{k}^T \boldsymbol{r}(t) \tag{3.7}$$

where:

$$\boldsymbol{r}(t) = \begin{bmatrix} \tilde{y}(t) & x_I(t) & x_{m_1}(t) & x_{m_2}(t) & x_{m_3}(t) & u_M(t) \end{bmatrix}^T$$

$$\boldsymbol{k} = \begin{bmatrix} K_P & K_I & K_{x_1} & K_{x_2} & K_{x_3} & K_{u_M} \end{bmatrix}^T$$

$$\tilde{y}(t) = y_m(t) - y_p(t)$$

Here, $\boldsymbol{k}$ is a vector of controller parameters. The 2DOF controller in Figure 3.3 can also be expressed in the transfer function form, where $C_r(s, \boldsymbol{k})$ and $C_y(s, \boldsymbol{k})$ are the feedforward and feedback controllers respectively, as:

$$u_p(t) = C_r(s, \boldsymbol{k}) u_m(t) - C_y(s, \boldsymbol{k}) y_p(t) \tag{3.8}$$

where:

$$C_r(s, \boldsymbol{k}) = \frac{1}{D_{cr}(s)} \left(K_{u_M} s^4 + K_{x_3} s^3 + K_{x_2} s^2 + (K_{x_1} + K_P)\, s + K_I \right) \tag{3.9}$$

$$C_y(s, \boldsymbol{k}) = \frac{K_P s + K_I}{s} \tag{3.10}$$

$$D_{cr}(s) = s(T_d s + 1)^3 \tag{3.11}$$

The following results are obtained using the CGT theory [9, 22]. Assuming that the controlled system satisfies the almost strictly positive real (ASPR) property and the reference signal $u_m(t)$ satisfy the PE condition, the ideal states $\boldsymbol{x}_p^*(t)$ and the ideal input $u_p^*(t)$, that is, the states and input when the output error $\tilde{y}(t)$ between the controlled system and the reference model is forced to zero, is expressable as:

$$\boldsymbol{x}_p^*(t) = \boldsymbol{S}_{11} \boldsymbol{x}_m(t) + \boldsymbol{s}_{12} u_M(t) \tag{3.12}$$

$$u_p^*(t) = \boldsymbol{s}_{21}^T \boldsymbol{x}_m(t) + s_{22} u_M(t) \tag{3.13}$$

From (3.1), (3.2), (3.5), and (3.6), along with the above equations, it follows that:

$$\begin{aligned} \dot{\boldsymbol{x}}_p^*(t) &= \boldsymbol{S}_{11} \dot{\boldsymbol{x}}_m(t) + \boldsymbol{s}_{12} \dot{u}_M(t) \\ &= \boldsymbol{S}_{11} \boldsymbol{A}_m \boldsymbol{x}_m(t) + \boldsymbol{S}_{11} \boldsymbol{b}_m u_M(t) \\ &= \boldsymbol{A}_p \boldsymbol{x}_p^*(t) + \boldsymbol{b}_p u_p^*(t) \\ &= \left(\boldsymbol{A}_p \boldsymbol{S}_{11} + \boldsymbol{b}_p \boldsymbol{s}_{21}^T \right) \boldsymbol{x}_m(t) + \left(\boldsymbol{A}_p \boldsymbol{s}_{12} + \boldsymbol{b}_p s_{22} \right) u_M(t) \end{aligned} \tag{3.14}$$

In the first line of (3.14), $\dot{u}_M(t) \to 0$ when the input is a step signal. Since $u_p^*(t)$ signifies that $y_m(t) = y_p(t)$, we also have:

$$\begin{aligned} y_m(t) &= \boldsymbol{c}_p^T \boldsymbol{x}_p^*(t) \\ &= \boldsymbol{c}_p^T \boldsymbol{S}_{11} \boldsymbol{x}_m(t) + \boldsymbol{c}_p^T \boldsymbol{s}_{12} u_M(t) \\ &= \boldsymbol{c}_m^T \boldsymbol{x}_m(t) \end{aligned} \tag{3.15}$$

It follows from (3.14) and (3.15) that:

$$\left.\begin{aligned} \boldsymbol{S}_{11}\boldsymbol{A}_m &= \boldsymbol{A}_p\boldsymbol{S}_{11} + \boldsymbol{b}_p\boldsymbol{s}_{21}^T \\ \boldsymbol{S}_{11}\boldsymbol{b}_m &= \boldsymbol{A}_p\boldsymbol{s}_{12} + \boldsymbol{b}_p s_{22} \\ \boldsymbol{c}_m^T &= \boldsymbol{c}_p^T\boldsymbol{S}_{11},\ \ 0 = \boldsymbol{c}_p^T\boldsymbol{s}_{12} \end{aligned}\right\} \tag{3.16}$$

Note from (3.13) that $\boldsymbol{s}_{21}$ and s_{22} are the linear coefficients of the reference model states and input that produce the ideal input signal. They correspond to the ideal gains of the proposed feedforward controller when the error is forced to zero. Solving (3.16) yields the following relationship between the controller gains defined in (3.7) and the ideal controller gains in (3.13):

PROPERTY 3.1 *If the control input can force the output error $\tilde{y}$ to zero, the controller gains converge to:*

$$\left.\begin{aligned} \lim_{\tilde{y}\to 0} K_{x_1} &= C_1 + C_2 \\ \lim_{\tilde{y}\to 0} K_{x_2} &= J_1 + J_2 - K_1 C_2^2 \\ \lim_{\tilde{y}\to 0} K_{x_3} &= -2K_1 C_2 J_2 + K_1^2 C_2^3 \\ \lim_{\tilde{y}\to 0} K_{u_M} &= -K_1 J_2^2 - K_1^3 C_2^4 + 3K_1^2 C_2^2 J_2 \end{aligned}\right\} \tag{3.17}$$

Proof: The proposed feedforward controller is derived by noting that $u_p^*(t)$ corresponds to the ideal control input when the error is minimized. This input is expressable as a linear combination of the reference model input and states, given in (3.13). The proposed feedforward controller structure is designed to include the reference model and input generator, so that as the gains approach $\boldsymbol{s}_{21}$ and s_{22}, the ideal control input signal will be realized. Let $\boldsymbol{S}_{11}$, $\boldsymbol{s}_{12}$, $\boldsymbol{s}_{21}$ and s_{22} in (3.13) be denoted as:

$$\boldsymbol{S}_{11} = \begin{bmatrix} w_{1,1} & \cdots & w_{1,3} \\ \vdots & \ddots & \vdots \\ w_{3,1} & \cdots & w_{3,3} \end{bmatrix}, \quad \boldsymbol{s}_{12} = \begin{bmatrix} x_1 \\ \vdots \\ x_3 \end{bmatrix}$$
$$\boldsymbol{s}_{21}^T = \begin{bmatrix} y_1 & \cdots & y_3 \end{bmatrix}, \qquad s_{22} = z \tag{3.18}$$

Then, solving for the components of $\boldsymbol{s}_{21}$ and s_{22} will yield the ideal feedforward gains. Using the CGT theory, the relationships in (3.16) are determined. Given the controlled system and reference state space model in (3.1), (3.2), (3.5) and (3.6), it is now possible to solve for $\boldsymbol{S}_{11}$, $\boldsymbol{s}_{12}$, $\boldsymbol{s}_{21}$ and s_{22} by rewriting (3.16) as:

$$\underline{\boldsymbol{A}_p\boldsymbol{S}_{11} + \boldsymbol{b}_p\boldsymbol{s}_{21}^T = \boldsymbol{S}_{11}\boldsymbol{A}_m :}$$

$$\begin{bmatrix} -C_1/J_1 & -1/J_1 & 0 \\ 1/K_1 & 0 & -1/K_1 \\ 0 & 1/J_2 & -C_2/J_2 \end{bmatrix} \begin{bmatrix} w_{1,1} & \cdots & w_{1,3} \\ \vdots & \ddots & \vdots \\ w_{3,1} & \cdots & w_{3,3} \end{bmatrix} + \begin{bmatrix} 1/J_1 \\ 0 \\ 0 \end{bmatrix} \begin{bmatrix} y_1 \\ \vdots \\ y_3 \end{bmatrix}^T$$

$$= \begin{bmatrix} w_{1,1} & \cdots & w_{1,3} \\ \vdots & \ddots & \vdots \\ w_{3,1} & \cdots & w_{3,3} \end{bmatrix} \begin{bmatrix} 0 & 1 & 0 \\ 0 & 0 & 1 \\ 0 & 0 & 0 \end{bmatrix} \tag{3.19}$$

$\underline{\boldsymbol{A}_p\boldsymbol{s}_{12} + \boldsymbol{b}_p s_{22} = \boldsymbol{S}_{11}\boldsymbol{b}_m :}$

$$\begin{bmatrix} -C_1/J_1 & -1/J_1 & 0 \\ 1/K_1 & 0 & -1/K_1 \\ 0 & 1/J_2 & -C_2/J_2 \end{bmatrix} \begin{bmatrix} x_1 \\ \vdots \\ x_3 \end{bmatrix} + \begin{bmatrix} 1/J_1 \\ 0 \\ 0 \end{bmatrix} z = \begin{bmatrix} w_{1,1} & \cdots & w_{1,3} \\ \vdots & \ddots & \vdots \\ w_{3,1} & \cdots & w_{3,3} \end{bmatrix} \begin{bmatrix} 0 \\ 0 \\ 1 \end{bmatrix} \tag{3.20}$$

$\underline{\boldsymbol{c}_p^T\boldsymbol{S}_{11} = \boldsymbol{c}_m^T :}$

$$\begin{bmatrix} 1 & 0 & 0 \end{bmatrix} \begin{bmatrix} w_{1,1} & \cdots & w_{1,3} \\ \vdots & \ddots & \vdots \\ w_{3,1} & \cdots & w_{3,3} \end{bmatrix} = \begin{bmatrix} 1 \\ 0 \\ 0 \end{bmatrix}^T \tag{3.21}$$

$\underline{\boldsymbol{c}_p^T\boldsymbol{s}_{12} = 0 :}$

$$\begin{bmatrix} 1 & 0 & 0 \end{bmatrix} \begin{bmatrix} x_1 \\ \vdots \\ x_3 \end{bmatrix} = 0 \tag{3.22}$$

Solving these equations will yield $\boldsymbol{S}_{11}$, $\boldsymbol{s}_{12}$, $\boldsymbol{s}_{21}$ and s_{22}. The calculation is straightforward, with the solutions $\boldsymbol{s}_{21}$ and s_{22} given by:

$\underline{\boldsymbol{s}_{21} :}$

$$y_1 = C_1 + C_2$$

$$y_2 = J_1 + J_2 - K_1C_2^2$$

$$y_3 = -2K_1C_2J_2 + K_1^2C_2^3$$

$\underline{s_{22} :}$

$$z = -K_1J_2^2 - K_1^3C_2^4 + 3K_1^2C_2^2J_2$$

Comparing (3.7) and (3.13), the solution of $\boldsymbol{s}_{21}$ and s_{22} leads directly to Property 3.1. □

This relationship between the feedforward controller gains and the true physical model parameters leads to the definition of the ideal controller gains as:

$$\boldsymbol{k}^* = \begin{bmatrix} \boldsymbol{k}_{PI}^{*\,T} & \boldsymbol{k}_x^{*T} & K_{u_M}^* \end{bmatrix}^T \tag{3.23}$$

where:

$$\boldsymbol{k}_{PI}^* = \begin{bmatrix} K_P^* & K_I^* \end{bmatrix}^T$$
$$\boldsymbol{k}_x^* = \begin{bmatrix} K_{x_1}^* & K_{x_2}^* & K_{x_3}^* \end{bmatrix}^T$$

Here, K_P^* and K_I^* are the optimal but previously unknown PI gains, while $\boldsymbol{k}_x^*$ and $K_{u_M}^*$ are defined by (3.17).

3.3.2 Discrete-Time Implementation

In practical implementation, the control action is discrete-time. Note that for a discrete-time system with sampling interval T_s, the proposed controller can be modified by replacing the Laplace s-operator with the following δ-operator:

$$\delta = \frac{(1 - z^{-1})}{T_s z^{-1}} \tag{3.24}$$

Here, z^{-1} is the backward shift operator with respect to sampling time T_s, given as $z^{-1} = e^{-T_s s}$. To preserve the ASPR property of the controlled system when it is discretized with a zero-order holder, the following phase-lead compensator may be included in the controlled system [27]:

$$u_p'(m) = \frac{2T_s\delta + 1}{T_s\delta + 1} u_p(m) \tag{3.25}$$

This is shown in Figure 3.4(a). The equivalent transfer function of the controlled system, which consists of the two-mass motor and a phase-lead compensator, when discretized with the δ-operator, is expressed as:

$$G_{eq}(\delta) = \left(\frac{2T_s\delta + 1}{T_s\delta + 1} \right) G_o(\delta) \tag{3.26}$$

Here, $G_o(\delta)$ refers to the discretized transfer function of the two-mass motor system given in (3.4). The complete closed-loop system is illustrated in Figure 3.4(b), where $C(\delta, \boldsymbol{k}) = \{C_r(\delta, \boldsymbol{k})\ C_y(\delta, \boldsymbol{k})\}$ are the feedforward and feedback controllers in (3.9) and (3.10), when discretized with the δ-operator.

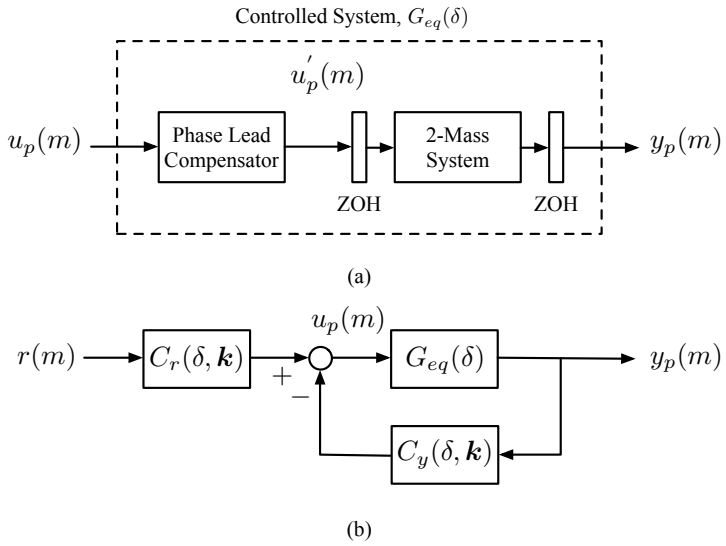

Figure 3.4: (a) Controlled system with phase lead compensator, and (b) closed-loop system, discretized with the δ-operator.

3.4 Proposed Tuning Algorithm

3.4.1 Conventional Iterative Feedback Tuning

The proposed iterative tuning scheme makes use of Property 3.1, which establishes a direct relationship between the feedforward controller and the physical model parameters of the system. This information is essential for eliminating the gradient experiments required by conventional IFT [18, 19].

A brief discussion of the conventional IFT method is considered. Assume an unknown system whose transfer function is described by (3.26), and the controller in (3.8) when discretized by the δ-operator. The control objective is the tracking of the desired response $y_m(m)$. Without using Property 3.1, the controller is parameterized at iteration i by the gain vector $\boldsymbol{k}^{(i)}$. In this paper, the performance criterion is chosen as a quadratic function based upon N measured, discrete-time, error signals given as:

$$J(\boldsymbol{k}^{(i)}) = \frac{1}{2N} \sum_{m=1}^{N} (L_y \tilde{y}(m, \boldsymbol{k}^{(i)}))^2 \tag{3.27}$$

In (3.27), the notation $\tilde{y}(m, \boldsymbol{k}^{(i)})$ signifies the error signal at sampling instant mT_s, with the controller $C(\delta, \boldsymbol{k}^{(i)})$ operating in the closed loop. For the sake of simplicity, the frequency weighted filter L_y is taken to be 1. The optimal controller parameter $\boldsymbol{k}^*$ is defined by:

$$\boldsymbol{k}^* = \arg\min_{\boldsymbol{k}} J(\boldsymbol{k}) \tag{3.28}$$

This can be obtained by the following iterative algorithm:

$$\boldsymbol{k}^{(i+1)} = \boldsymbol{k}^{(i)} - \gamma^{(i)} \boldsymbol{R}(\boldsymbol{k}^{(i)})^{-1} \frac{\partial J(\boldsymbol{k}^{(i)})}{\partial \boldsymbol{k}} \tag{3.29}$$

$$\frac{\partial J(\boldsymbol{k}^{(i)})}{\partial \boldsymbol{k}} = \frac{1}{N} \sum_{m=1}^{N} \left(\tilde{y}(m, \boldsymbol{k}^{(i)}) \frac{\partial \tilde{y}(m, \boldsymbol{k}^{(i)})}{\partial \boldsymbol{k}} \right) \tag{3.30}$$

Here, $\gamma^{(i)}$ is a sequence of positive real numbers that determines the step-size, and $\boldsymbol{R}(\boldsymbol{k}^{(i)})$ is a sequence of positive definite matrices. This study defines $\boldsymbol{R}(\boldsymbol{k}^{(i)})$ as:

$$\boldsymbol{R}(\boldsymbol{k}^{(i)}) = \frac{1}{N} \sum_{m=1}^{N} \operatorname{diag} \left(\left(\frac{\partial \tilde{y}(m, \boldsymbol{k}^{(i)})}{\partial K_P} \right)^2, \ldots, \left(\frac{\partial \tilde{y}(m, \boldsymbol{k}^{(i)})}{\partial K_{u_M}} \right)^2 \right) \tag{3.31}$$

Notice that the solution of (3.30) requires the gradient of the output with respect to each controller parameter in $\boldsymbol{k}^{(i)}$. For the discrete-time, closed-loop system shown in Fig. 3.4, the gradient is given as:

$$\frac{\partial \tilde{y}(m, \boldsymbol{k}^{(i)})}{\partial \boldsymbol{k}} = T_o(\delta, \boldsymbol{k}^{(i)}) \left(\frac{\partial C_r(\delta, \boldsymbol{k}^{(i)})}{\partial \boldsymbol{k}} u_m(m) - \frac{\partial C_y(\delta, \boldsymbol{k}^{(i)})}{\partial \boldsymbol{k}} y_p(m, \boldsymbol{k}^{(i)}) \right) \tag{3.32}$$

where:

$$T_o(\delta, \boldsymbol{k}^{(i)}) = \frac{G_{eq}(\delta)}{1 + C_y(\delta, \boldsymbol{k}^{(i)}) G_{eq}(\delta)}$$

To calculate the error gradient in (3.32), it is obvious that the transfer function $G_{eq}(\delta)$ is necessary. Without this information, conventional IFT requires additional experiments to be performed in order to obtain a suitable estimate of the gradient, or the use of separate system identification procedures. Instead, the novel iterative algorithm presented in this study can simplify the tuning process by eliminating these extra procedures.

3.4.2 Novel Iterative Tuning Algorithm

This study proposes using the derived relationship between feedforward controller parameters and the physical parameters in Property 3.1 to achieve the iterative feedback tuning of the unknown two-mass controlled system. First, the physical model parameter estimates, which also includes the PI gains, are defined as:

$$\boldsymbol{\rho} = \begin{bmatrix} K_P & K_I & \hat{J}_1 & \hat{J}_2 & \hat{C}_1 & \hat{C}_2 & \hat{K}_1 \end{bmatrix}^T \tag{3.33}$$

The feedforward controller gains are then restated in terms of $\boldsymbol{\rho}$ as:

$$\left.\begin{aligned} K_{x_1} &= \hat{C}_1 + \hat{C}_2 \\ K_{x_2} &= \hat{J}_1 + \hat{J}_2 - \hat{K}_1\hat{C}_2^2 \\ K_{x_3} &= -2\hat{K}_1\hat{C}_2\hat{J}_2 + \hat{K}_1^2\hat{C}_2^3 \\ K_{u_M} &= -\hat{K}_1\hat{J}_2^2 - \hat{K}_1^3\hat{C}_2^4 + 3\hat{K}_1^2\hat{C}_2^2\hat{J}_2 \end{aligned}\right\} \tag{3.34}$$

The feedforward and feedback controllers in (3.9) and (3.10) can also be expressed as $C(s,\boldsymbol{\rho}) = \{C_r(s,\boldsymbol{\rho})\ C_y(s,\boldsymbol{\rho})\}$, using (3.34). This allows for direct tuning of the controller by physical model parameter estimates to achieve output error minimization. A key component of this proposed algorithm is that the physical model estimates can be used to construct an estimated system transfer function for iterative tuning.

PROPERTY 3.2 *The convergence of physical model estimates $\boldsymbol{\rho}$ to the ideal parameters $\boldsymbol{\rho}^*$ as the output error $\tilde{y}(m)$ approaches zero is guaranteed by using Property 3.1 and (3.34), where*

$$\boldsymbol{\rho}^* = \begin{bmatrix} K_P^* & K_I^* & J_1 & J_2 & C_1 & C_2 & K_1 \end{bmatrix}^T \tag{3.35}$$

Proof: The ideal input is defined as:

$$u_p^*(t) = \boldsymbol{k}^{*T}\boldsymbol{r}(t) \tag{3.36}$$

Therefore, the actual input and controller parameters can be expressed as:

$$u_p(t) = \boldsymbol{k}^T\boldsymbol{r}(t) \tag{3.37}$$

$$\boldsymbol{k} = \boldsymbol{k}^* + \Delta\boldsymbol{k} \tag{3.38}$$

where $\Delta\boldsymbol{k}$ is a small deviation from $\boldsymbol{k}^*$. Similarly, the estimated physical parameters can also be expressed approximately as:

$$\boldsymbol{\rho} = \boldsymbol{\rho}^* + \Delta\boldsymbol{\rho} \tag{3.39}$$

The relationship between $\Delta \boldsymbol{k}$ and $\Delta \boldsymbol{\rho}$ can be determined as:

$$\Delta \boldsymbol{k} = \boldsymbol{M} \Delta \boldsymbol{\rho} \tag{3.40}$$

$$\boldsymbol{M} = \begin{bmatrix} 1 & 0 & 0 & 0 & 0 & 0 & 0 \\ 0 & 1 & 0 & 0 & 0 & 0 & 0 \\ 0 & 0 & 0 & 0 & 1 & 1 & 0 \\ 0 & 0 & 1 & 1 & 0 & m_{4,6} & m_{4,7} \\ 0 & 0 & 0 & m_{5,4} & 0 & m_{5,6} & m_{5,7} \\ 0 & 0 & 0 & m_{6,4} & 0 & m_{6,6} & m_{6,7} \end{bmatrix} \tag{3.41}$$

where:

$$\begin{aligned} m_{4,6} &= -2K_1C_2 \\ m_{4,7} &= -C^2 \\ m_{5,4} &= -2K_1C_2 \\ m_{5,6} &= 3K_1^2C_2^2 - 2K_1J_2 \\ m_{5,7} &= 2K_1C_2^3 - 2C_2J_2 \\ m_{6,4} &= 3K_1^2C_2^2 - 2K_1J_2 \\ m_{6,6} &= 6K_1^2C_2J_2 - 4K_1^3C_2^3 \\ m_{6,7} &= 6K_1C_2^2J_2 - 3K_1^2C_2^4 - J_2^2 \end{aligned}$$

Substituting (3.37) into (3.1):

$$\begin{aligned} \dot{\boldsymbol{x}}_p(t) &= \boldsymbol{A}_p\boldsymbol{x}_p(t) + \boldsymbol{b}_p u_p(t) \\ &= \boldsymbol{A}_p\boldsymbol{x}_p(t) + \boldsymbol{b}_p\boldsymbol{k}^T\boldsymbol{r}(t) \\ &= \boldsymbol{A}_p\boldsymbol{x}_p(t) + \boldsymbol{b}_pK_P\tilde{y}(t) + \boldsymbol{b}_pK_Ix_I(t) + \boldsymbol{b}_p{\boldsymbol{k}_x}^T\boldsymbol{x}_m(t) + \boldsymbol{b}_pK_{u_M}u_M(t) \end{aligned} \tag{3.42}$$

Define the state error as:

$$\tilde{\boldsymbol{x}}(t) = \boldsymbol{x}_p(t) - \boldsymbol{x}_p^*(t) \tag{3.43}$$

Then, the state error dynamics becomes:

$$\begin{aligned} \dot{\tilde{\boldsymbol{x}}}(t) &= \dot{\boldsymbol{x}}_p(t) - \dot{\boldsymbol{x}}_p^*(t) \\ &= \boldsymbol{A}_p\boldsymbol{x}_p(t) + \boldsymbol{b}_pK_P\tilde{y}(t) + \boldsymbol{b}_pK_Ix_I(t) + \boldsymbol{b}_p{\boldsymbol{k}_{\boldsymbol{x}}}^T\boldsymbol{x}_m(t) + \boldsymbol{b}_pK_{u_M}u_M(t) - \boldsymbol{A}_p\boldsymbol{x}_p^*(t) \\ &\quad -\boldsymbol{b}_pK_I^*x_I(t) - \boldsymbol{b}_p{\boldsymbol{k}_x^*}^T\boldsymbol{x}_m(t) - \boldsymbol{b}_pK_{u_M}^*u_M(t) \\ &= \left(\boldsymbol{A}_p + \boldsymbol{b}_pK_P^*\boldsymbol{c}_p^T\right)\tilde{\boldsymbol{x}}(t) + \boldsymbol{b}_p\Delta\boldsymbol{k}^T\boldsymbol{r}(t) \end{aligned} \tag{3.44}$$

Substituting (3.40) into (3.44) gives:

$$\dot{\tilde{\boldsymbol{x}}}(t) = \left(\boldsymbol{A}_p + \boldsymbol{b}_p K_P^* \boldsymbol{c}_p^T\right) \tilde{\boldsymbol{x}}(t) + \boldsymbol{b}_p \left[\boldsymbol{M}\Delta\boldsymbol{\rho}\right]^T \boldsymbol{r}(t) \tag{3.45}$$

Therefore, the output error can be expressed as:

$$\begin{aligned} \tilde{y}(t) &= y_p(t) - y_m(t) \\ &= \boldsymbol{c}_p^T(\boldsymbol{x}_p(t) - \boldsymbol{x}_p^*(t)) = \boldsymbol{c}_p^T \tilde{\boldsymbol{x}}(t) \\ &= W(s)\left[\Delta\boldsymbol{\rho}^T \boldsymbol{M}^T \boldsymbol{r}(t)\right] \end{aligned} \tag{3.46}$$

where

$$W(s) = \boldsymbol{c}_p^T(s\boldsymbol{I} - (\boldsymbol{A}_p + \boldsymbol{b}_p K_P^* \boldsymbol{c}_p^T))^{-1}\boldsymbol{b}_p$$

It can easily be shown that the two-mass system is output stablizable, and therefore $W(s)$ is SPR. Therefore, assuming that $\boldsymbol{M}^T\boldsymbol{r}(t)$ satisfies the PE condition, it is guaranteed that $\boldsymbol{\rho} \to \boldsymbol{\rho}^*$ as the output error is minimized. □

The novel tuning process is summarized as:

(Step 1) Start the iterative procedure with an arbitrary stabilizing controller $C(\delta, \boldsymbol{\rho}^{(1)})$, parameterized by $\boldsymbol{\rho}$ according to (3.33) and (3.34). Set iteration number $i = 1$.

(Step 2) With the controller $C(\delta, \boldsymbol{\rho}^{(i)})$ in the loop, perform one experiment with the reference signal $u_m(m)$. Substitute the physical model estimates $\boldsymbol{\rho}^{(i)}$ into (3.26) to obtain the estimated transfer function $\hat{G}_{eq}^{(i)}(\delta)$.

(Step 3) Tuning directly by the physical parameter estimates, the performance criterion is redefined as:

$$J(\boldsymbol{\rho}^{(i)}) = \frac{1}{2N}\sum_{m=1}^{N}(L_y\tilde{y}(m, \boldsymbol{\rho}^{(i)}))^2 \tag{3.47}$$

and the iterative algorithm becomes:

$$\boldsymbol{\rho}^{(i+1)} = \boldsymbol{\rho}^{(i)} - \gamma^{(i)}\boldsymbol{R}(\boldsymbol{\rho}^{(i)})^{-1}\frac{\partial J(\boldsymbol{\rho}^{(i)})}{\partial \boldsymbol{\rho}} \tag{3.48}$$

where:

$$\frac{\partial J(\boldsymbol{\rho}^{(i)})}{\partial \boldsymbol{\rho}} = \frac{1}{N}\sum_{m=1}^{N}\left(\tilde{y}(m, \boldsymbol{\rho}^{(i)})\frac{\partial \tilde{y}(m, \boldsymbol{\rho}^{(i)})}{\partial \boldsymbol{\rho}}\right) \tag{3.49}$$

$$\boldsymbol{R}(\boldsymbol{\rho}^{(i)}) = \frac{1}{N}\sum_{m=1}^{N}\mathrm{diag}\left(\left(\frac{\partial \tilde{y}(m, \boldsymbol{\rho}^{(i)})}{\partial K_P}\right)^2, \ldots, \left(\frac{\partial \tilde{y}(m, \boldsymbol{\rho}^{(i)})}{\partial \hat{K}_1}\right)^2\right) \tag{3.50}$$

The gradient is then estimated by:

$$\frac{\partial\hat{\tilde{y}}(m,\boldsymbol{\rho}^{(i)})}{\partial\boldsymbol{\rho}} = \hat{T}_o(\delta,\boldsymbol{\rho}^{(i)})\left(\frac{\partial C_r(\delta,\boldsymbol{\rho}^{(i)})}{\partial\boldsymbol{\rho}}u_m(m) - \frac{\partial C_y(\delta,\boldsymbol{\rho}^{(i)})}{\partial\boldsymbol{\rho}}y_p(m,\boldsymbol{\rho}^{(i)})\right) \tag{3.51}$$

$$\hat{T}_o(\delta,\boldsymbol{\rho}^{(i)}) = \frac{\hat{G}_{eq}^{(i)}(\delta)}{1+C_y(\delta,\boldsymbol{\rho}^{(i)})\hat{G}_{eq}^{(i)}(\delta)} \tag{3.52}$$

Notice that the gradient experiments of IFT are no longer required because $\hat{G}_{eq}^{(i)}(\delta)$ is available. The exact mathematical expressions for $\partial C_r(\delta,\boldsymbol{\rho}^{(i)})/\partial\boldsymbol{\rho}$ and $\partial C_y(\delta,\boldsymbol{\rho}^{(i)})/\partial\boldsymbol{\rho}$ can be derived as:

$$\begin{aligned}
\frac{\partial C_r(\delta,\boldsymbol{\rho})}{\partial K_P} &= \frac{\delta}{D_{cr}(\delta)}\\
\frac{\partial C_r(\delta,\boldsymbol{\rho})}{\partial K_I} &= \frac{1}{D_{cr}(\delta)}\\
\frac{\partial C_r(\delta,\boldsymbol{\rho})}{\partial \hat{J}_1} &= \frac{\delta^2}{D_{cr}(\delta)}\\
\frac{\partial C_r(\delta,\boldsymbol{\rho})}{\partial \hat{J}_2} &= \frac{\left(3\hat{C}_2^2\hat{K}_1^2 - 2\hat{J}_2\hat{K}_1\right)\delta^4 - 2\hat{C}_2\hat{K}_1\delta^3 + \delta^2}{D_{cr}(\delta)}\\
\frac{\partial C_r(\delta,\boldsymbol{\rho})}{\partial \hat{C}_1} &= \frac{\delta}{D_{cr}(\delta)}\\
\frac{\partial C_r(\delta,\boldsymbol{\rho})}{\partial \hat{C}_2} &\approx \frac{6\hat{J}_2\hat{C}_2\hat{K}_1^2\delta^4 - 2\hat{J}_2\hat{K}_1\delta^3 - 2\hat{C}_2\hat{K}_1\delta^2 + \delta}{D_{cr}(\delta)}\\
\frac{\partial C_r(\delta,\boldsymbol{\rho})}{\partial \hat{K}_1} &\approx \frac{-\hat{J}_2^2\delta^4 - 2\hat{J}_2\hat{C}_2\delta^3 - \hat{C}_2^2\delta^2}{D_{cr}(\delta)}
\end{aligned}$$

Similarly, the controller gradient of the feedback controller $C_y(\delta,\boldsymbol{\rho})$ in (3.10) discretized by the δ-operator is also derived as:

$$\begin{aligned}
\frac{\partial C_y(\delta,\boldsymbol{\rho})}{\partial \hat{K}_P} &= 1\\
\frac{\partial C_y(\delta,\boldsymbol{\rho})}{\partial \hat{K}_I} &= \frac{1}{\delta}\\
\frac{\partial C_y(\delta,\boldsymbol{\rho})}{\partial \hat{J}_1} &= \ldots = \frac{\partial C_y(\delta,\boldsymbol{\rho})}{\partial \hat{K}_1} = 0
\end{aligned}$$

Thus, all the gradients can be calculated analytically.

(Step 4) With the controller $C(\delta,\boldsymbol{\rho}^{(i+1)})$ in the loop, repeat from step (2) with $i = i+1$ until a suitable performance level is reached.

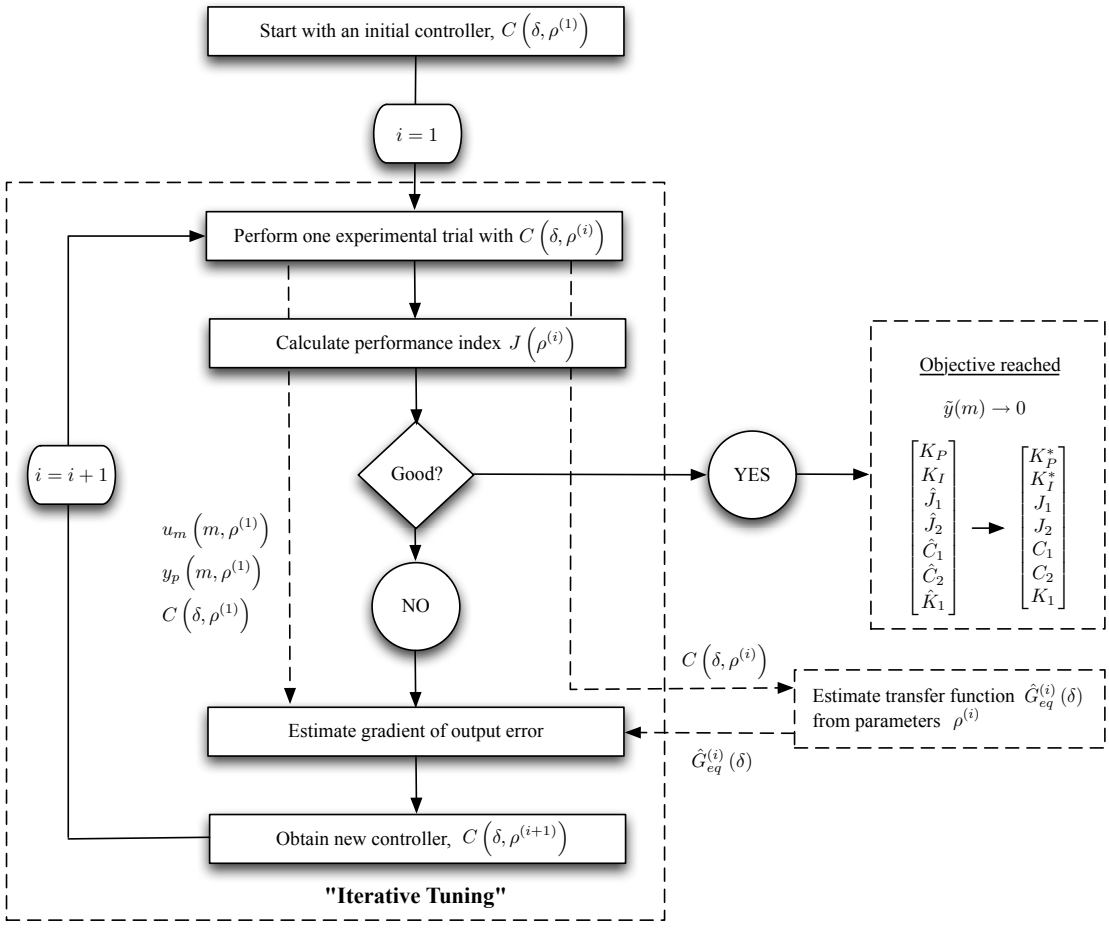

Figure 3.5: Novel iterative tuning algorithm.

Thus, the proposed iterative tuning scheme combines the CGT theory and the IFT algorithm to greatly simplify the tuning process. The flow chart of the proposed tuning algorithm based upon feedforward estimation is shown in Figure 3.5. In tuning the feedforward controller parameters directly by physical model estimates, the transfer function $\hat{G}_{eq}^{(i)}(\delta)$ of the system and the controller gradients are available. Therefore, the additional gradient experiments of IFT are no longer required, providing an advantageous decrease in experimental time and cost. It is also no longer necessary to perform closed-loop identification at every iteration. The proposed algorithm depends only on input-output data to achieve trajectory tracking of a completely unknown system, thus preserving the essence of IFT. From a system identification viewpoint,

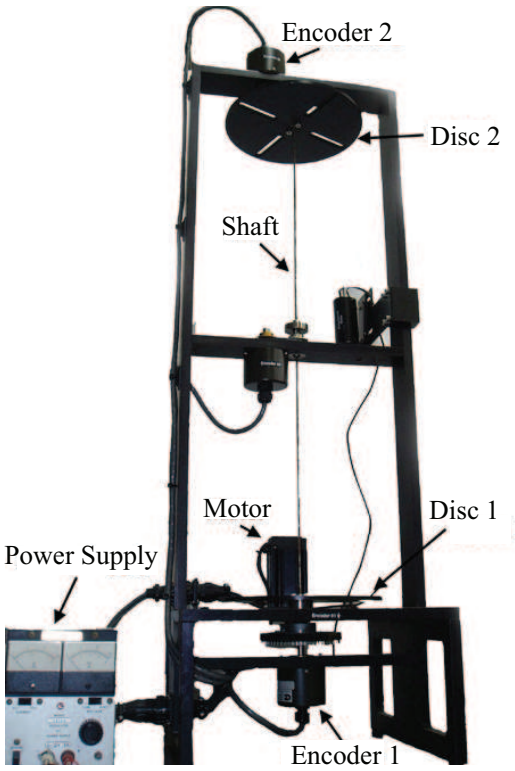

Figure 3.6: Experimental set-up (Torsional Control System Model 205a, manufactured by ECP).

it also provides an additional benefit of determining all the physical parameters and transfer function of the system. Clearly, the efficiency of the algorithm increases as $\hat{G}_o(\delta) \rightarrow G_o(\delta)$.

3.5 Experimental Results

The proposed scheme is verified by using the two-mass motor system in Figure 3.6. The experimental apparatus is a Torsional Control System Model 205a, manufactured by Educational Control Products (ECP), and configured with two inertial masses. Other experimental components include the Interface PCI-6201 Encoder Board, PCI-3521 Digital/Analog Board, PCI-6103 Timer Board, and a computer unit. The experiment is implemented in discrete-time, with sampling interval $T_s = 0.01$ [s]. The time constant of the reference model is chosen as $T_d = 0.03$ [s].

The true plant parameters are determined using off-line, open-loop identification for com-

Table 3.1: Physical parameters estimated by feedforward identification (Inertia Ratio 1:1).

Parameters	Initial	Converged	Open Loop
K_P	0	0.15924	–
K_I	0	0.01125	–
$\hat{J}_1$ (kg-m^2)	5.00×10^{-3}	2.43×10^{-3}	$2.43 \pm 0.00 \times 10^{-3}$
$\hat{C}_1$ (N-m/rad/s)	4.00×10^{-3}	1.35×10^{-3}	$1.26 \pm 0.27 \times 10^{-3}$
$\hat{J}_2$ (kg-m^2)	4.00×10^{-3}	1.92×10^{-3}	$1.89 \pm 0.06 \times 10^{-3}$
$\hat{C}_2$ (N-m/rad/s)	3.00×10^{-3}	1.02×10^{-3}	$1.14 \pm 0.29 \times 10^{-3}$
$\hat{K}_1$ (rad/N-m)	1.00×10^{0}	8.11×10^{-1}	$8.07 \pm 0.09 \times 10^{-1}$

parison with the parameters identified by the proposed on-line iterative tuning algorithm. The prediction error method (PEM) is employed to identify the transfer function and physical parameters of the system. Ten identification trials were conducted by exciting the two-mass motor system with varying input signals of persistently exciting condition. The input voltage signals consist of random gaussian noise and steady-state components. An example of the input voltage and the measured output velocity used for identification are shown in Figure 3.7. Two experimental configurations are used, with inertia ratio of 1:1 and 1:3. The average values and standard deviations of the physical model parameters determined by open-loop identification are given in Tables 3.1 and 3.2. The bode diagram for the nominal transfer functions constructed from the average values are shown in Figure 3.8. This average transfer function is considered as the nominal system in this experiment and will be used to compare with the physical parameter identification results.

The effectiveness of the proposed iterative algorithm in tuning the controller (3.8) for high performance tracking is illustrated for a two-mass system with inertia ratio of 1:1 and 1:3. The experiment time per iteration is 150 seconds. At each iteration, an estimated transfer function model of the system and the estimated gradients are constructed from the updated physical model parameters. Thus the controller parameter tuning as well as the physical model parameter identification can be executed simultaneously.

For an inertia ratio of 1:1, the estimated parameters converge to the true physical parameters after 40 iterations. The initial and converged values are compared to the true open-loop

Table 3.2: Physical parameters estimated by feedforward identification (Inertia Ratio 1:3).

Parameters	Initial	Converged	Open Loop
K_P	0.02	0.15764	–
K_I	0.002	0.00272	–
$\hat{J}_1$ (kg-m^2)	5.00×10^{-3}	2.43×10^{-3}	$2.43 \pm 0.00 \times 10^{-3}$
$\hat{C}_1$ (N-m/rad/s)	4.00×10^{-3}	1.25×10^{-3}	$1.26 \pm 0.27 \times 10^{-3}$
$\hat{J}_2$ (kg-m^2)	1.60×10^{-2}	7.46×10^{-3}	$7.44 \pm 0.09 \times 10^{-3}$
$\hat{C}_2$ (N-m/rad/s)	3.00×10^{-3}	1.05×10^{-3}	$1.14 \pm 0.29 \times 10^{-3}$
$\hat{K}_1$ (rad/N-m)	1.00×10^{0}	8.08×10^{-1}	$8.07 \pm 0.09 \times 10^{-1}$

identified system in Table 3.1, and Figures 3.9 and 3.10. The converged controller parameters are shown in Figures 3.11 and 3.12. It is evident from the performance index J in Figure 3.13 that the iterative tuning algorithm is successful in minimizing tracking error. To analyze this, Figure 3.14 shows the output velocity and tracking error of the initial controller. It is clear that the tracking performance is unacceptable. This is compared to Figure 3.15, which corresponds to the output velocity and tracking of the final controller obtained by the proposed iterative tuning algorithm. The performance has been significantly improved. It is also noted that the proposed algorithm requires 40 experimental trials over 40 iterations. In conventional IFT, three experiments are required per iteration. The first two experiments are necessary for gradient estimation, while the last experiment determines the output error. Therefore, the conventional IFT approach would have required 120 experimental trials over 40 iterations.

The validity of the proposed algorithm is further demonstrated by the second configuration with inertia ratio 1:3. This exemplifies sudden variations in inertial coefficients. For this case, the estimated parameters converge to the true physical parameters after 70 iterations. The initial and converged values are compared to the true open-loop identified system in Table 3.2, and Figures 3.16 and 3.17. The converged controller parameters are shown in Figures 3.18 and 3.19. It is evident from the performance index J in Figure 3.20 that the iterative tuning algorithm is successful in minimizing tracking error. To analyze this, Figure 3.21 shows the output velocity and tracking error of the initial controller. It is clear that the tracking performance is unacceptable. This is compared to Figure 3.22, which corresponds to the output

velocity and tracking of the final controller obtained by the proposed iterative tuning algorithm. The performance has been significantly improved.

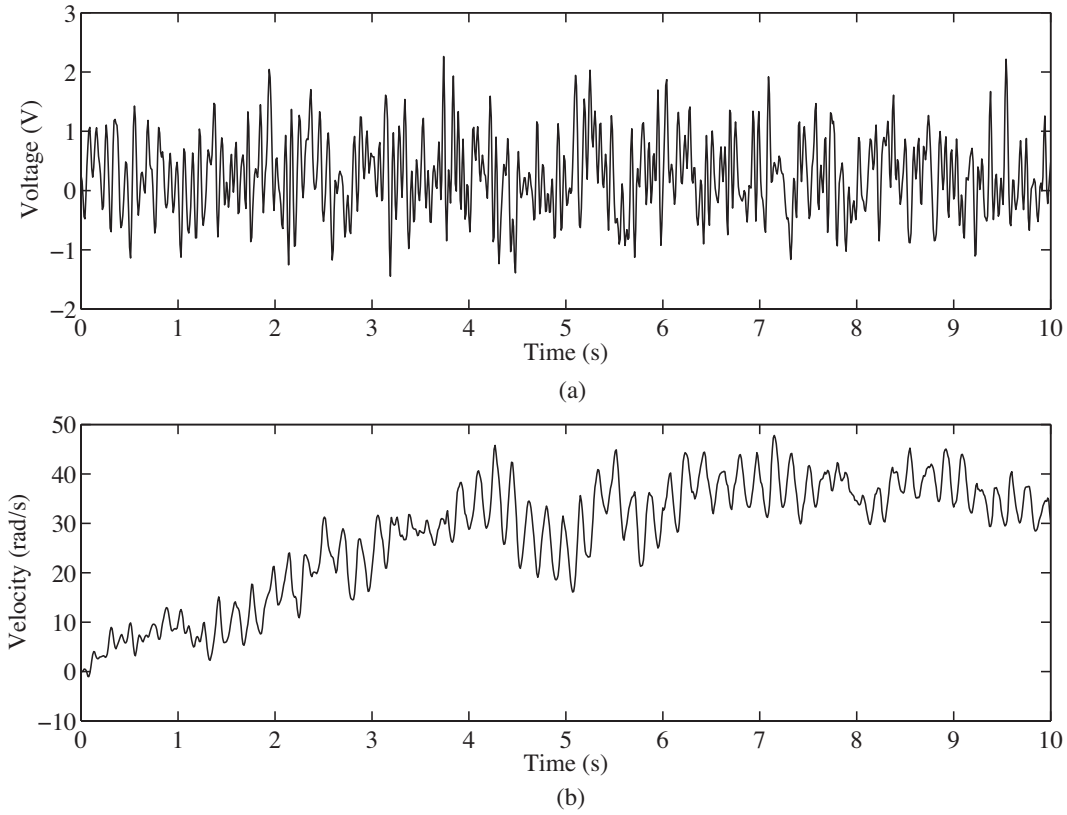

Figure 3.7: Input voltage and measured output velocity for open-loop identification.

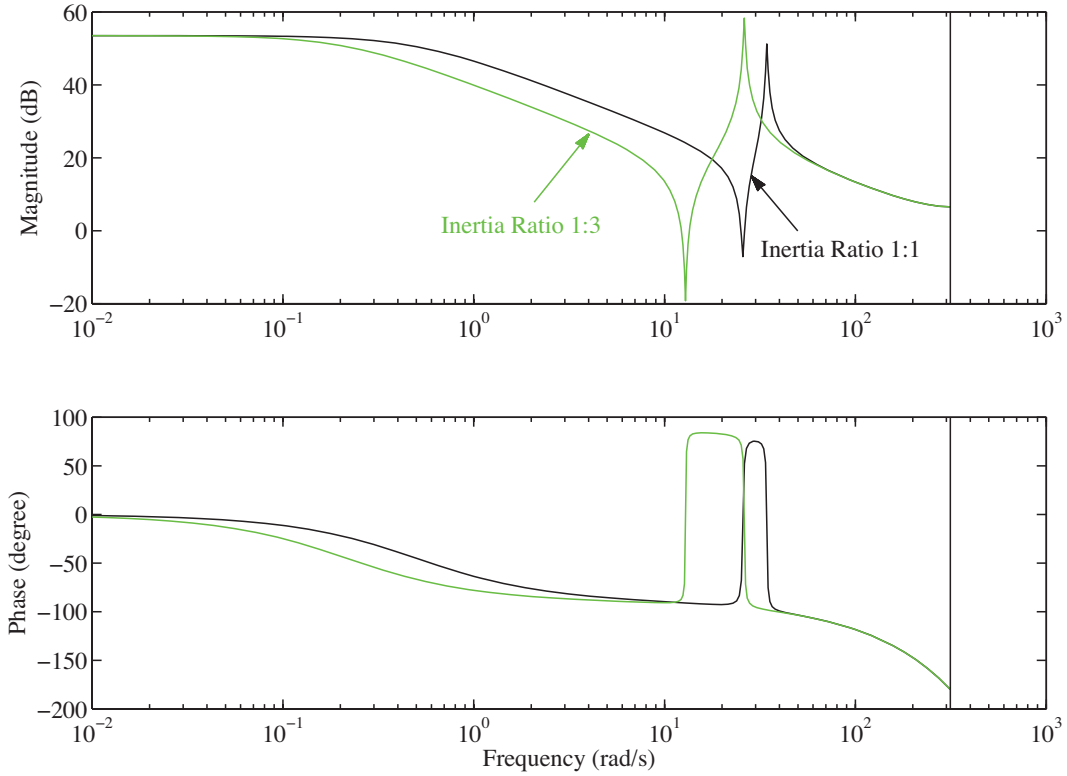

Figure 3.8: Nominal plant determined from open-loop identification for inertia ratio 1:1 and 1:3.

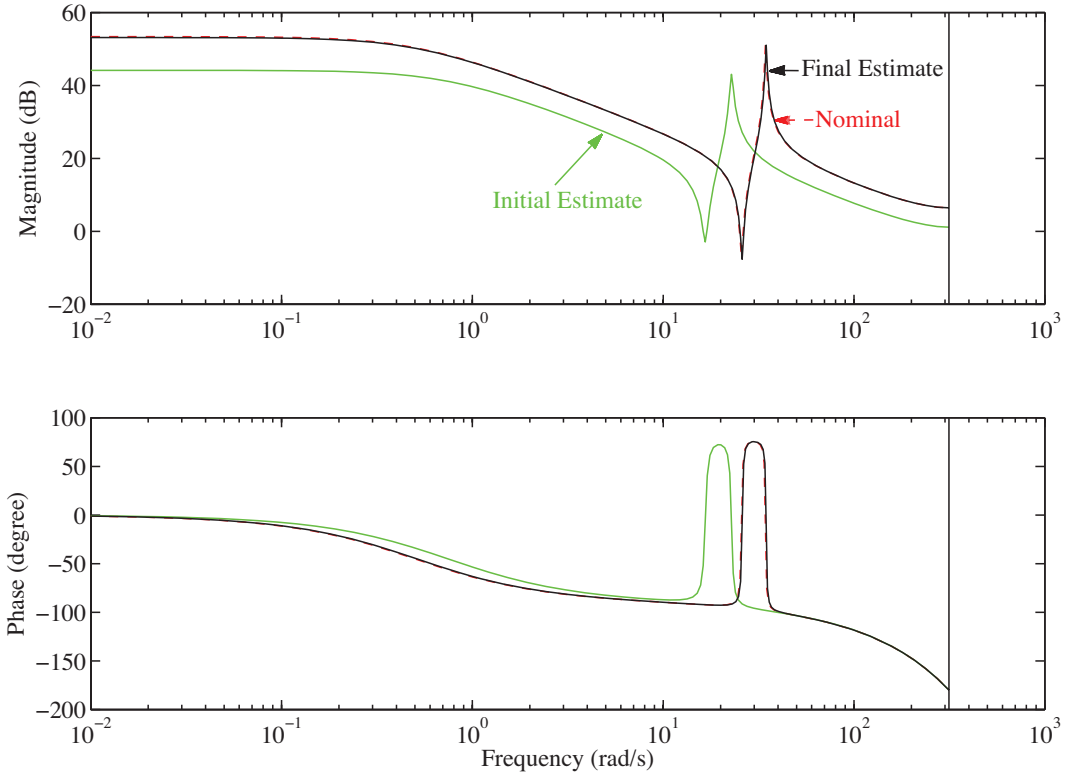

Figure 3.9: Bode diagram comparison of results for inertia ratio 1:1.

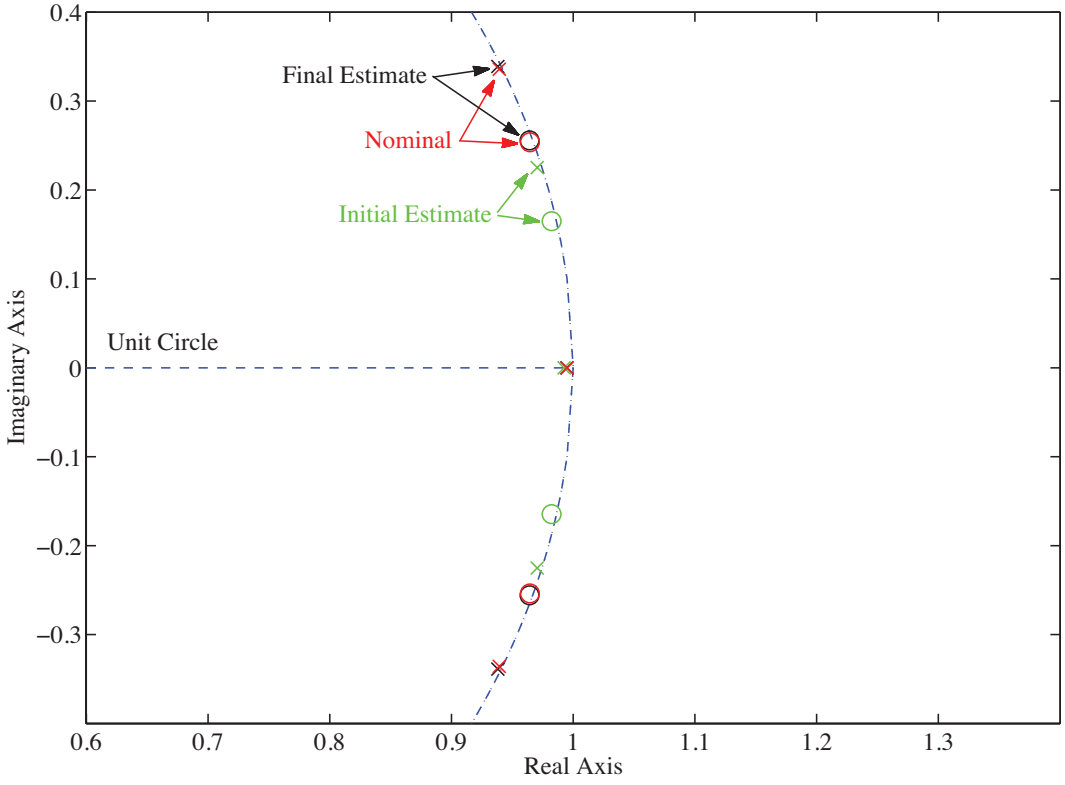

Figure 3.10: Discrete-time pole-zero plot of results for inertia ratio 1:1.

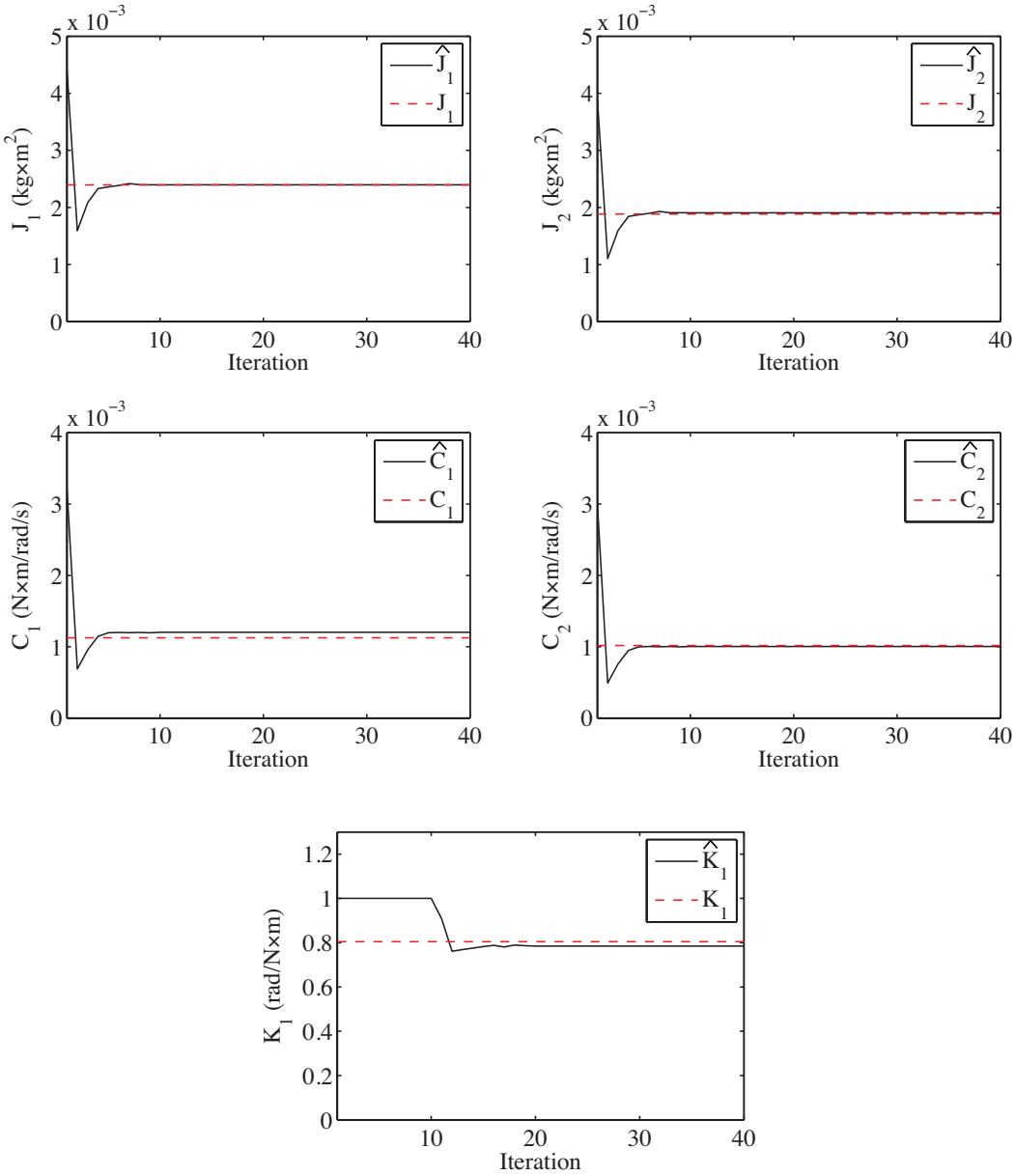

Figure 3.11: Convergence of physical parameter estimates for inertia ratio 1:1.

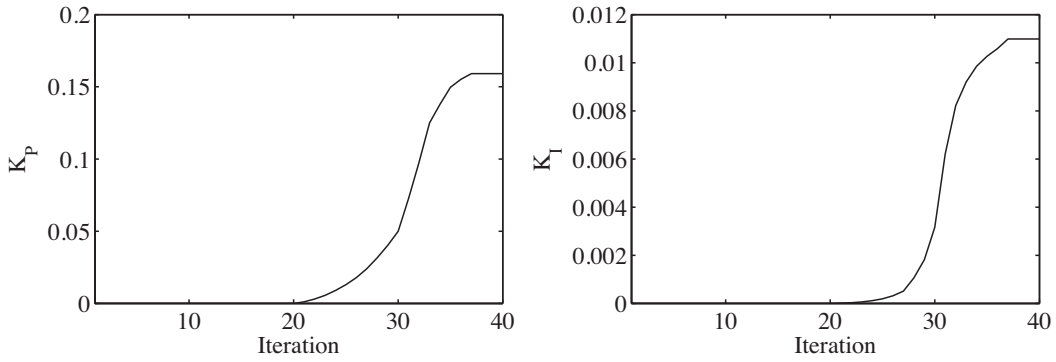

Figure 3.12: Convergence of PI gains for inertia ratio 1:1.

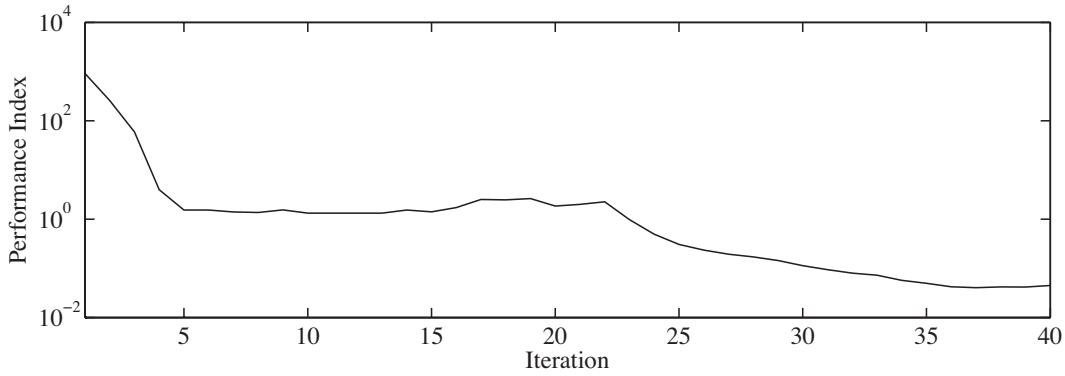

Figure 3.13: Performance index J for inertia ratio 1:1.

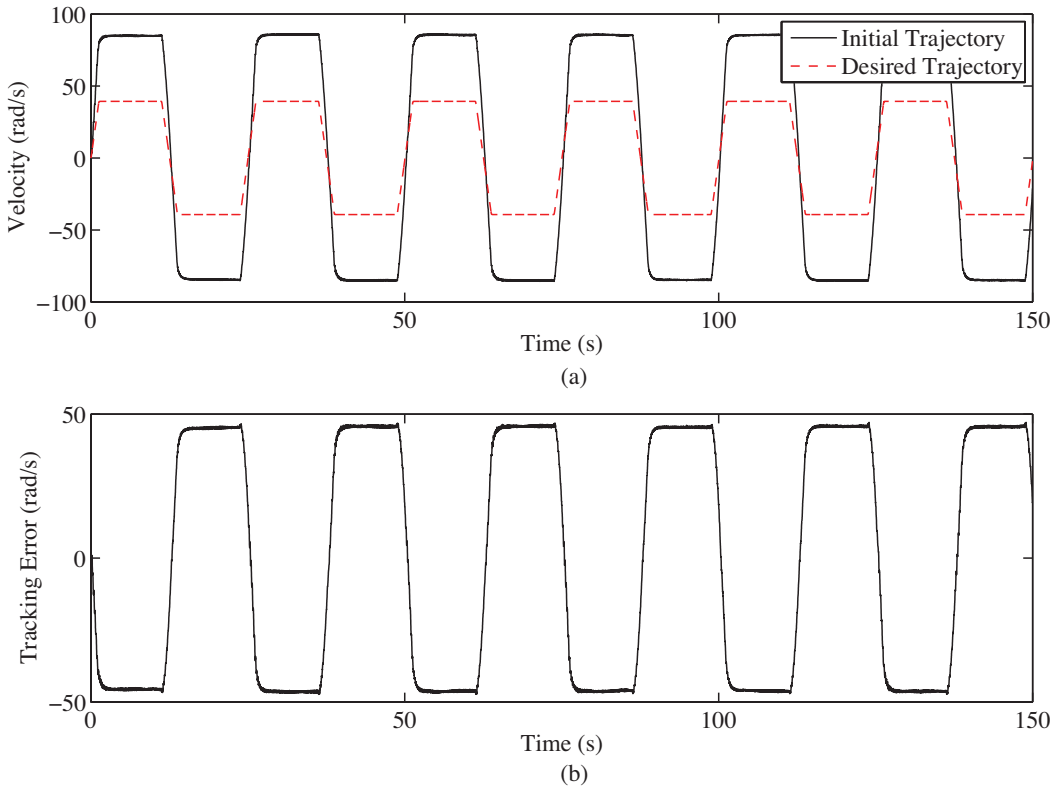

Figure 3.14: Velocity output and tracking error of initial iteration for inertia ratio 1:1.

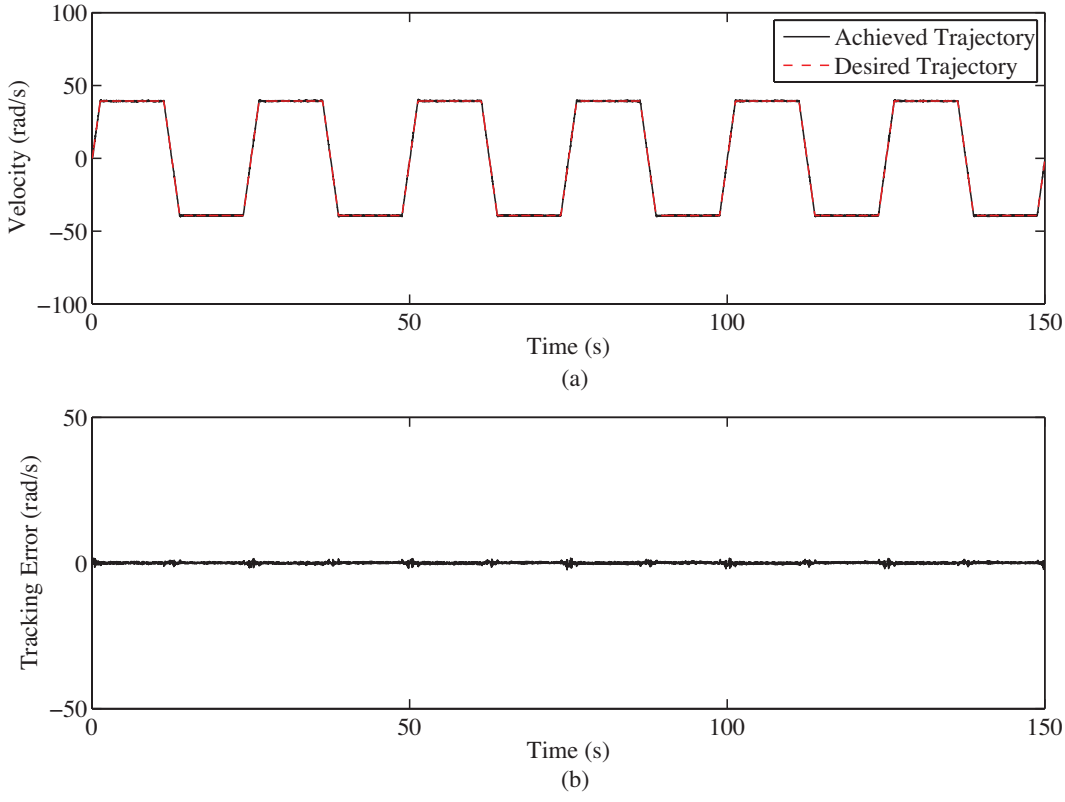

Figure 3.15: Velocity output and input after 40 iterations for inertia ratio 1:1.

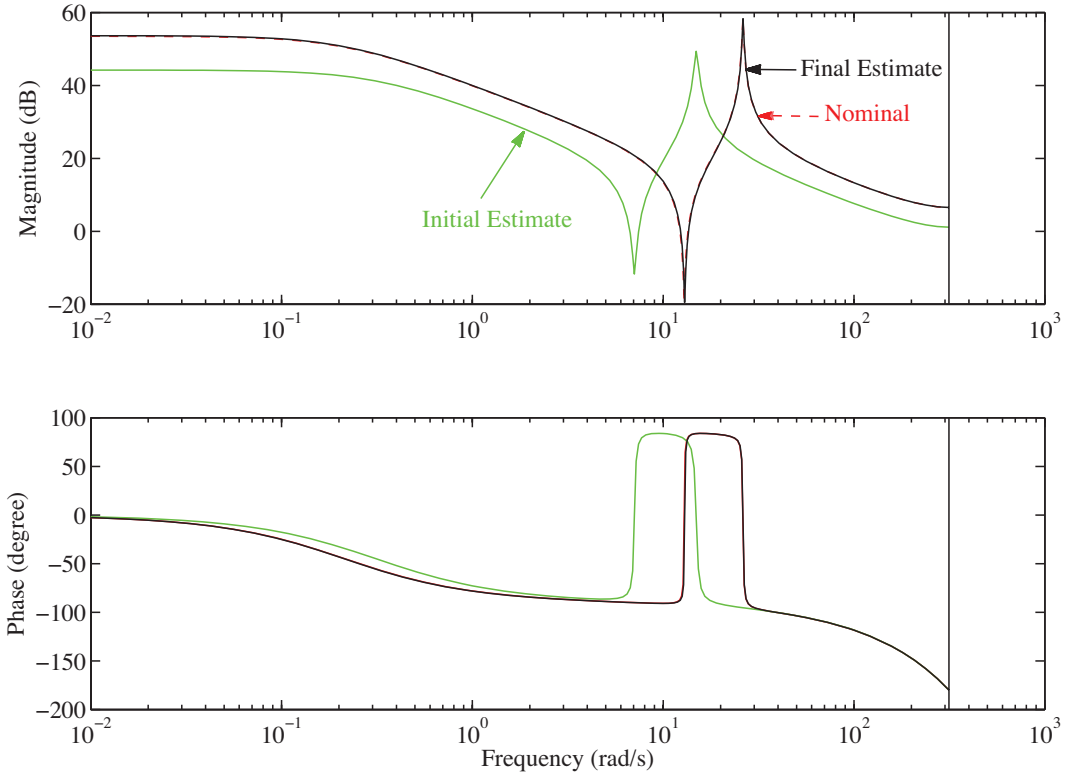

Figure 3.16: Bode diagram comparison of results for inertia ratio 1:3.

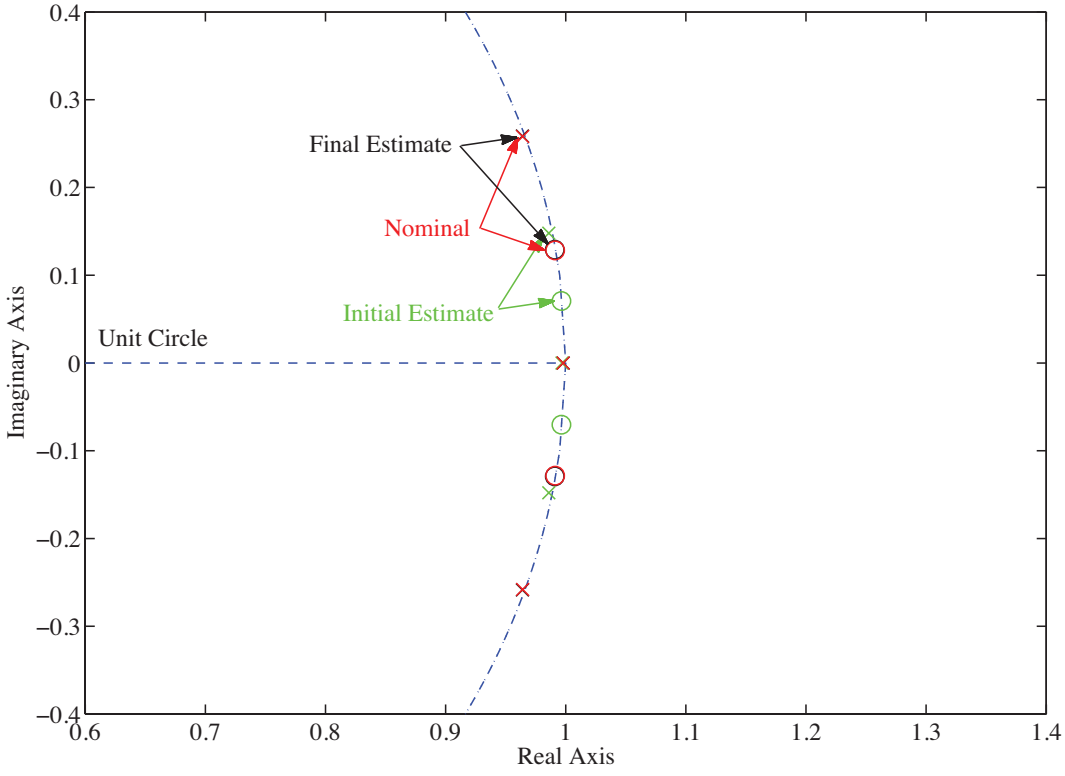

Figure 3.17: Discrete-time pole-zero plot of results for inertia ratio 1:3.

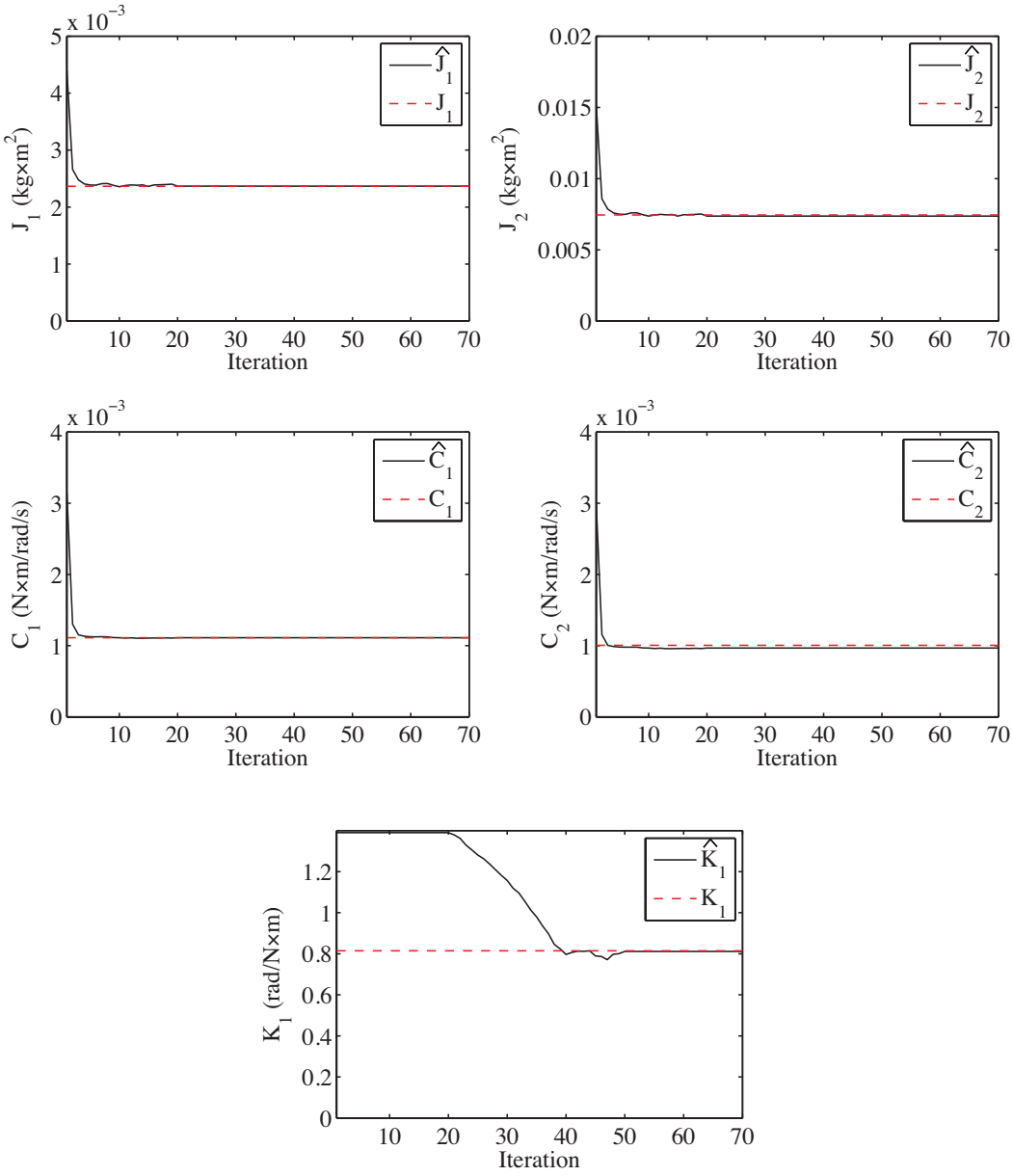

Figure 3.18: Convergence of physical parameter estimates for inertia ratio 1:3.

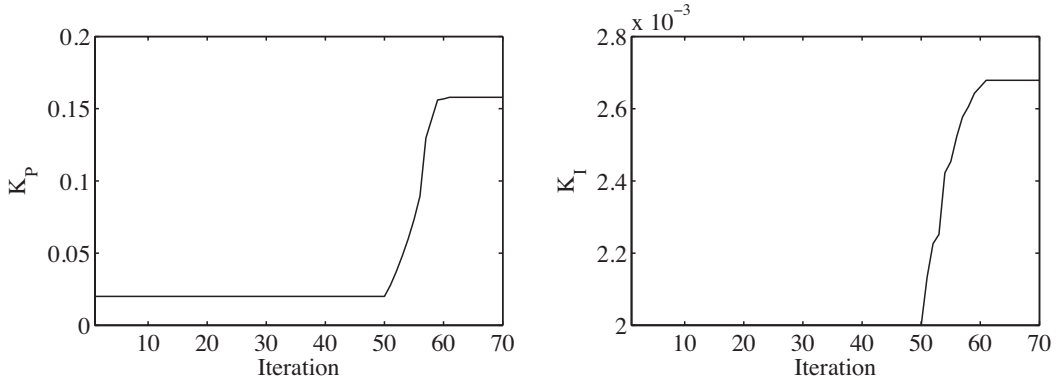

Figure 3.19: Convergence of PI gains for inertia ratio 1:3.

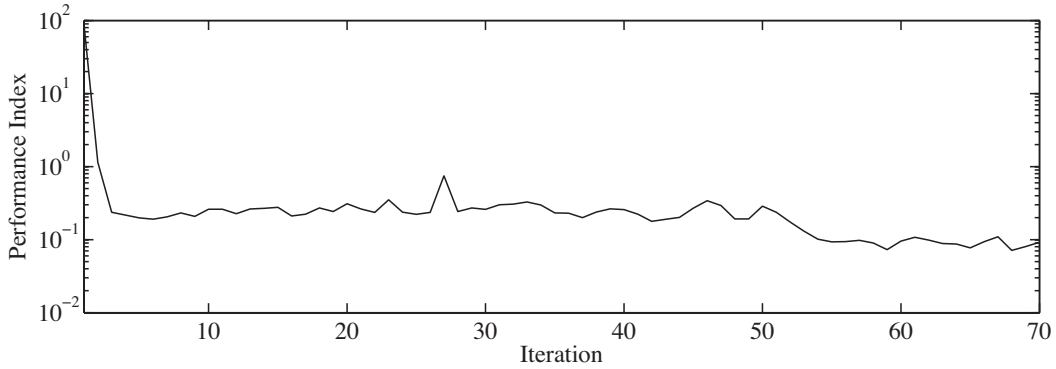

Figure 3.20: Performance index J for inertia ratio 1:3.

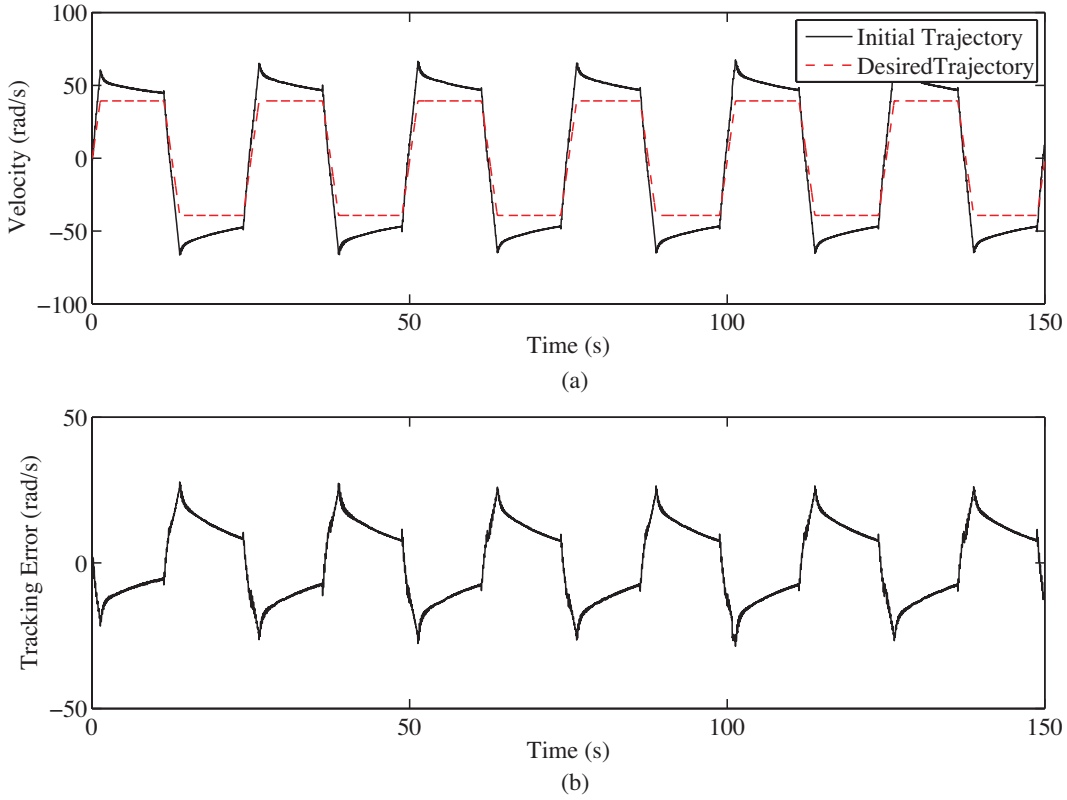

Figure 3.21: Velocity output and tracking error of initial iteration for inertia ratio 1:3.

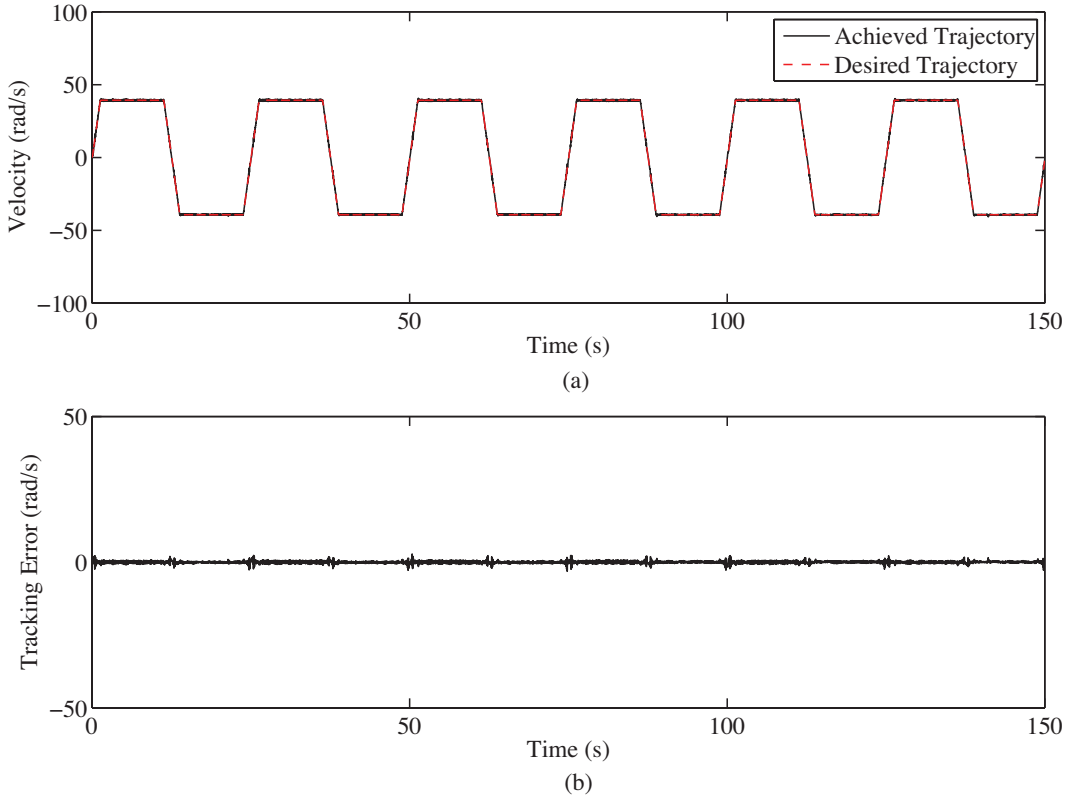

Figure 3.22: Velocity output and input after 70 iterations for inertia ratio 1:3.

3.6 Summary

A new iterative tuning algorithm has been proposed based on the CGT theory, allowing for the simultaneous achievement of trajectory tracking and identification of all physical paramters in a two-mass motor system. The resulting tuning procedure is simple and self-sufficient, requiring no prior knowledge about the system or extra gradient experiments needed by conventional IFT. The merits of the proposed iterative tuning algorithm are summarized as:

- By including the physical model parameters in the tuning parameters, the tracking performance and the physical model identification can be attained simultaneously. This eliminates the need to perform separate system identification experiments prior to controller tuning by IFT.
- The additional experiments required by conventional IFT for gradient estimation of an unknown system are no longer necessary. The number of experiments per iteration is greatly reduced.
- The two-mass model parameters can be estimated accurately by using the established relationship between the feedforward controller parameters and the physical model parameters as the output error is minimized.

Experimentation results show the effectiveness of the algorithm in achieving both high performance tracking characteristics and estimating all plant parameters.

Chapter 4

Adaptive Damper Control of Suspension System

This chapter is concerned with the development of an adaptive semi-active control scheme for suspension systems installed with magnetorheological (MR) dampers that involve parametric uncertainties. It considers two separate cases: when the MR damper is unknown but other suspension parameters are available; and when both the MR damper and suspension parameters are unknown or time varying. The proposed approach consists of two control algorithms. The first is an adaptive inverse control for compensating the nonlinear hysteresis dynamics of the MR damper, which can be realized by identifying a forward model of MR damper and then calculating the input voltage to generate a reference damping force. It can also be realized directly by updating an inverse model of MR damper without identification of the forward model, which then works as an adaptive inverse controller. The other is a robust linear quadratic (LQ) controller or an adaptive reference feedback controller which gives the desired damping force to match the seat dynamics to a specified reference dynamics even in the presence of uncertainties in the suspension structure. The stability of the total system is discussed and its stability condition is explored. Validity of the proposed algorithm is also examined by experimentation and simulation studies.

4.1 Introduction

Magnetorheological (MR) damper is a promising semi-active device in areas of vibration isolation for suspension systems and civil structures. The viscosity of MR fluid is controllable depending on input voltage or current. It inherently has hysteresis characteristics in nonlinear friction mechanism, and many efforts have been devoted to the modeling of nonlinear behavior from static and dynamic points of view [49, 58]. Static or quasi-static models include no dynamics but can express a nonlinear mapping from velocity to damping force [13,40,58]. It is not easy to identify the hysteresis curve by using a small number of model parameters from actual road suface excitation data. To model the hysteresis dynamics explicitly, the Bouc-Wen model and its variations have also been investigated, in which the input-output relation is expressed by a set of nonlinear differential equations [49, 58]. Hammerstein class of nonlinear model was also investigated [48]. These models can simulate the nonlinear behavior of the MR damper, however it includes too many nonlinear model parameters to be identified in a real-time manner. Alternative modeling is based on the LuGre friction model [41] which was originally developed to describe nonlinear friction phenomena [11]. It has a rather simple structure and the number of model parameters can also be reduced. However, it is not adequate for real-time design of an inverse controller. Thus, an MR damper model based on the LuGre model and an analytical method for adaptive inverse controller design has been explored [42, 54].

It is desired that the input to MR damper be determined so that the specified damping force is produced to attenuate vibrations of the suspension system. The necessary damping force can be calculated to minimize the linear quadratic (LQ) or linear quadratic gaussian (LQG) performance when the linear dynamic equation is given for the controlled structure. A clipped-optimal control algorithm has also been applied [15], in which a linear optimal controller is combined with a force feedback loop designed to adjust the input voltage. Its modification was also considered in [28, 59]. These approaches did not use any inversion dynamics of MR damper. By regarding the total system including the MR damper and structure as a nonlinear controlled system, nonlinear control design methods can also be applied, such as neuro-control approach [12], sliding mode control [28], adaptive skyhook control [60], gain scheduled control [38], bilinear H_∞ control [46] and others.

The purpose of this research is to provide a new fully adaptive control approach which can deal with uncertainties in both models of MR damper and suspension mechanism. The

proposed approach consists of two adaptive controllers. The first is an adaptive inverse control for compensating the nonlinear hysteresis dynamics of the MR damper, which can be realized by identifying a forward model of the MR damper and then calculating the input voltage to MR damper to generate a reference damping force. It can also be realized by directly updating the inverse model of MR damper without identification of the forward model, which works as an adaptive inverse controller. The other is an adaptive reference control based on an adaptive skyhook approach [60], which gives the desired damping force to match the seat dynamics to a specified reference dynamics even in the presence of uncertainties in the suspension structure. Another purpose of this chapter is to clarify stability condition for the total system consisting of the two adaptation algorithms. Validity of the proposed algorithm is also examined in simulation studies.

4.2 Suspension System

Figure 4.1 illustrates a simple suspension system installed with the MR damper between the car chassis and the wheel assembly. The dynamic equation of this system is expressed by:

$$M_s\ddot{x}_s + C_s(\dot{x}_s - \dot{x}_u) + K_s(x_s - x_u) = -F_{MR}(\dot{x}, v) \tag{4.1}$$

$$M_u\ddot{x}_u + C_s(\dot{x}_u - \dot{x}_s) + K_s(x_u - x_s) + K_t(x_u - x_r) = F_{MR}(\dot{x}, v) \tag{4.2}$$

$$x = x_s - x_u \tag{4.3}$$

where x is the relative displacement between the car chassis and the wheel assembly; M_s is the sprung mass, which represents the car chassis; M_u is the unsprung mass, which represents the wheel assembly; C_s and K_s are damping and stiffness of the uncontrolled suspension system, respectively; K_t serves to model the compressibility of the pneumatic tyre. x_s and x_u are the displacements of the sprung and unsprung mass, respectively; x_r is the road displacement input; $F_{MR}(\dot{x}, v)$ is the damping force supplied by the MR damper, subjected to an applied voltage v. This can be represented in the state-space form as:

$$\dot{\boldsymbol{x}}_p = \boldsymbol{A}\boldsymbol{x}_p + \boldsymbol{b}F_{MR} + \boldsymbol{e}\dot{x}_r \tag{4.4}$$

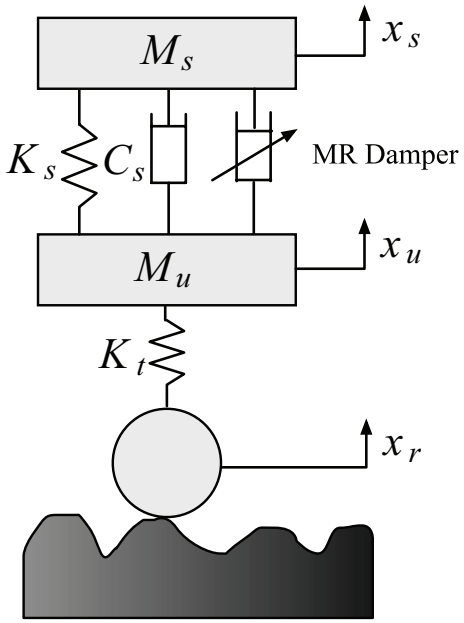

Figure 4.1: Suspension system with MR damper.

where:

$$\boldsymbol{x}_p = \begin{bmatrix} x_s - x_u & x_u - x_r & \dot{x}_s & \dot{x}_u \end{bmatrix}^T$$

$$\boldsymbol{A} = \begin{bmatrix} 0 & 0 & 1 & -1 \\ 0 & 0 & 0 & 1 \\ -K_s/M_s & 0 & -C_s/M_s & C_s/M_s \\ K_s/M_u & -K_t/M_u & C_s/M_u & -C_s/M_u \end{bmatrix}$$

$$\boldsymbol{b} = \begin{bmatrix} 0 & 0 & -1/M_s & 1/M_u \end{bmatrix}^T$$

$$\boldsymbol{e} = \begin{bmatrix} 0 & -1 & 0 & 0 \end{bmatrix}^T$$

4.3 Magnetorheological Damper

MR damper is a semi-active device in which the viscosity of the fluid is controllable by the input voltage or current. A variety of approaches have been taken to model the nonlinear

hysteresis behavior of the MR damper. Compared to the Bouc-Wen model [49, 58], the LuGre model has a simpler structure and smaller number of parameters is needed for expression of its behavior [41]. The LuGre model may also be modified so that a necessary input voltage can be analytically calculated to produce the specified command damping force F_A [42].

The damping force F_{MR} is expressed by:

$$F_{MR} = \sigma_a z + \sigma_0 z v + \sigma_1 \dot{z} + \sigma_2 \dot{x} + \sigma_b \dot{x} v, \tag{4.5}$$

$$\dot{z} = \dot{x} - a_0 |\dot{x}| z \tag{4.6}$$

where z [m] is an internal state variable [m], x is the relative displacement between the car chassis and the wheel assembly, σ_0 [N/(m·V)] is the stiffness of z influenced by the applied voltage, v [V], σ_1 [N·s/m] is the damping coefficient of z, σ_2 [N·s/m] is the viscous damping coefficient, σ_a [N/m] is the stiffness of z, σ_b [N·s/(m·V)] is the viscous damping coefficient influenced by v, and a_0 [V/N] is a constant value. The model was validated by experimental data and the results are presented in the appendix of this chapter [54].

Substituting (4.6) into (4.5) gives the input-output relation as:

$$\begin{aligned} F_{MR} &= \sigma_a z + \sigma_0 z v - \sigma_1 a_0 |\dot{x}| z + (\sigma_1 + \sigma_2)\, \dot{x} + \sigma_b \dot{x} v \\ &= \boldsymbol{\theta}_f^T \boldsymbol{\varphi}_f + \boldsymbol{\theta}_g^T \boldsymbol{\varphi}_g v \end{aligned} \tag{4.7}$$

where:

$$\boldsymbol{\theta}_f = \begin{bmatrix} \sigma_a & \sigma_1 a_0 & \sigma_1 + \sigma_2 \end{bmatrix}^T \tag{4.8}$$

$$\boldsymbol{\varphi}_f = \begin{bmatrix} z & -|\dot{x}| z & \dot{x} \end{bmatrix}^T \tag{4.9}$$

$$\boldsymbol{\theta}_g = \begin{bmatrix} \sigma_0 & \sigma_b \end{bmatrix}^T \tag{4.10}$$

$$\boldsymbol{\varphi}_g = \begin{bmatrix} z & \dot{x} \end{bmatrix}^T \tag{4.11}$$

4.4 LQ-Based Adaptive Semi-Active Control Algorithm

This section considers the adaptive semi-active damper control problem when the parameters of the MR damper is not available, but the suspension is assumed to be known *a priori*. Figures 4.2 and 4.3 show schematic diagrams of the proposed adaptive semi-active control for the suspension system. The adaptive algorithm consists of two controllers: the first is a robust

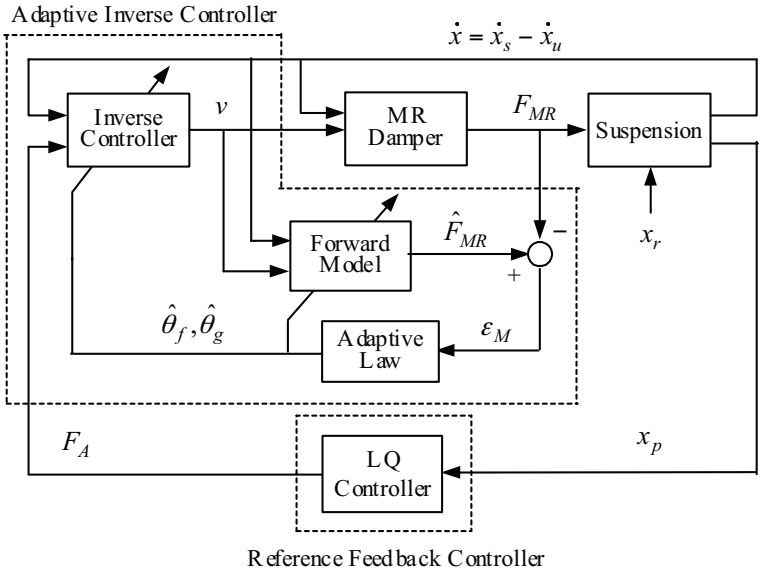

Figure 4.2: Proposed adaptive semi-active control scheme based on *forward* modeling.

LQ controller with full-state feedback that generates a command damping force F_A, when the parameters of the suspension system are known; the second is an adaptive inverse controller which can give required input voltage v to MR damper so that the damping force F_{MR} is equal to F_A. If the adaptive inverse controller is designed so that the linearization from F_A to F_{MR} can be attained, that is, $F_A = F_{MR}$, almost active control performance is achieved. For construction of the inverse controller, the forward model of MR damper is identified and then the input voltage to MR damper is calculated as shown in Figure 4.2. Figure 4.3 gives an alternative scheme in which the inverse controller is directly updated without identification of MR damper.

4.4.1 Robust LQ Control with Dissipativity

This section uses robust LQ control to design the active damping force F_A. The semi-active constraint of the MR damper signifies that $F_{MR} \neq F_A$ and therefore it is necessary to define the following disturbance term:

$$\delta_{MR} = F_{MR} - F_A \tag{4.12}$$

which is assumed to be bounded by:

$$\|\delta_{MR}\|_2 \leq \Delta_{MR} \tag{4.13}$$

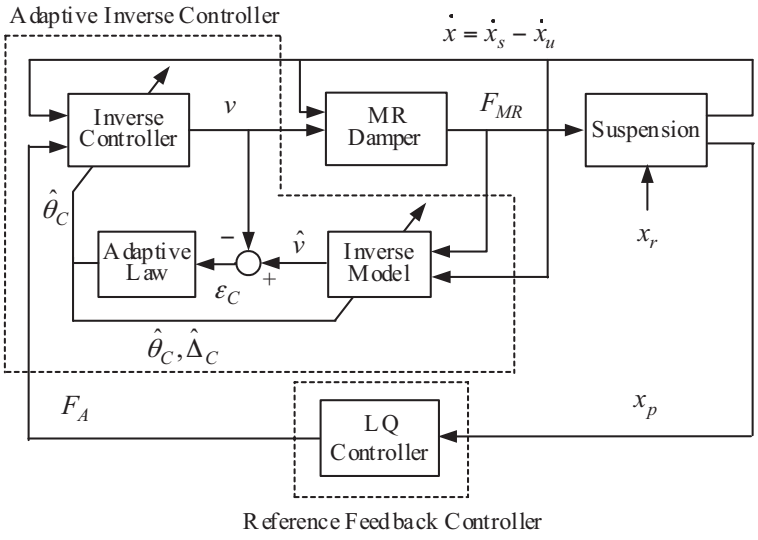

Figure 4.3: Proposed adaptive semi-active control scheme based on *inverse* modeling.

Restating (4.4) in terms of F_A and δ_{MR}:

$$\dot{\boldsymbol{x}}_p = \boldsymbol{A}\boldsymbol{x}_p + \boldsymbol{b}F_A + \boldsymbol{b}\delta_{MR} + \boldsymbol{e}\dot{x}_r \tag{4.14}$$

The robust control objective becomes:

$$J_\infty = \sup_{\delta_{MR} \in L_2} \frac{\|z\|_2}{\|\delta_{MR}\|_2} < \gamma \tag{4.15}$$

where:

$$z = \begin{bmatrix} \left(\boldsymbol{Q} - r^{-1}\boldsymbol{s}\boldsymbol{s}^T\right)^{\frac{1}{2}} & \boldsymbol{0} \\ r^{-\frac{1}{2}}\boldsymbol{s}^T & r^{\frac{1}{2}} \end{bmatrix} \begin{bmatrix} \boldsymbol{x}_p \\ F_A \end{bmatrix} \tag{4.16}$$

Here, $\boldsymbol{Q} = q\boldsymbol{I}$ and $\boldsymbol{s} = \begin{bmatrix} \boldsymbol{0}^T & s_1 & s_2 \end{bmatrix}^T$, while $q > 0$ and $r > 0$. Therefore:

$$\begin{aligned} \|z\|_2 &= \int_0^\infty \begin{bmatrix} \boldsymbol{x}_p^T & F_A \end{bmatrix} \begin{bmatrix} \boldsymbol{Q} & \boldsymbol{s} \\ \boldsymbol{s}^T & r \end{bmatrix} \begin{bmatrix} \boldsymbol{x}_p \\ F_A \end{bmatrix} dt \\ &= \int_0^\infty \left(\boldsymbol{x}_p^T \boldsymbol{Q}\boldsymbol{x}_p + 2\boldsymbol{x}_p^T \boldsymbol{s} F_A + r F_A^2\right) dt \end{aligned} \tag{4.17}$$

Assuming that the road perturbation $\dot{x}_r$ is a random signal with zero mean, the active control force considering the disspativity is given by:

$$F_A = -\boldsymbol{k}^T \boldsymbol{x}_p \tag{4.18}$$

$$\boldsymbol{k} = \frac{\boldsymbol{P}\boldsymbol{b} + \boldsymbol{s}}{r} \tag{4.19}$$

and $\boldsymbol{P}$ is the solution of the corresponding Riccati equation:

$$\boldsymbol{Q} + \boldsymbol{P}\boldsymbol{A} + \boldsymbol{A}^T\boldsymbol{P} - \boldsymbol{P}\boldsymbol{b}\left(1 - \gamma^{-2}\right)\boldsymbol{b}^T\boldsymbol{P} = \boldsymbol{0} \tag{4.20}$$

If all of the states are not available, an observer can be designed from the sensor data, for instance $x_s - x_u$ and $\ddot{x}_s$, and an output controller is implemented.

4.4.2 Adaptive Inverse Damper Control

Adaptive Inverse Damper Control via Forward Modeling

Since the internal state z of the MR damper model cannot be measured, the regressor vectors should be replaced with their estimates as:

$$\hat{\boldsymbol{\varphi}}_f = \begin{bmatrix} \hat{z} & -|\dot{x}|\hat{z} & \dot{x} \end{bmatrix}^T \tag{4.21}$$

$$\hat{\boldsymbol{\varphi}}_g = \begin{bmatrix} \hat{z} & \dot{x} \end{bmatrix}^T \tag{4.22}$$

where the estimate $\hat{z}$ is given later by using the updated model parameters.

The output of the identification model is now described as:

$$\hat{F}_{MR} = \hat{\boldsymbol{\theta}}_f^T\hat{\boldsymbol{\varphi}}_f + \hat{\boldsymbol{\theta}}_g^T\hat{\boldsymbol{\varphi}}_g v \tag{4.23}$$

where $\hat{\boldsymbol{\theta}}_f$ and $\hat{\boldsymbol{\theta}}_g$ are the parameter estimates. By using the damping force estimation error defined by $\varepsilon_M = \hat{F}_{MR} - F_{MR}$, and the identified parameter $\hat{a}_0$, the estimate $\hat{z}$ of the internal state can be calculated as:

$$\dot{\hat{z}} = \dot{x} - \hat{a}_0|\dot{x}|\hat{z} - l\varepsilon_M, \tag{4.24}$$

where l is an observer gain such that $0 \leq l \leq 1/\hat{\sigma}_{1\max}$, and the upper bound is decided by the stability of the adaptive observer [54]. The adaptive laws for updating the model parameters are given as:

$$\dot{\hat{\boldsymbol{\theta}}}_f = -\boldsymbol{\Gamma}_f\hat{\boldsymbol{\varphi}}_f\varepsilon_M - \sigma_f\boldsymbol{\Gamma}_f\hat{\boldsymbol{\theta}}_f \tag{4.25}$$

$$\dot{\hat{\boldsymbol{\theta}}}_g = -\boldsymbol{\Gamma}_g\hat{\boldsymbol{\varphi}}_g v\varepsilon_M - \sigma_g\boldsymbol{\Gamma}_g\hat{\boldsymbol{\theta}}_g \tag{4.26}$$

where $\boldsymbol{\Gamma}_f$ and $\boldsymbol{\Gamma}_g$ are positive definite matrices, σ_f and σ_g are positive design constants. Though $\boldsymbol{\Gamma}_f$ and $\boldsymbol{\Gamma}_g$ may vary with time, it is defined by this research as constant for practical implementation.

The role of the adaptive inverse controller shown in Figure 4.2 is to decide the control input voltage v to the MR damper so that the actual damping force F_{MR} approaches the specified command damping force F_A, even in the presence of uncertainty in the MR damper model. The input voltage giving F_A can be analytically calculated from the identified forward model of MR damper. Actually using the identified model parameters, the input voltage v is obtained from (4.7) as:

$$\rho = \hat{\boldsymbol{\theta}}_g^T \hat{\boldsymbol{\varphi}}_g \tag{4.27}$$

$$d_\rho = \begin{cases} \rho & \text{for} \quad \rho < -\delta, \quad \delta < \rho \\ \delta \, \text{sgn}(\rho) & \text{for} \quad -\delta \leq \rho \leq \delta \end{cases} \tag{4.28}$$

$$v_A = \frac{F_A - \hat{\boldsymbol{\theta}}_f^T \hat{\boldsymbol{\varphi}}_f - l\varepsilon_M}{d_\rho} \tag{4.29}$$

$$v = sat(v_A), \quad 0 \leq v \leq V_{\max} \tag{4.30}$$

where F_A is the optimal control force as determined by the robust LQ controller. v_A is assumed to be fixed near $\rho = 0$ to avoid division by zero. Due to these saturation effects, the semi-active force F_{MR} may not fully match the active optimal control force F_A. Stability analysis results are similar to the case of adaptive control via inverse modeling, which is presented in the following section.

Adaptive Inverse Damper Control via Inverse Modeling

In the previous section, the inverse controller is obtained analytically from the estimated parameters of the forward model of MR damper. However, as expressed in (4.29), some adjustable parameters appear in the denominator of the inverse controller and so zero-division should be avoided. Therefore, linearly parameterized *inverse* model is considered, as shown in Figure 4.3. Since the damper force F_{MR} is given as a function of the velocity $\dot{x}$, input voltage v and internal state z as shown in (4.7), its inverse model for the input voltage v can be expressed as a function of $\dot{x}$, z and F_{MR}. Hence, an inverse model which is expressed by a linearly parameterized polynomial function is considered as:

$$v = \sum_{j=0}^{n} \sum_{i=0}^{m} h_{i+(m+1)k+1} \left|\dot{x}\right|^i \left|z\right|^j F_{MR} \text{sgn}(\dot{x}) + \delta_C \tag{4.31}$$

where the inverse model has three inputs of $\dot{x}$, z and F_{MR}, and one output of v. z is an internal state of the MR damper, which can be calculated as given previously by:

$$\dot{z} = \dot{x} - a_0|\dot{x}|z \tag{4.32}$$

where a nominal value of a_0 is assumed to be known via the forward modeling. δ_C represents the unknown approximation error, which is assumed to be bounded:

$$\sup|\delta_C| \leq \Delta_C \tag{4.33}$$

The unknown bound Δ_C can be made arbitrary small by increasing the order of polynomial approximation. In simulation, an inverse model with $m = 4$ and $n = 1$ is adopted.

The inverse model is also expressed in vector form as:

$$v = \boldsymbol{\theta}_C^T \boldsymbol{\varphi}_C + \delta_C \tag{4.34}$$

where:

$$\boldsymbol{\theta}_C = \begin{bmatrix} h_1 & h_2 & \dots & h_{(n+1)(m+1)} \end{bmatrix}^T \tag{4.35}$$

$$\boldsymbol{\varphi}_C = \begin{bmatrix} F_{MR}\text{sgn}(\dot{x}) & |\dot{x}|F_{MR}\text{sgn}(\dot{x}) & \dots & |z|F_{MR}\text{sgn}(\dot{x}) \\ & & & |\dot{x}||z|F_{MR}\text{sgn}(\dot{x}) & \dots & |\dot{x}|^m|z|^n F_{MR}\text{sgn}(\dot{x}) \end{bmatrix}^T \tag{4.36}$$

Then the identified model is expressed as:

$$\hat{v} = \hat{\boldsymbol{\theta}}_C^T \boldsymbol{\varphi}_C + \mu \tag{4.37}$$

where the identification error ε_C is defined as:

$$\varepsilon_C = \hat{v} - v \tag{4.38}$$

and μ is a robustifying term given as:

$$\mu = \hat{\Delta}_C \eta_C \tanh((a + bt)\varepsilon_C) \tag{4.39}$$

Here, $\eta_C > 1$ and $a, b > 0$. The adaptive parameters $\hat{\boldsymbol{\theta}}_C$ and $\hat{\Delta}_C$ are adjusted in an on-line manner so as to minimize the identification error according to the following adaptive laws:

$$\dot{\hat{\boldsymbol{\theta}}}_C = -\boldsymbol{\Gamma}_C \boldsymbol{\varphi}_C \varepsilon_C - \sigma_C \boldsymbol{\Gamma}_C \hat{\boldsymbol{\theta}}_C \tag{4.40}$$

$$\dot{\hat{\Delta}}_C = \gamma_{\Delta_C}|\varepsilon_C| - \sigma_{\Delta_C}\gamma_{\Delta_C}\hat{\Delta}_C \tag{4.41}$$

where $\mathbf{\Gamma}_C$ is a positive definite matrix, γ_{Δ_C}, σ_C and σ_{Δ_C} are positive design constants. For practical implementation, $\mathbf{\Gamma}_C$ is chosen constant.

Figure 4.3 describes the adaptive damper control via inverse modeling. The control input voltage v is given as:

$$v_A = \hat{\boldsymbol{\theta}}_C^T \boldsymbol{\varphi}_A \tag{4.42}$$

$$v = \begin{cases} 0 & \text{for } v_A \leq 0 \\ v_A & \text{for } 0 < v_A \leq V_{\max} \\ V_{\max} & \text{for } V_{\max} < v_A \end{cases} \tag{4.43}$$

where:

$$\boldsymbol{\varphi}_A = \Big[F_A \text{sgn}(\dot{x}) \quad |\dot{x}| F_A \text{sgn}(\dot{x}) \quad \dots \quad |z| F_A \text{sgn}(\dot{x}) \quad |\dot{x}||z| F_A \text{sgn}(\dot{x}) \quad \dots \quad |\dot{x}|^m |z|^n F_A \text{sgn}(\dot{x}) \Big]^T \tag{4.44}$$

Again due to the semi-active nature of the MR damper, F_{MR} may not fully match the active optimal control force F_A. The stability result of the total system given in Figure 4.3 is presented in the following theorem.

THEOREM 4.1 *Assume $\kappa > 0$ is satisfied, and a_0 is known. Then the control law (4.18), along with the adaptive laws (4.40) and (4.41) guarantee that all error signals remain bounded and converge to a small neighborhood of the origin.*

Proof: It is assumed that a_0 is known. From this assumption, the internal state is directly accessible, *i.e.*, $\hat{z} = z$. Define a candidate of the Lyapunov function as:

$$V = \frac{1}{2} \boldsymbol{x}_p^T P \boldsymbol{x}_p + \frac{1}{2} \tilde{\boldsymbol{\theta}}_C^T \mathbf{\Gamma}_C^{-1} \tilde{\boldsymbol{\theta}}_C + \frac{1}{2\gamma_{\Delta_C}} \tilde{\Delta}_C^2 \tag{4.45}$$

where $\tilde{\boldsymbol{\theta}}_C = \hat{\boldsymbol{\theta}}_C - \boldsymbol{\theta}_C$ and $\tilde{\Delta}_C = \hat{\Delta}_C - \Delta_C$. Taking the time-derivative of (4.45), using the control law as defined in (4.42), and applying the adaptive laws (4.40) and (4.41) gives:

$$\begin{aligned} \dot{V}_1 &= \frac{1}{2} \boldsymbol{x}_p^T \left(\boldsymbol{P}\boldsymbol{A} + \boldsymbol{A}^T \boldsymbol{P} - 2\boldsymbol{P}\boldsymbol{b}\boldsymbol{k}^T \right) \boldsymbol{x}_p \\ &\quad - \tilde{\boldsymbol{\theta}}_C^T \boldsymbol{\varphi}_C \varepsilon_C + \tilde{\Delta}_C |\varepsilon_C| - \sigma_C \tilde{\boldsymbol{\theta}}_C^T \hat{\boldsymbol{\theta}}_C - \sigma_{\Delta_C} \tilde{\Delta}_C \hat{\Delta}_C \\ &= -\frac{1}{2} \boldsymbol{x}_p^T \left(\boldsymbol{Q} - 2\boldsymbol{s}\boldsymbol{k}^T + r\boldsymbol{k}\boldsymbol{k}^T \right) \boldsymbol{x}_p \\ &\quad - \varepsilon_C^2 + \delta_C \varepsilon_C - \mu \varepsilon_C + \tilde{\Delta}_C |\varepsilon_C| - \sigma_C \tilde{\boldsymbol{\theta}}_C^T \hat{\boldsymbol{\theta}}_C - \sigma_{\Delta_C} \tilde{\Delta}_C \hat{\Delta}_C \end{aligned} \tag{4.46}$$

The following relationship will be employed:

$$-\sigma\tilde{\boldsymbol{\theta}}^T\hat{\boldsymbol{\theta}} \leq -\frac{\sigma}{2}\tilde{\boldsymbol{\theta}}^T\tilde{\boldsymbol{\theta}} + \frac{\sigma}{2}\boldsymbol{\theta}^T\boldsymbol{\theta} \tag{4.47}$$

along with (4.33) to obtain:

$$\begin{aligned}\dot{V}_1 \leq & -\frac{1}{2}\boldsymbol{x}_p^T\left(\boldsymbol{Q} - 2\boldsymbol{s}\boldsymbol{k}^T + r\boldsymbol{k}\boldsymbol{k}^T\right)\boldsymbol{x}_p \\ & +\hat{\Delta}_C\left(1 - \eta_C\tanh((a+bt)|\varepsilon_C|)\right)|\varepsilon_C| \\ & -\frac{\sigma_C}{2}\tilde{\boldsymbol{\theta}}_C^T\tilde{\boldsymbol{\theta}}_C - \frac{\sigma_{\Delta_C}}{2}\tilde{\Delta}_C^2 + \frac{\sigma_C}{2}\boldsymbol{\theta}_C^T\boldsymbol{\theta}_C + \frac{\sigma_{\Delta_C}}{2}\Delta_C^2\end{aligned} \tag{4.48}$$

Notice that the condition:

$$1 - \eta_C\tanh\left((a+bt)|\varepsilon_C|\right) \leq 0 \tag{4.49}$$

is satisfied when:

$$|\varepsilon_C| \geq \nu_C = \frac{1}{a+bt}\ln\left(\frac{\eta_C+1}{\eta_C-1}\right), \quad \eta_C > 1 \tag{4.50}$$

As $t \to \infty$ and $b > 0$, the region defined by ν_C goes to zero, and thus the condition (4.49) is satisfied as $t \to \infty$. It can be shown that there exists $\boldsymbol{M}$ such that:

$$\boldsymbol{Q} - 2\boldsymbol{s}\boldsymbol{k}^T + r\boldsymbol{k}\boldsymbol{k}^T = \boldsymbol{M}\boldsymbol{M}^T > 0 \tag{4.51}$$

Therefore:

$$\dot{V}_1 \leq -c_1V_1 + \lambda_1 \tag{4.52}$$

where:

$$\begin{aligned}c_1 &= \min\left\{\frac{\lambda_{\min}(\boldsymbol{M}\boldsymbol{M}^T)}{\lambda_{\max}(\boldsymbol{P})}, \frac{\sigma_c}{\lambda_{\max}(\boldsymbol{\Gamma}_C^{-1})}, \gamma_{\Delta_C}\sigma_{\Delta_C}\right\} \\ \lambda_1 &= \frac{\sigma_C}{2}\boldsymbol{\theta}_C^T\boldsymbol{\theta}_C + \frac{\sigma_{\Delta_C}}{2}\Delta_C^2\end{aligned} \tag{4.53}$$

As $\lambda_1/c_1 > 0$, (4.52) results in:

$$0 \leq V_1(t) \leq \lambda_1/c_1 + (V_1(0) - \lambda_1/c_1)e^{-c_1t} \tag{4.54}$$

Therefore all system states $\boldsymbol{x}_p$, error signals $\tilde{\boldsymbol{\theta}}_C$ and $\tilde{\Delta}_C$ are uniformly bounded and converge to a small neighborhood of the origin. □

4.5 Simulation Results

This section presents simulation results for the proposed control algorithm when the suspension system parameters are known. The control algorithm consists of a robust LQ controller, designed to minimize the seat acceleration and seat-tire displacement, and an adaptive inverse controller to achieve linearization of the MR damper. The adaptive inverse controller is designed using the forward modeling approach and the inverse modeling approach, as shown in Figures 4.2 and 4.3.

Consider a suspension system shown in Fig. 4.1, where the parameters are set as $M_s = 504.5$ [kg], $M_u = 62$ [kg], $C_s = 400$ [Ns/m], $K_s = 1.31 \times 10^4$ [N/m] and $K_t = 2.52 \times 10^5$ [N/m]. The parameters of the MR damper are specified as: $\sigma_0 = 4.0 \times 10^4$ [N/mV], $\sigma_1 = 2.0 \times 10^2$ [Ns/m], $\sigma_2 = 1.0 \times 10^2$ [Ns/m], $\sigma_a = 1.5 \times 10^4$ [N/m], $\sigma_b = 2.5 \times 10^3$ [Ns/(mV)], $a_0 = 1.9 \times 10^2$, which are all unknown. An upper limit of input voltage to the MR damper is set at 2.5[V], so v varies between 0 to 2.5[V]. The base of the dynamic system in Fig. 4.1 is excited by the road surface, which is given by a random signal sequence with a frequency range of 0-3.5 Hz. To analyze the effectiveness of each control schemes for various frequency ranges, the road excitation was designed so that the bandwidth increases every ten seconds from 1Hz, 1.5Hz, 2.5Hz to 3.5Hz. The initial period of ten seconds has a bandwidth of 3.5Hz to allow for parameter convergences of the adaptive schemes. The displacement and velocity profile of the road excitation is shown in Figure 4.4. The following schemes are compared: (1) Passive low damping with 0 [V] fixed, (2) Passive high damping with 2.5 [V] fixed, (3) Active LQ-based scheme, (4) Forward modeling based scheme (Proposed), and (5) Inverse modeling based scheme (Proposed).

First, the role of the dissipativity term in the robust LQ design is demonstrated. This study considered the case when $\boldsymbol{s} = \mathbf{0}$ and when $\boldsymbol{s} = \begin{bmatrix} 0 & 4 \times 10^3 \end{bmatrix}^T$. Figure 4.5 shows a comparison of the active damping force F_A and the measured damping force F_{MR} for both the non-dissipative and dissipative LQ controllers. The dissipativity term $\boldsymbol{s}$ serves to prevent the active control action from behaving too aggressively, thus allowing the MR damper a greater chance to match the active damping force. This is reflected in Figure 4.6, where the dissipative LQ controller produces slightly higher RMS acceleration than the non-dissipative LQ controller, due to its less aggressive actions.

Next, the results of the various control algorithms are presented. The damping results are compared by the following criterions: (1) the RMS seat acceleration in Figure 4.7, and (2) the

Table 4.1: Ride comfort evaluation (ISO 2631).

Frequency Range (Hz)	ISO 2631-1 ($\leq$ 1 hour)	Low Damping	High Damping	LQ Active	LQ + MR Forward	LQ + MR Inverse
0-1	0.8000	0.2491	0.1322	0.1140	0.1705	0.2221
0-1.5	0.6400	0.3746	0.3353	0.1936	0.2781	0.3493
0-2.5	0.5120	0.3724	*0.8875*	0.2492	0.3291	0.4385
0-3.5	0.4200	0.2702	*1.0164*	0.2346	0.2874	0.4001

RMS positional deflection of the seat and the tire in Figure 4.8. The results in Figures 4.7 and 4.8 can be analyzed as follows. The passive low damping produces a small damping force and therefore is suited for higher level of frequencies. The passive high damping provides the stiffest damping, and performs better during the low frequency ranges. The trade off between low and high damping can clearly be seen as the bandwidth of the road excitation is increased. The active control meanwhile provides the best performance regardless of the level of excitation. The semi-active forward and inverse modeling schemes also perform better overall than the fixed damping, as it is able to adjust the stiffness to account for the road excitation. It is noted that there is a trade-off between acceleration and displacement. The performance criterion should therefore be taken into careful consideration during design of the LQ controller. The convergence of the feedforward modeling parameters are shown in Figure 4.9. A comparison of the active and semi-active damping force is given in Figures 4.10 and 4.11.

The evaluation of ride comfort is conducted by comparing the RMS seat acceleration results with the permissible acceleration as specified by ISO 2631. The amount of RMS acceleration that a human being can sustain while remaining comfortable is a function of vibration time and frequency of excitation. For a ride duration of 1 hour, ISO 2631 specifies these values as given in Table 4.1. By comparing with the results for each methods, it is noted that all values fall within the permissible range, except for high damping at 2.5 and 3.5Hz excitation, thus ensuring that the proposed control methods are able to guarantee ride comfort to the human occupants.

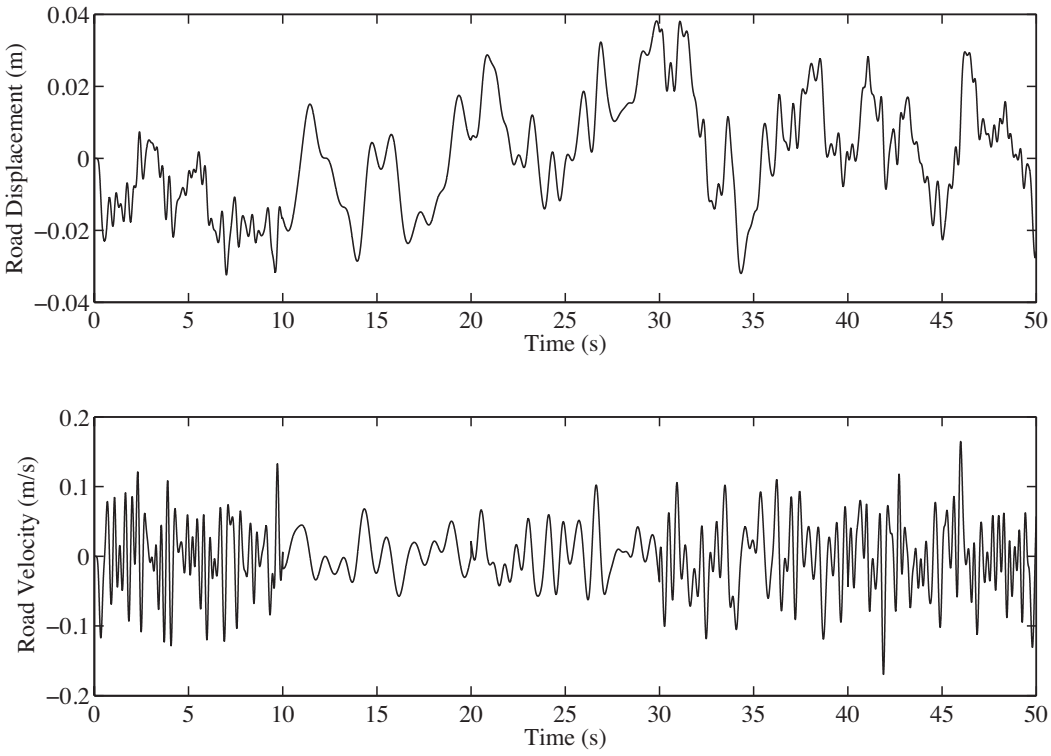

Figure 4.4: Road excitation, displacement x_r and velocity $\dot{x}_r$.

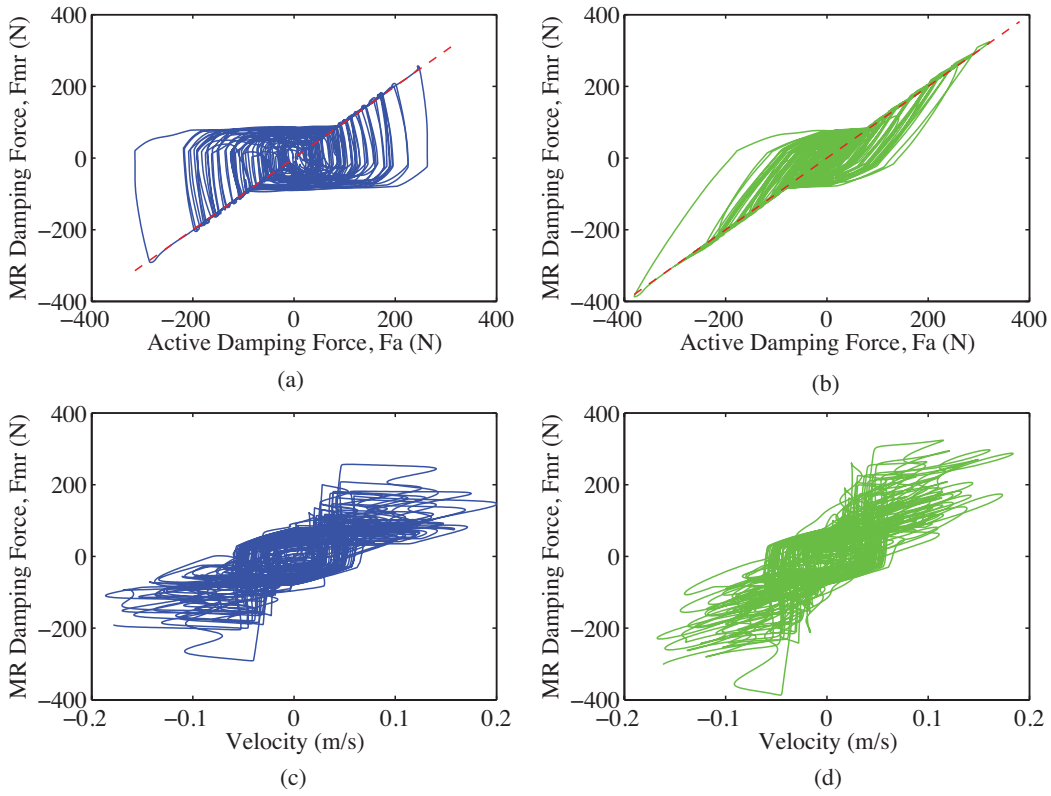

Figure 4.5: Comparison of F_A and F_{MR} for (a,c) non-dissipative LQ, and (b,d) dissipative LQ.

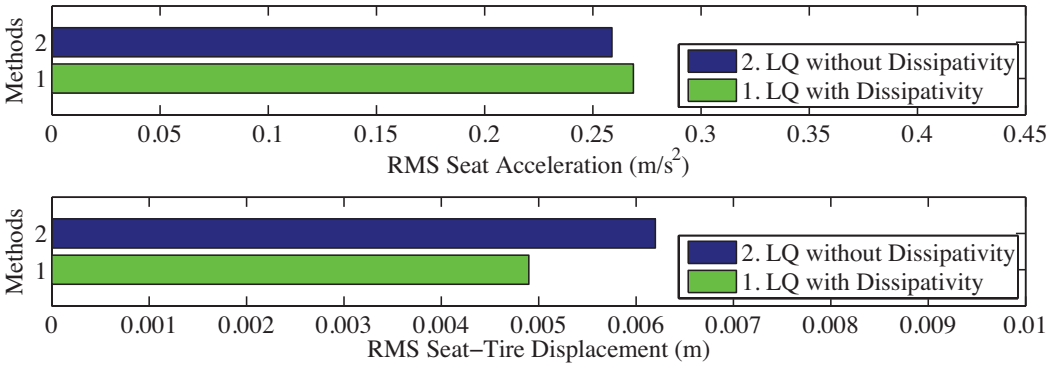

Figure 4.6: RMS seat acceleration and RMS seat-tire displacement for non-dissipative and dissipative LQ.

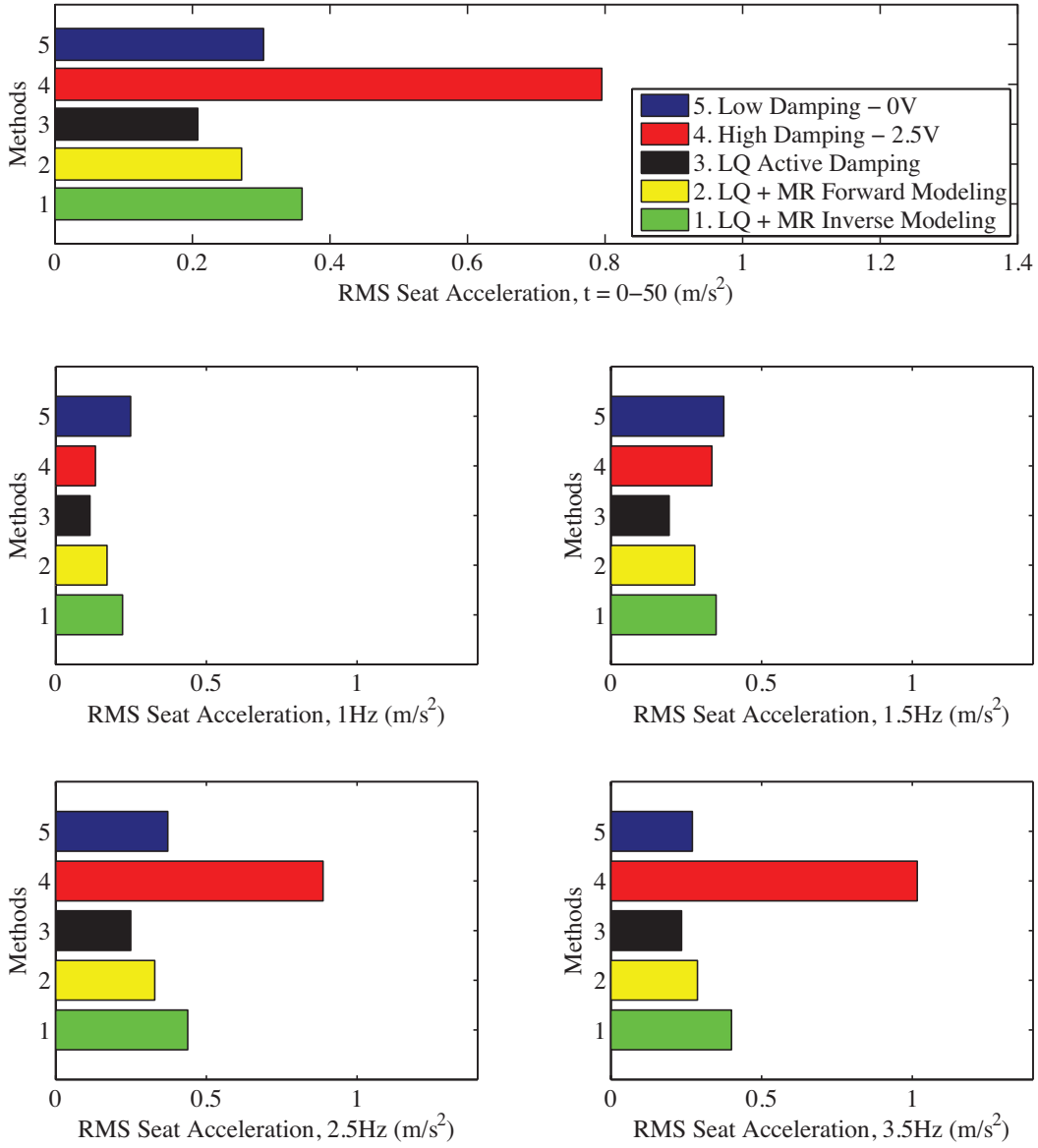

Figure 4.7: Comparison of RMS seat acceleration for the entire simulation, and divided into frequency ranges.

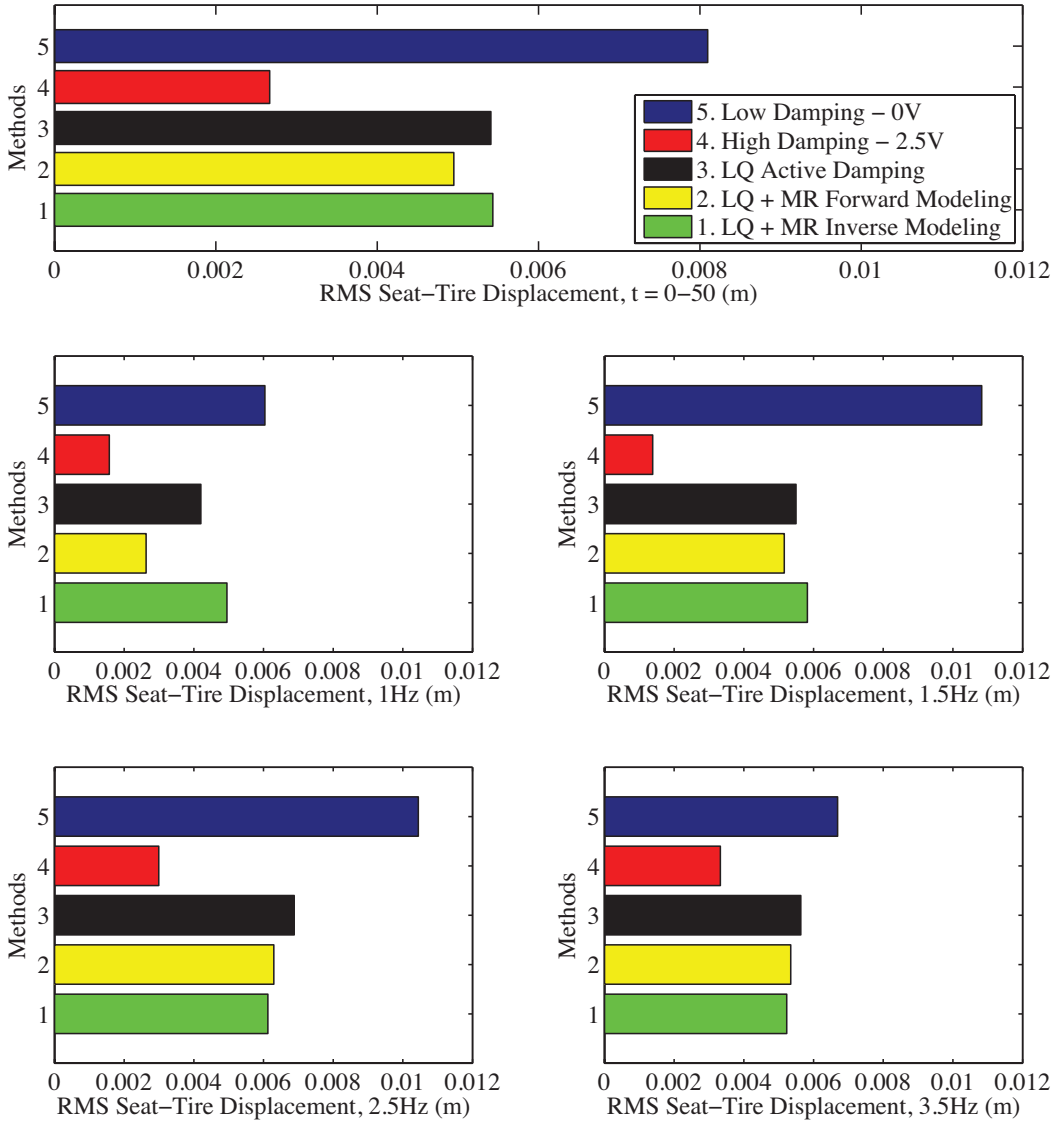

Figure 4.8: Comparison of RMS seat-tire displacement for the entire simulation, and divided into different frequency ranges.

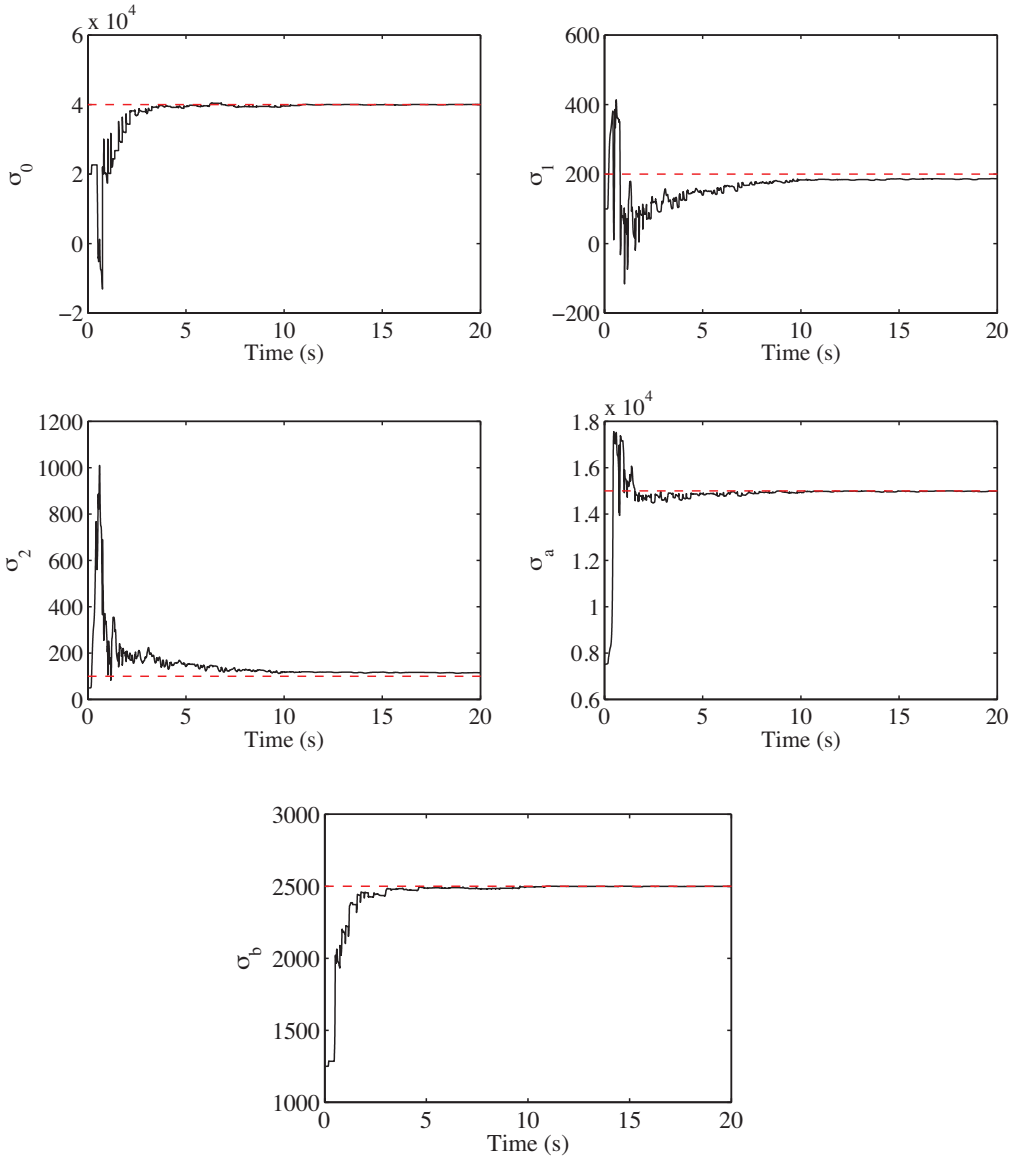

Figure 4.9: Convergence of MR parameter estimates for LQ control with forward modeling.

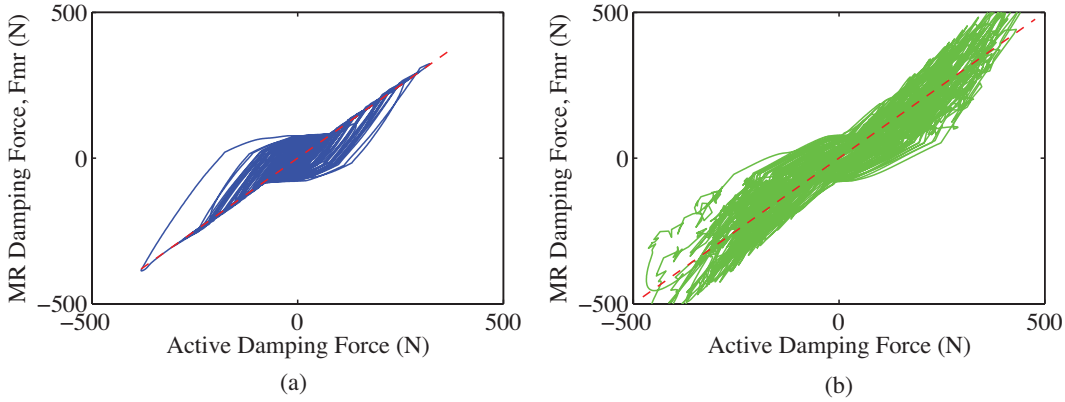

Figure 4.10: Comparison of F_A and F_{MR} for (a) LQ with forward modeling and (b) LQ with inverse modeling.

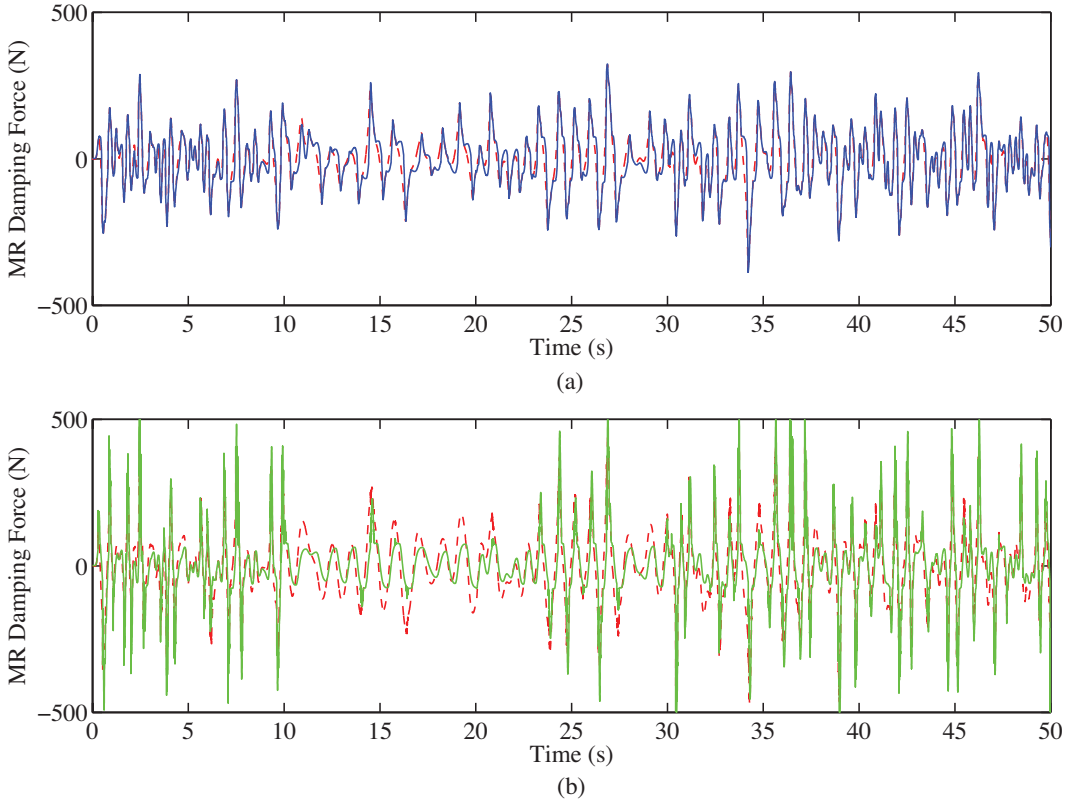

Figure 4.11: Plot of F_A (red, dashed) and F_{MR} versus time for (a) LQ with forward modeling and (blue, solid) (b) LQ with inverse modeling (green, solid).

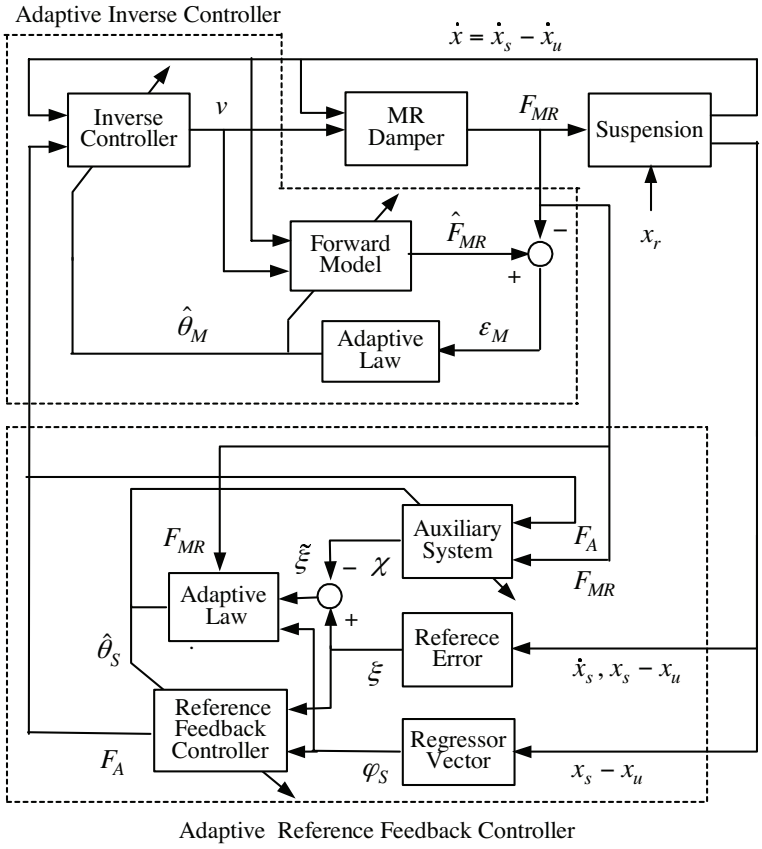

Figure 4.12: Proposed fully adaptive sem-iactive control scheme based on *forward* modeling.

4.6 Fully Adaptive Semi-active Control Algorithm

This section considers the case when both the MR damper and suspension parameters are unknown or uncertain. In this case, LQ-based controller design cannot be employed and a fully adaptive approach is necessary. Figures 4.12 and 4.13 show schematic diagrams of the proposed fully adaptive semi-active control for the suspension system. The adaptive algorithm consists of two controllers. The first is an adaptive inverse controller which provides the required input voltage v to MR damper so that the damping force F_{MR} approaches a specified command damping force F_A. If the adaptive inverse controller is designed so that the linearization from F_A to F_{MR} can be attained, that is, $F_A = F_{MR}$, almost active control performance can be realized. For construction of the inverse controller, the forward model of MR damper is identified and then the input voltage to MR damper is calculated as shown in Figure 4.12. Figure 4.13

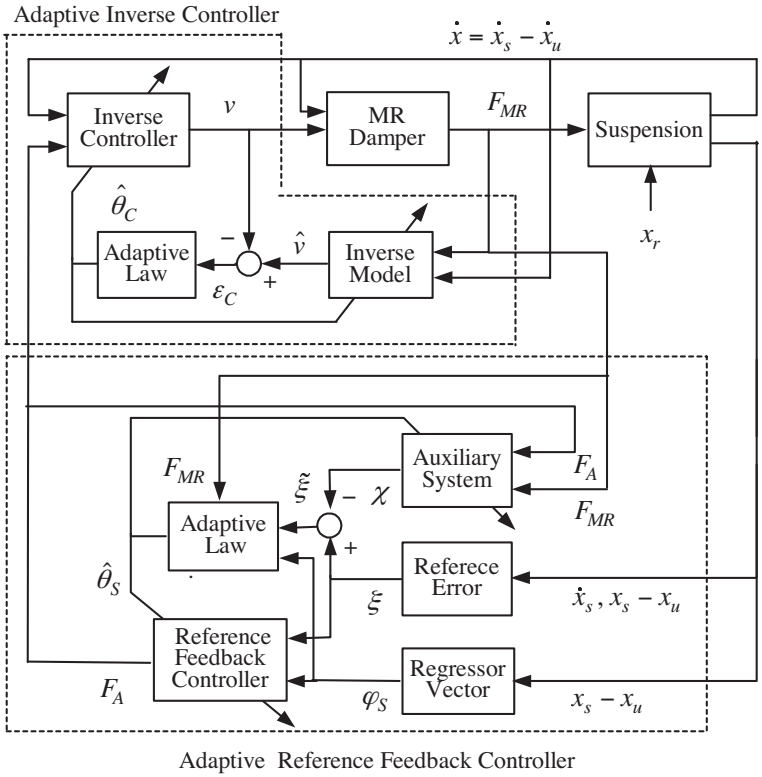

Figure 4.13: Proposed fully adaptive semi-active control scheme based on *inverse* modeling.

gives an alternative scheme in which the inverse controller is directly updated without identification of MR damper. The adaptive reference feedback control can match the chassis dynamic response to a desired reference dynamics even when the suspension system involves parametric uncertainty in M_s, C_s and K_s. Since the MR damper is actually a nonlinear semi-active device, it is difficult to make it behave in an active manner, and fine and complicated tuning is required for both the adaptive inverse and adaptive reference controllers.

4.6.1 Adaptive Reference Feedback Control

The role of the adaptive reference feedback controller is to provide a desired damper force F_A to the adaptive inverse controller so that the car chassis dynamics can match the reference dynamics. The desired damper force is decided by the skyhook approach in the case when the mass and spring constants are both unknown. Following the adaptive scheme [60], the desired

reference dynamics is specified by:

$$\ddot{x}_s + 2\zeta\omega\dot{x}_s + \omega^2(x_s - x_u) = 0 \tag{4.55}$$

where ω is the natural frequency, and ζ is a damping constant. Then, the control error ξ is given by:

$$\xi = \dot{x}_s + (s + 2\zeta\omega)^{-1}\omega^2(x_s - x_u) \tag{4.56}$$

Taking the derivative of (4.56), and employing (4.1):

$$\begin{aligned}\dot{\xi} &= \ddot{x}_s + (s + 2\zeta\omega)^{-1}\omega^2 s(x_s - x_u) \\ &= -\frac{C_s}{M_s}(\dot{x}_s - \dot{x}_u) - \frac{K_s}{M_s}(x_s - x_u) - \frac{1}{M_s}F_{MR} + (s + 2\zeta\omega)^{-1}\omega^2 s(x_s - x_u) \\ &= -\boldsymbol{\theta}_{S,1}^T\boldsymbol{\varphi}_{S,1} - \theta_{S,2}F_{MR} + (s + 2\zeta\omega)^{-1}\omega^2 s(x_s - x_u)\end{aligned} \tag{4.57}$$

where:

$$\boldsymbol{\theta}_{S,1} = \begin{bmatrix}\frac{C_s}{M_s} & \frac{K_s}{M_s}\end{bmatrix}^T \tag{4.58}$$

$$\boldsymbol{\varphi}_{S,1} = \begin{bmatrix}\dot{x}_s - \dot{x}_u & x_s - x_u\end{bmatrix}^T \tag{4.59}$$

$$\theta_{S,2} = \frac{1}{M_s} \tag{4.60}$$

Then the adaptive control law is given as:

$$F_A = \frac{1}{\hat{\theta}_{S,2}}\left(\kappa\xi - \hat{\boldsymbol{\theta}}_{S,1}^T\boldsymbol{\varphi}_{S,1} + (s + 2\zeta\omega)^{-1}\omega^2 s(x_s - x_u)\right) \tag{4.61}$$

where $\kappa > 0$ is a design constant, and $\hat{\boldsymbol{\theta}}_{S,1}$ and $\hat{\theta}_{S,2}$ are corresponding parameter estimates. Due to parametric uncertainties and the semi-active nature of the MR damper, F_{MR} cannot match F_A as given in (4.61). To develop stable adaptive control laws in the presense of this semi-active constraint, it is necessary to define an auxiliary signal χ as:

$$\dot{\chi} = -\kappa\chi + \hat{\theta}_{S,2}\left(F_A - F_{MR}\right) \tag{4.62}$$

A modified error signal is given by:

$$\tilde{\xi} = \xi - \chi \tag{4.63}$$

Employing this modified error signal, the adjustable parameters $\hat{\boldsymbol{\theta}}_{S,1}$ and $\hat{\theta}_{S,2}$ are updated by:

$$\dot{\hat{\boldsymbol{\theta}}}_{S,1} = -\dot{\tilde{\boldsymbol{\theta}}}_{S,1} = -\boldsymbol{\Gamma}_{S,1}\boldsymbol{\varphi}_{S,1}\tilde{\xi} - \sigma_{S,1}\boldsymbol{\Gamma}_{S,1}\hat{\boldsymbol{\theta}}_{S,1} \tag{4.64}$$

$$\dot{\hat{\theta}}_{S,2} = -\dot{\tilde{\theta}}_{S,2} = -\gamma_{S,2}\tilde{\xi}F_{MR} - \sigma_{S,2}\gamma_{S,2}\hat{\theta}_{S,2} \tag{4.65}$$

where $\tilde{\boldsymbol{\theta}}_{S,1} = \hat{\boldsymbol{\theta}}_{S,1} - \boldsymbol{\theta}_{S,1}$ and $\tilde{\theta}_{S,2} = \hat{\theta}_{S,2} - \theta_{S,2}$. $\boldsymbol{\Gamma}_{S,1}$ is a positive-definite matrix, $\gamma_{S,2} > 0$, $\sigma_{S,1}$ and $\sigma_{S,2}$ are positive design constants. For practical implementation, $\boldsymbol{\Gamma}_{S,1}$ and $\gamma_{S,2}$ are chosen constant. The main stability result for the adaptive reference feedback controller is presented in the following theorem.

THEOREM 4.2 *Assume $M_s > 0$ and $\kappa > 0$ are satisfied. Then the control law (4.61), along with the adaptive laws (4.64) and (4.65), guarantee that the modified error signal $\tilde{\xi}$ and the parameter estimation errors $\tilde{\boldsymbol{\theta}}_{S,1}$ and $\tilde{\theta}_{S,2}$ remain bounded and converge to a small neighborhood of the origin. Furthermore, if $F_{MR} = F_A$, then the control error ξ also converges to a small neighborhood of the origin.*

Proof: Consider a candidate of the Lyapunov function as:

$$V_S = \frac{1}{2}\tilde{\xi}^2 + \frac{1}{2}\tilde{\boldsymbol{\theta}}_{S,1}^T\boldsymbol{\Gamma}_{S,1}^{-1}\tilde{\boldsymbol{\theta}}_{S,1} + \frac{1}{2\gamma_{S,2}}\tilde{\theta}_{S,2}^2 \tag{4.66}$$

Taking the time-derivative of V_S and using the control law (4.61):

$$\begin{aligned}
\dot{V}_S &= \tilde{\xi}\dot{\tilde{\xi}} + \tilde{\boldsymbol{\theta}}_{S,1}^T\boldsymbol{\Gamma}_{S,1}^{-1}\dot{\tilde{\boldsymbol{\theta}}}_{S,1} + \frac{1}{\gamma_{S,2}}\tilde{\theta}_{S,2}\dot{\tilde{\theta}}_{S,2} \\
&= \tilde{\xi}\left(\dot{\xi} - \dot{\chi}\right) + \tilde{\boldsymbol{\theta}}_{S,1}^T\boldsymbol{\Gamma}_{S,1}^{-1}\dot{\tilde{\boldsymbol{\theta}}}_{S,1} + \frac{1}{\gamma_{S,2}}\tilde{\theta}_{S,2}\dot{\tilde{\theta}}_{S,2} \\
&= \tilde{\xi}\left(-\boldsymbol{\theta}_{S,1}^T\boldsymbol{\varphi}_{S,1} - \theta_{S,2}F_{MR} + (s+2\zeta\omega)^{-1}\omega^2 s(x_s - x_u) + \kappa\chi - \hat{\theta}_{S,2}\left(F_A - F_{MR}\right)\right) \\
&\quad + \tilde{\boldsymbol{\theta}}_{S,1}^T\boldsymbol{\Gamma}_{S,1}^{-1}\dot{\tilde{\boldsymbol{\theta}}}_{S,1} + \frac{1}{\gamma_{S,2}}\tilde{\theta}_{S,2}\dot{\tilde{\theta}}_{S,2} \\
&= -\kappa\tilde{\xi}^2 + \tilde{\boldsymbol{\theta}}_{S,1}^T\boldsymbol{\varphi}_{S,1}\tilde{\xi} + \tilde{\theta}_{S,2}\tilde{\xi}F_{MR} + \tilde{\boldsymbol{\theta}}_{S,1}^T\boldsymbol{\Gamma}_{S,1}^{-1}\dot{\tilde{\boldsymbol{\theta}}}_{S,1} + \frac{1}{\gamma_{S,2}}\tilde{\theta}_{S,2}\dot{\tilde{\theta}}_{S,2}
\end{aligned} \tag{4.67}$$

Now using the adaptive laws (4.64) and (4.65):

$$\begin{aligned}
\dot{V}_S &= -\kappa\tilde{\xi}^2 - \sigma_{S,1}\tilde{\boldsymbol{\theta}}_{S,1}^T\hat{\boldsymbol{\theta}}_{S,1} - \sigma_{S,2}\tilde{\theta}_{S,2}\hat{\boldsymbol{\theta}}_{S,2} \\
&\leq -\kappa\tilde{\xi}^2 - \frac{\sigma_{S,1}}{2}\tilde{\boldsymbol{\theta}}_{S,1}^T\tilde{\boldsymbol{\theta}}_{S,1} - \frac{\sigma_{S,2}}{2}\tilde{\theta}_{S,2}^2 + \frac{\sigma_{S,1}}{2}\boldsymbol{\theta}_{S,1}^T\boldsymbol{\theta}_{S,1} + \frac{\sigma_{S,2}}{2}\theta_{S,2}^2
\end{aligned} \tag{4.68}$$

Thus:

$$\dot{V}_S \leq -c_S V_S + \lambda_S \tag{4.69}$$

where:

$$c_S = \min\left\{2\kappa, \frac{\sigma_{S,1}}{\lambda_{\max}(\mathbf{\Gamma}_{S,1}^{-1})}, \gamma_{S,2}\sigma_{S,2}\right\} \tag{4.70}$$

$$\lambda_S = \frac{\sigma_{S,1}}{2}\boldsymbol{\theta}_{S,1}^T\boldsymbol{\theta}_{S,1} + \frac{\sigma_{S,2}}{2}\theta_{S,2}^2 \tag{4.71}$$

Since κ, $\sigma_{S,1}$ and $\sigma_{S,2}$ are positive design constants, $\lambda_S/c_S > 0$ and the following result is obtained:

$$0 \leq V_S(t) \leq \lambda_S/c_S + (V_S(0) - \lambda_S/c_S)\, e^{-c_S t} \tag{4.72}$$

Thus, the modified error $\tilde{\xi}$ and the parameter estimation errors $\tilde{\boldsymbol{\theta}}_{S,1}$ and $\tilde{\theta}_{S,2}$ are uniformly bounded and converge to a small neighborhood of the origin. The assumption that $M_s > 0$ and some type of parameter projection method is necessary to ensure that $\hat{\theta}_{S,2}$ does not approach zero. From (4.62), it is clear that if $F_{MR} = F_A$ then $\chi \to 0$, and therefore the control error ξ also converges to a small neigborhood of the origin. □

4.6.2 Adaptive Inverse Damper Control

Adaptive Inverse Damper Control via Forward Modeling

Since the internal state z of the MR damper model cannot be measured, the regressor vector $\boldsymbol{\varphi}_M$ should be replaced with its estimate $\hat{\boldsymbol{\varphi}}_M$ as:

$$\hat{\boldsymbol{\varphi}}_M = (\hat{z},\ \hat{z}v,\ -|\dot{x}|\hat{z},\ \dot{x},\ \dot{x}v)^T \tag{4.73}$$

where the estimate $\hat{z}$ is given later by using the updated model parameters. The output of the identification model is now described as:

$$\hat{F}_{MR} = \hat{\boldsymbol{\theta}}_M^T\hat{\boldsymbol{\varphi}}_M \tag{4.74}$$

By using the damping force estimation error defined by $\varepsilon_M = \hat{F}_{MR} - F_{MR}$, and the identified parameter $\hat{a}_0$, the estimate $\hat{z}$ of the internal state can be calculated as:

$$\dot{\hat{z}} = \dot{x} - \hat{a}_0|\dot{x}|\hat{z} - L\varepsilon_M \tag{4.75}$$

where L is an observer gain such that $0 \leq L \leq 1/\hat{\sigma}_{1\max}$, and the upper bound is decided by the stability of the adaptive observer [54].

To assure the stability of the adaptive identification algorithm, introduce the normalizing signal as $N_M = \left(c_1 + \hat{\boldsymbol{\varphi}}_M^T \hat{\boldsymbol{\varphi}}_M\right)^{1/2}$, where $c_1 > 0$. By dividing the signals and errors by N_M as $\boldsymbol{\varphi}_{M_N} = \boldsymbol{\varphi}_M / N_M$, $\hat{\boldsymbol{\varphi}}_{M_N} = \hat{\boldsymbol{\varphi}}_M / N_M$ and $\varepsilon_{M_N} = \hat{F}_{MR_N} - F_{MR_N}$, where $F_{MR_N} = F_{MR}/N_M$ and $\hat{F}_{MR_N} = \hat{\boldsymbol{\theta}}_M^T \hat{\boldsymbol{\varphi}}_{M_N}$, the adaptive law for updating the model parameters is given as:

$$\dot{\hat{\boldsymbol{\theta}}}_M = -\boldsymbol{\Gamma}_M \hat{\boldsymbol{\varphi}}_{M_N} \varepsilon_{M_N} - \sigma_M \boldsymbol{\Gamma}_M \hat{\boldsymbol{\theta}}_M \tag{4.76}$$

where $\tilde{\boldsymbol{\theta}}_M = \hat{\boldsymbol{\theta}}_M - \boldsymbol{\theta}_M$. $\boldsymbol{\Gamma}_M$ is a positive-definite matrix and σ_M is a positive design constant. For practical implementation, $\boldsymbol{\Gamma}_M$ is chosen constant. Thus, the physical model parameters can be calculated from the relation (4.7).

The role of the adaptive inverse controller shown in Figure 4.12 is to decide the control input voltage v to the MR damper so that the actual damping force F_{MR} may coincide with the specified command damping force F_A, even in the presence of uncertainty in the MR damper model. The input voltage giving F_A can be analytically calculated from the identified forward model of MR damper (4.7). Actually using the identified model parameters, the input voltage v is obtained from (4.7) as:

$$\rho = \hat{\sigma}_0 \hat{z} + \hat{\sigma}_b \dot{x} \tag{4.77}$$

$$d_\rho = \begin{cases} \rho & \text{for } \rho < -\delta, \quad \delta < \rho \\ \delta \, \mathrm{sgn}(\rho) & \text{for } -\delta \le \rho \le \delta \end{cases} \tag{4.78}$$

$$v_A = \frac{F_A - \{\hat{\sigma}_a \hat{z} - \hat{\sigma}_1 \hat{a}_0 |\dot{x}| \hat{z} + (\hat{\sigma}_1 + \hat{\sigma}_2)\dot{x} - L\varepsilon_M\}}{d_\rho} \tag{4.79}$$

$$v = \begin{cases} 0 & \text{for } v_A \le 0 \\ v_A & \text{for } 0 < v_A \le V_{\max} \\ V_{\max} & \text{for } V_{\max} < v_A \end{cases} \tag{4.80}$$

where F_A is the specified command damping force. v is assumed to be fixed near $\rho = 0$ to avoid division by zero. Due to the semi-active nature of the MR damper, F_{MR} may not fully match the desired control force F_A. The stability result of the total system given in Figure 4.12 is presented in the following theorem.

THEOREM 4.3 *Assume $M_s > 0$ and $\kappa > 0$ are satisfied, and a_0 is known. Then the control law (4.61), along with the adaptive laws (4.64), (4.65) and (4.76) guarantee that all error signals remain bounded and converge to a small neighborhood of the origin. Furthermore, if $F_{MR} = F_A$, then the control error ξ also converges to a small neighborhood of the origin.*

Proof: Let a candidate Lyapunov function to the total system with forward modeling be denoted by:

$$V_M = V_S + \frac{1}{2}\tilde{\boldsymbol{\theta}}_M^T \boldsymbol{\Gamma}_M^{-1} \tilde{\boldsymbol{\theta}}_M \tag{4.81}$$

From the assumption that a_0 is known, the internal state z is available and the regressor vector $\boldsymbol{\varphi}_{M_N}$ can be employed in (4.76). Taking the time-derivative of V_M and using the results of Theorem 4.2, along with the adaptive law (4.76), leads to:

$$\begin{aligned}
\dot{V}_M &= \dot{V}_S + \tilde{\boldsymbol{\theta}}_M^T \boldsymbol{\Gamma}_M^{-1} \dot{\tilde{\boldsymbol{\theta}}}_M \\
&= \dot{V}_S - \tilde{\boldsymbol{\theta}}_M^T \boldsymbol{\varphi}_{M_N} \varepsilon_{M_N} - \sigma_M \tilde{\boldsymbol{\theta}}_M^T \hat{\boldsymbol{\theta}}_M \\
&= \dot{V}_S - \varepsilon_{M_N}^2 - \sigma_M \tilde{\boldsymbol{\theta}}_M^T \hat{\boldsymbol{\theta}}_M \\
&\leq \dot{V}_S - \frac{\sigma_M}{2} \tilde{\boldsymbol{\theta}}_M^T \tilde{\boldsymbol{\theta}}_M + \frac{\sigma_M}{2} \boldsymbol{\theta}_M^T \boldsymbol{\theta}_M
\end{aligned} \tag{4.82}$$

Therefore:

$$\dot{V}_M \leq -c_M V_M + \lambda_M \tag{4.83}$$

where:

$$c_M = \min \left\{ c_S, \frac{\sigma_M}{\lambda_{\max}(\boldsymbol{\Gamma}_M^{-1})} \right\} \tag{4.84}$$

$$\lambda_M = \lambda_S + \frac{\sigma_M}{2} \boldsymbol{\theta}_M^T \boldsymbol{\theta}_M \tag{4.85}$$

As $\lambda_M / c_M > 0$, the following result is obtained:

$$0 \leq V_M(t) \leq \lambda_M / c_M + \left(V_M(0) - \lambda_M / c_M \right) e^{-c_M t} \tag{4.86}$$

Thus, all the error signals associated with the total system, along with the parameter estimation error $\tilde{\boldsymbol{\theta}}_M$, are uniformly bounded and converge to a small neighborhood of the origin. Furthermore, if $F_{MR} = F_A$, then the control error ξ also converges to a small neighborhood of the origin. □

Adaptive Inverse Damper Control via Inverse Modeling

In the previous section, the inverse controller is obtained analytically from the estimated parameters of the forward model of MR damper. However, as expressed in (4.80), some adjustable

parameters appear in the denominator of the inverse controller and so zero-division should be avoided. Therefore, we consider a linearly parameterized *inverse* model, as shown in Fig. 4.13. Since the damper force F_{MR} is given as a function of the velocity $\dot{x}$, input voltage v and internal state z as shown in (4.7), its inverse model for the input voltage v can be expressed as a function of $\dot{x}$, z and F_{MR}. Hence, an approximate inverse model, which is expressed by a linearly parameterized polynomial function, is considered as:

$$v = \sum_{j=0}^{n} \sum_{i=0}^{m} h_{i+(m+1)k+1} \left|\dot{x}\right|^i \left|z\right|^j F_{MR}\mathrm{sgn}(\dot{x}) + \delta_C \tag{4.87}$$

where δ_C is an approximation error term, and is assumed to have an unknown constant bound $|\delta_C| \leq \Delta_C$. The inverse model has three inputs of $\dot{x}$, z and F_{MR}, and one output of v. z is an internal state of the MR damper, which can be calculated as given previously by:

$$\dot{z} = \dot{x} - a_0|\dot{x}|z \tag{4.88}$$

where a nominal value of a_0 is assumed to be known via the forward modeling. In simulation, an inverse model with $m = 4$ and $n = 1$ is adopted.

The inverse model is also expressed in vector form as:

$$v = \boldsymbol{\theta}_C^T \boldsymbol{\varphi}_C + \delta_C \tag{4.89}$$

where:

$$\boldsymbol{\theta}_C = \begin{bmatrix} h_1 & h_2 & \dots & h_{(n+1)(m+1)} \end{bmatrix}^T \tag{4.90}$$

$$\boldsymbol{\varphi}_C = \begin{bmatrix} F_{MR}\mathrm{sgn}(\dot{x}) & |\dot{x}|F_{MR}\mathrm{sgn}(\dot{x}) & \dots & |z|F_{MR}\mathrm{sgn}(\dot{x}) \\ & & & |\dot{x}||z|F_{MR}\mathrm{sgn}(\dot{x}) & \dots & |\dot{x}|^m|z|^n F_{MR}\mathrm{sgn}(\dot{x}) \end{bmatrix}^T \tag{4.91}$$

Then the identified model is expressed as:

$$\hat{v} = \hat{\boldsymbol{\theta}}_C^T \boldsymbol{\varphi}_C + \mu \tag{4.92}$$

The identification error ε_C is defined as:

$$\varepsilon_C = \hat{v} - v \tag{4.93}$$

and μ is a robustifying term given as:

$$\mu = -\hat{\Delta}_C \eta_C \tanh((a + bt)\varepsilon_C) \tag{4.94}$$

with $\eta_C > 1$ and $a, b > 0$. To assure the stability of the adaptive identification algorithm, introduce the normalizing signal as $N_C = \left(c_2 + \boldsymbol{\varphi}_C^T \boldsymbol{\varphi}_C\right)^{1/2}$, where $c_2 > 0$. By dividing the signals and errors by N_C as $\boldsymbol{\varphi}_{C_N} = \boldsymbol{\varphi}_C / N_C$, and $\varepsilon_{C_N} = \hat{v}_N - v_N$, where $v_N = v/N_C$ and $\hat{v}_N = \hat{\boldsymbol{\theta}}_C^T \hat{\boldsymbol{\varphi}}_{C_N} + \mu_N$, and $\mu_N = -\hat{\Delta}_C \eta_C \tanh((a+bt)\varepsilon_{C_N})$, the adaptive laws for updating the model parameters are given as:

$$\dot{\hat{\boldsymbol{\theta}}}_C = -\boldsymbol{\Gamma}_C \boldsymbol{\varphi}_{C_N} \varepsilon_{C_N} - \sigma_C \boldsymbol{\Gamma}_C \hat{\boldsymbol{\theta}}_C \tag{4.95}$$

$$\dot{\hat{\Delta}}_C = \gamma_{\Delta_C} |\varepsilon_{C_N}| - \sigma_{\Delta_C} \gamma_{\Delta_C} \hat{\Delta}_C \tag{4.96}$$

where $\tilde{\boldsymbol{\theta}}_C = \hat{\boldsymbol{\theta}}_C - \boldsymbol{\theta}_C$ and $\tilde{\Delta}_C = \hat{\Delta}_C - \Delta_C$. $\boldsymbol{\Gamma}_C$ is a positive definite matrix, γ_{Δ_C}, σ_C and σ_{Δ_C} are positive design constants. For practical implementation, $\boldsymbol{\Gamma}_C$ and γ_{Δ_C} are chosen constant.

Figure 4.13 describes the adaptive damper control via inverse modeling. The control input voltage v is given as:

$$v_A = \hat{\boldsymbol{\theta}}_C^T \boldsymbol{\varphi}_A \tag{4.97}$$

$$v = \begin{cases} 0 & \text{for } v_A \le 0 \\ v_A & \text{for } 0 < v_A \le V_{\max} \\ V_{\max} & \text{for } V_{\max} < v_A \end{cases} \tag{4.98}$$

where:

$$\boldsymbol{\varphi}_A = \Big[F_A \mathrm{sgn}(\dot{x}) \quad |\dot{x}| F_A \mathrm{sgn}(\dot{x}) \quad \dots \quad |z| F_A \mathrm{sgn}(\dot{x}) \quad |\dot{x}||z| F_A \mathrm{sgn}(\dot{x}) \quad \dots \quad |\dot{x}|^m |z|^n F_A \mathrm{sgn}(\dot{x}) \Big]^T \tag{4.99}$$

Again due to the semi-active nature of the MR damper, F_{MR} may not fully match the desired control force F_A. The stability result of the total system given in Figure 4.13 is presented in the following theorem.

THEOREM 4.4 *Assume $M_s > 0$ and $\kappa > 0$ are satisfied, and a_0 is known. Then the control law (4.61), along with the adaptive laws (4.64), (4.65), (4.95) and (4.96) guarantee that all error signals remain bounded and converge to a small neighborhood of the origin. Furthermore, if $F_{MR} = F_A$, then the control error ξ also converges to a small neighborhood of the origin.*

Proof: Let a candidate Lyapunov function to the total system with inverse modeling be denoted by:

$$V_C = V_S + \frac{1}{2} \tilde{\boldsymbol{\theta}}_C^T \boldsymbol{\Gamma}_C^{-1} \tilde{\boldsymbol{\theta}}_C + \frac{1}{2\gamma_{\Delta_C}} \tilde{\Delta}_C^2 \tag{4.100}$$

Taking the time-derivative of V_C and using the results of Theorem 4.2, along with the control laws (4.95) and (4.96), leads to:

$$\begin{aligned}
\dot{V}_C &= \dot{V}_S + \tilde{\boldsymbol{\theta}}_C^T \boldsymbol{\Gamma}_C^{-1} \dot{\tilde{\boldsymbol{\theta}}}_C + \frac{1}{\gamma_{\Delta_C}} \tilde{\Delta}_C \dot{\tilde{\Delta}}_C \\
&= \dot{V}_S - \tilde{\boldsymbol{\theta}}_C^T \boldsymbol{\varphi}_{C_N} \varepsilon_{C_N} + \tilde{\Delta}_C |\varepsilon_{C_N}| - \sigma_C \tilde{\boldsymbol{\theta}}_C^T \hat{\boldsymbol{\theta}}_C - \sigma_{\Delta_C} \tilde{\Delta}_C \hat{\Delta}_C \\
&= \dot{V}_S - \varepsilon_{C_N}^2 + \mu_N \varepsilon_{C_N} - \delta_C \varepsilon_{C_N} + \tilde{\Delta}_C |\varepsilon_{C_N}| - \sigma_C \tilde{\boldsymbol{\theta}}_C^T \hat{\boldsymbol{\theta}}_C - \sigma_{\Delta_C} \tilde{\Delta}_C \hat{\Delta}_C \\
&\leq \dot{V}_S + \hat{\Delta}_C \left(1 - \eta_C \tanh((a+bt)|\varepsilon_{C_N}|)\right) |\varepsilon_{C_N}| \\
&\quad - \frac{\sigma_C}{2} \tilde{\boldsymbol{\theta}}_C^T \tilde{\boldsymbol{\theta}}_C - \frac{\sigma_{\Delta_C}}{2} \tilde{\Delta}_C^2 + \frac{\sigma_C}{2} \boldsymbol{\theta}_C^T \boldsymbol{\theta}_C + \frac{\sigma_{\Delta_C}}{2} \Delta_C^2
\end{aligned} \tag{4.101}$$

Notice that the condition:

$$1 - \eta_C \tanh\left((a+bt)|\varepsilon_{C_N}|\right) \leq 0 \tag{4.102}$$

is satisfied when:

$$|\varepsilon_{C_N}| \geq \nu_C = \frac{1}{a+bt} \ln\left(\frac{\eta_C + 1}{\eta_C - 1}\right), \quad \eta_C > 1 \tag{4.103}$$

As $t \to \infty$ and $b > 0$, the region defined by ν_C goes to zero, and thus the condition (4.102) is satisfied as $t \to \infty$. Therefore:

$$\begin{aligned}
\dot{V}_C &\leq \dot{V}_S - \frac{\sigma_C}{2} \tilde{\boldsymbol{\theta}}_C^T \tilde{\boldsymbol{\theta}}_C - \frac{\sigma_{\Delta_C}}{2} \tilde{\Delta}_C^2 + \frac{\sigma_C}{2} \boldsymbol{\theta}_C^T \boldsymbol{\theta}_C + \frac{\sigma_{\Delta_C}}{2} \Delta_C^2 \\
&\leq -c_C V_C + \lambda_C
\end{aligned} \tag{4.104}$$

where:

$$c_C = \min\left\{c_S, \frac{\sigma_C}{\lambda_{\max}(\boldsymbol{\Gamma}_C^{-1})}, \gamma_{\Delta_C} \sigma_{\Delta_C}\right\} \tag{4.105}$$

$$\lambda_C = \lambda_S + \frac{\sigma_C}{2} \boldsymbol{\theta}_C^T \boldsymbol{\theta}_C + \frac{\sigma_{\Delta_C}}{2} \Delta_C^2 \tag{4.106}$$

As $\lambda_C / c_C > 0$, the following result is obtained:

$$0 \leq V_C(t) \leq \lambda_C / c_C + \left(V_C(0) - \lambda_C / c_C\right) e^{-c_C t} \tag{4.107}$$

Thus, all the error signals associated with the total system, along with the parameter estimation errors $\tilde{\boldsymbol{\theta}}_C$ and $\tilde{\Delta}_C$, are uniformly bounded and converge to a small neighborhood of the origin. Furthermore, if $F_{MR} = F_A$, then the control error ξ also converges to a small neighborhood of the origin. $\square$

4.7 Simulation Results

This section presents simulation results for the proposed control algorithm when the suspension system parameters are unknown. The control algorithm consists of the adaptive skyhook method and an adaptive inverse controller to achieve linearization of the MR damper. The adaptive inverse controller can be designed using the forward modeling approach or inverse modeling approach, as shown in Figures 4.12 and 4.13.

Consider a suspension system shown in Fig. 4.1, where the parameters are set as $M_s = 504.5$ [kg], $M_u = 62$ [kg], $C_s = 400$ [Ns/m], $K_s = 1.31 \times 10^4$ [N/m] and $K_t = 2.52 \times 10^5$ [N/m]. The parameters of the MR damper are specified as: $\sigma_0 = 4.0 \times 10^4$ [N/mV], $\sigma_1 = 2.0 \times 10^2$ [Ns/m], $\sigma_2 = 1.0 \times 10^2$ [Ns/m], $\sigma_a = 1.5 \times 10^4$ [N/m], $\sigma_b = 2.5 \times 10^3$ [Ns/(mV)], $a_0 = 1.9 \times 10^2$, which are all unknown. An upper limit of input voltage to the MR damper is set at 2.5[V], so v varies between 0 to 2.5[V]. The base of the dynamic system in Fig. 4.1 is excited by the road surface, which is given by a random signal sequence with a frequency range of 0-3.5 Hz. To analyze the effectiveness of each control schemes for various frequency ranges, the road excitation was designed so that the bandwidth increases every ten seconds from 1Hz, 1.5Hz, 2.5Hz to 3.5Hz. The initial period of ten seconds has a bandwidth of 3.5Hz to allow for parameter convergences of the adaptive schemes. The displacement and velocity profile of the road excitation is shown in Figure 4.4. The following schemes are compared: (1) Passive low damping with 0 [V] fixed, (2) Passive high damping with 2.5 [V] fixed, (3) Active skyhook-based scheme, (4) Skyhook control with forward modeling based scheme (Proposed) and (5) Skyhook control with inverse modeling based scheme (Proposed).

Next, the results of the various control algorithms are presented. The damping results are compared by the following criterions: (1) the RMS seat acceleration in Figure 4.14, and (2) the RMS positional deflection of the seat and the tire in Figure 4.15. The results in Figures 4.14 and 4.15 are similar to the LQ control case, and can be analyzed as follows. The passive low damping produces a small damping force and therefore is suited for higher level of frequencies. The passive high damping provides the stiffest damping, and performs better during the low frequency ranges. The trade off between low and high damping can clearly be seen as the bandwidth of the road excitation is increased. The active control meanwhile provides the best performance regardless of the level of excitation. The semi-active forward and inverse modeling schemes also perform better overall than the fixed damping, as it is able

Table 4.2: Ride comfort evaluation (ISO 2631).

Frequency Range (Hz)	ISO 2631-1 ($\leq$ 1 hour)	Low Damping	High Damping	Skyhook Active	Skyhook + MR Forward	Skyhoook + MR Inverse
0-1	0.8000	0.2491	0.1322	0.0940	0.1744	0.2241
0-1.5	0.6400	0.3746	0.3353	0.1434	0.2727	0.3697
0-2.5	0.5120	0.3724	*0.8875*	0.1758	0.3197	0.3841
0-3.5	0.4200	0.2702	*1.0164*	0.1546	0.2667	0.2952

to adjust the stiffness to account for the road excitation. The convergence of the skyhook parameters estimates are shown in Figure 4.16. It is clear that the suspension parameters can be identified very rapidly and accurately, as shown in Figure 4.17. The convergence of the feedforward modeling parameters are shown in Figure 4.18. A comparison of the active and semi-active damping force is given in Figure 4.19. In contrast to the robust LQ control design with dissipativity, the adaptive skyhook method produces a more aggressive damping force and therefore results in more discrepancies between the desired damping force and the semi-active damping force. However, the auxiliary function introduced in this research guarantees that the adaptive algorithm remains robust with respect to this error.

The evaluation of ride comfort is conducted by comparing the RMS seat acceleration results with the permissible acceleration as specified by ISO 2631. The amount of RMS acceleration that a human being can sustain while remaining comfortable is a function of vibration time and frequency of excitation. For a ride duration of 1 hour, ISO 2631 specifies these values as given in Table 4.2. By comparing with the results for each methods, it is noted that all values fall within the permissible range, except for high damping at 2.5 and 3.5Hz excitation, thus ensuring that the proposed control methods are able to guarantee ride comfort to the human occupants.

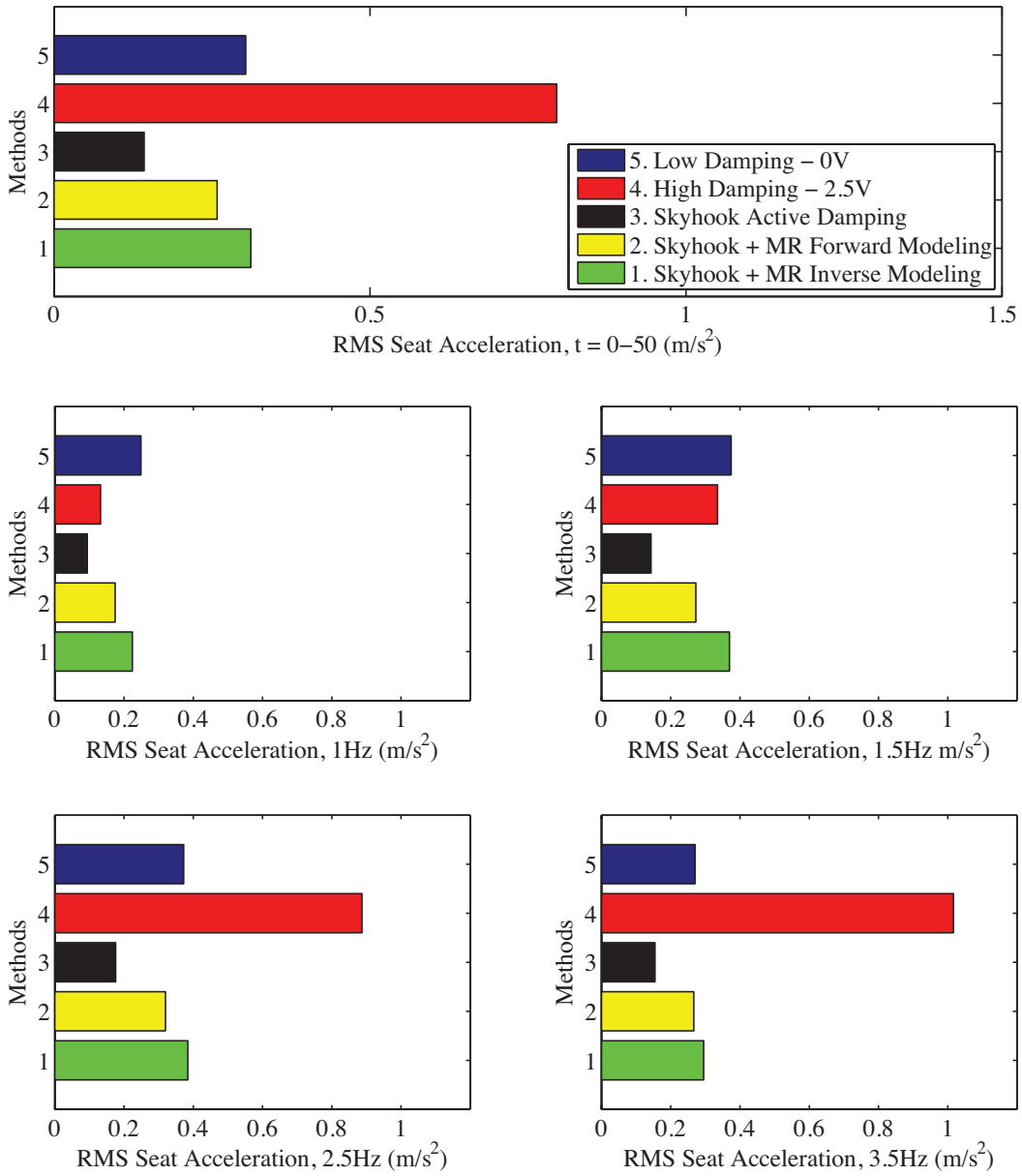

Figure 4.14: Comparison of RMS seat acceleration for the entire simulation, and divided into frequency ranges.

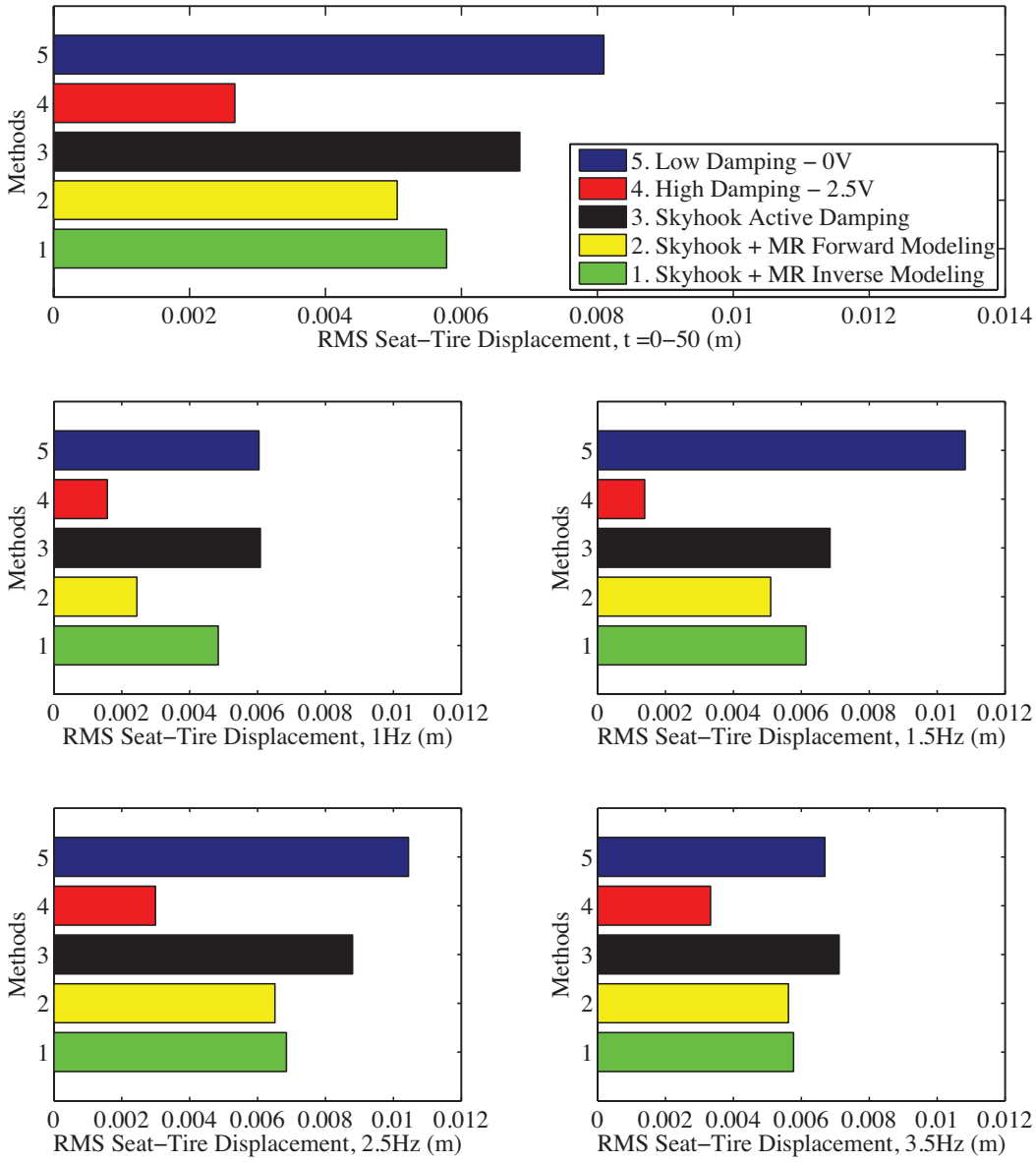

Figure 4.15: Comparison of RMS seat-tire displacement for the entire simulation, and divided into different frequency ranges.

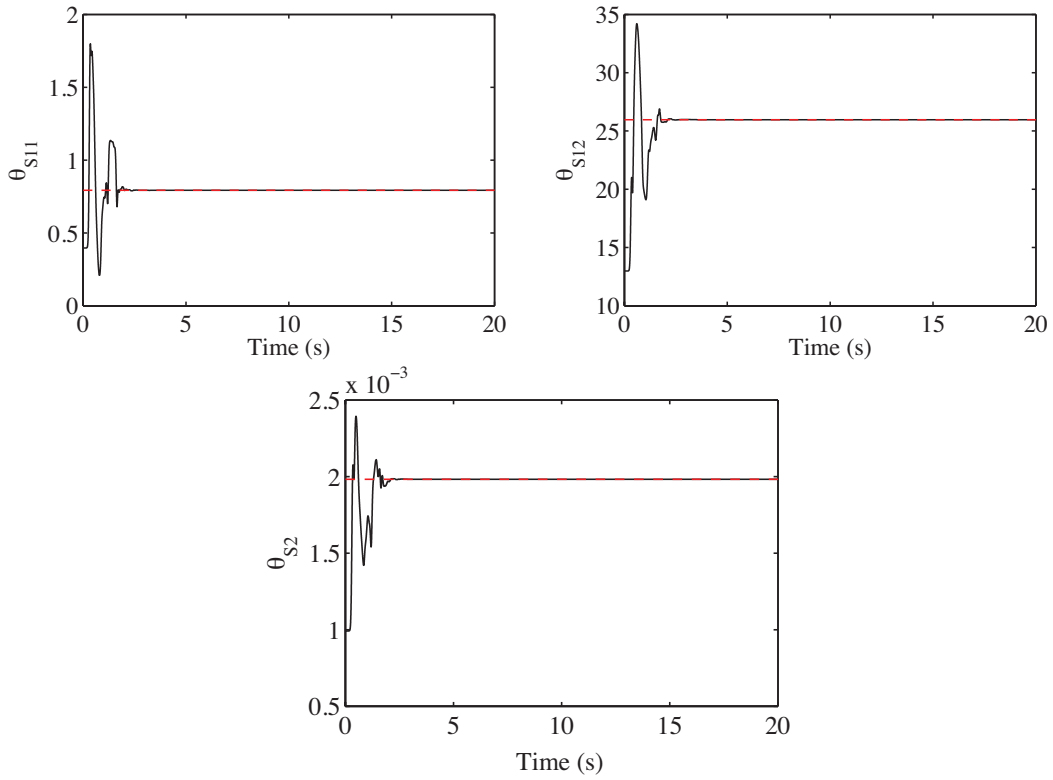

Figure 4.16: Convergence of skyhook parameter estimates.

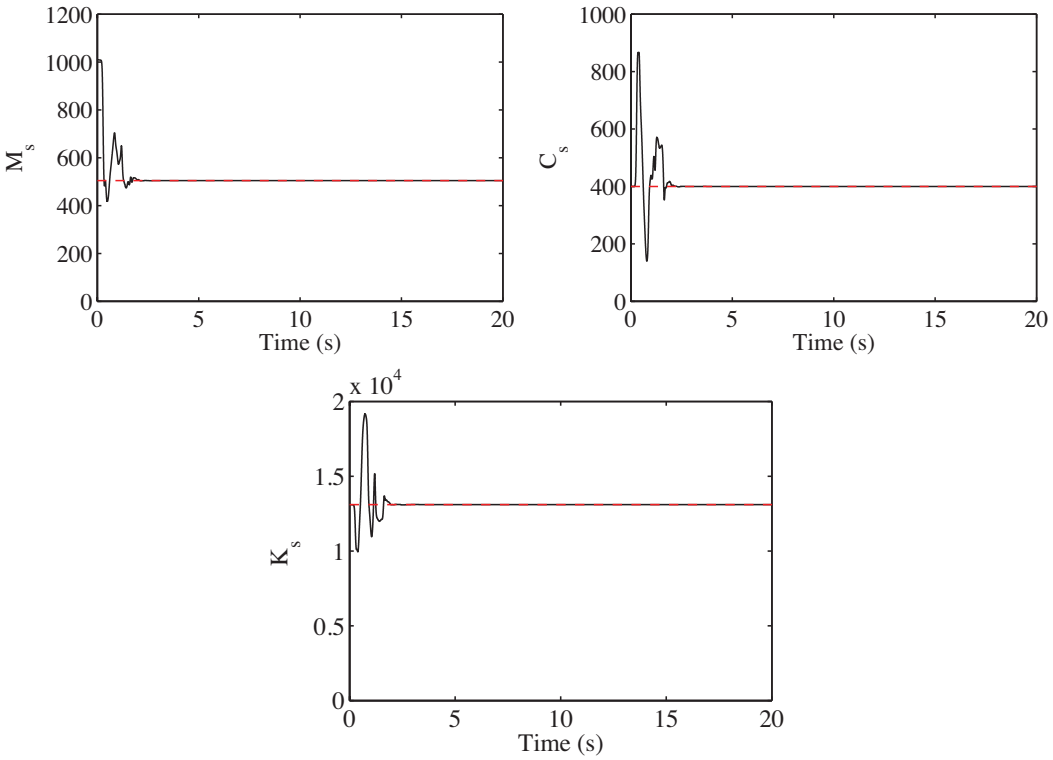

Figure 4.17: Convergence of suspension parameter estimates.

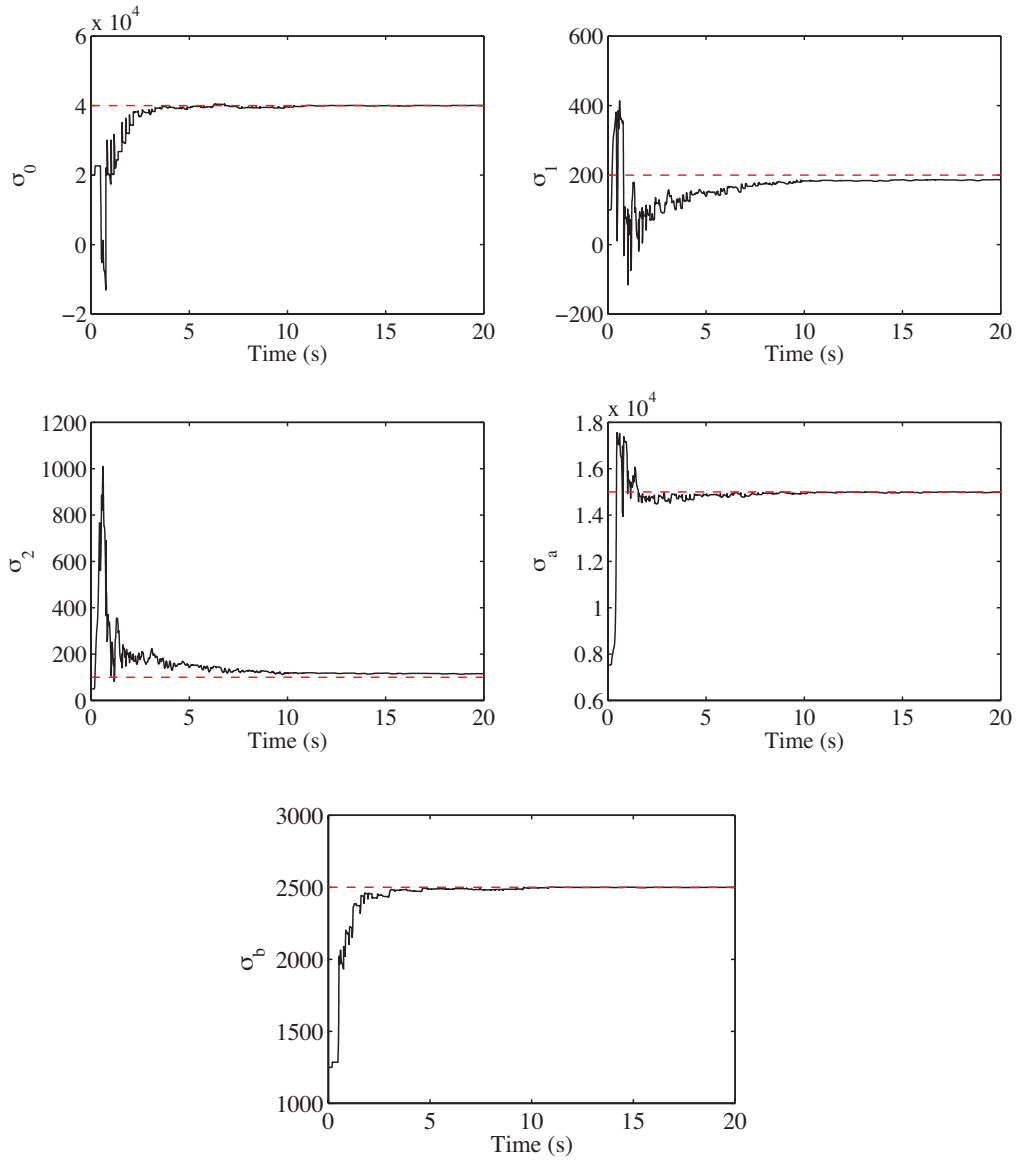

Figure 4.18: Convergence of MR parameter estimates for skyhook control with forward modeling.

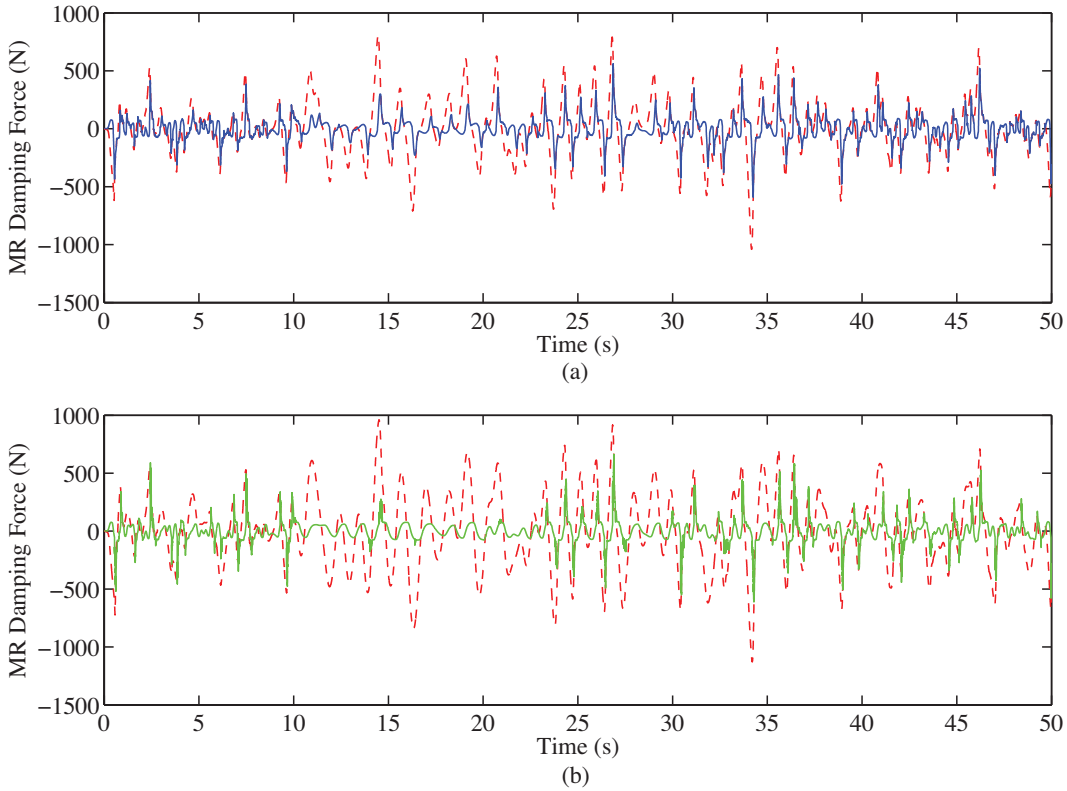

Figure 4.19: Plot of F_A (red, dashed) and F_{MR} versus time for (a) skyhook control with forward modeling (blue, solid) and (b) skyhook control with inverse modeling (green, solid).

4.8 Summary

This study presents a fully adaptive semi-active control algorithm which consists of the adaptive inverse controller compensating for nonlinear hysteresis dynamics of MR damper, and the adaptive reference controller matching the seat response to a reference dynamics even if the mass and spring constants are unknown. The forward modeling or inverse modeling scheme was introduced for realizing the adaptive inverse controller. Validation of the two modeling schemes was examined through identification experiments using an actual MR damper. Conditions for assuring stability of the total control system have been clarified, and the effectiveness of the proposed scheme has been validated in numerical simulation.

4.9 Appendix: Model Validation by Experiments

Experiments for the adaptive identification were made using a small type of MR damper (RD-1097-01) provided by Lord Corp. A laser sensor was placed to measure the displacement x of the piston rod of the MR damper, and a strain sensor was installed in series with the damper to measure the output force F_{MR}. The signals x, v and F_{MR} were sampled at a rate of 1 kHz. The identified forward model has two inputs of velocity $\dot{x}$ and voltage v and one output F_{MR}. The time profiles of the inputs $\dot{x}$ and v applied to the MR damper are illustrated in Figure 4.20. The convergence behavior of the forward model parameters $\hat{\boldsymbol{\theta}}_M$ of the MR damper is plotted in Figure 4.21. The dotted line shows the least squares parameter estimates obtained by batch processing, which are listed in Table 4.3.

To observe the hysteresis characteristics of the MR damper, a sinusoid displacement with amplitude of 1.5cm is applied for three constant voltages 0, 1 and 1.25 V. The measurement results show that the MR damper has a hysteresis behavior between the displacement x and damper force F_{MR} as shown in Figure 4.22(a), and the hysteresis property between F_{MR} and $\dot{x}$ shown in Figure 4.22(b). Figure 4.23(a)(b) gives the estimated hysteresis behavior obtained by the recursive forward modeling with the adaptive observer. The forward model is very precisely identified by the proposed adaptive scheme.

The inverse model with ten adjustable parameters ($m = 4$ and $n = 1$) were also identified using the data set of the two inputs F_{MR} and $\dot{x}$, and one output v. The profiles of the ten inverse model parameters are summarized in Figure 4.24. It can be seen that the inverse model

Table 4.3: Identified model parameters.

Parameters	LS estimate	Initial values
σ_0 [N/m· V]	3.95×10^4	2.90×10^4
σ_1 [N·s/m]	0.131	-
σ_2 [N·s/m]	92.5	8.00
σ_a [N/m]	1.51×10^4	3.50×10^3
σ_b [N·s/(m·V)]	24.9	5.00
a_0 [m^{-1}]	2.85×10^3	2.00×10^4

parameters converge very quickly to the LS estimates obtained by batch processing.

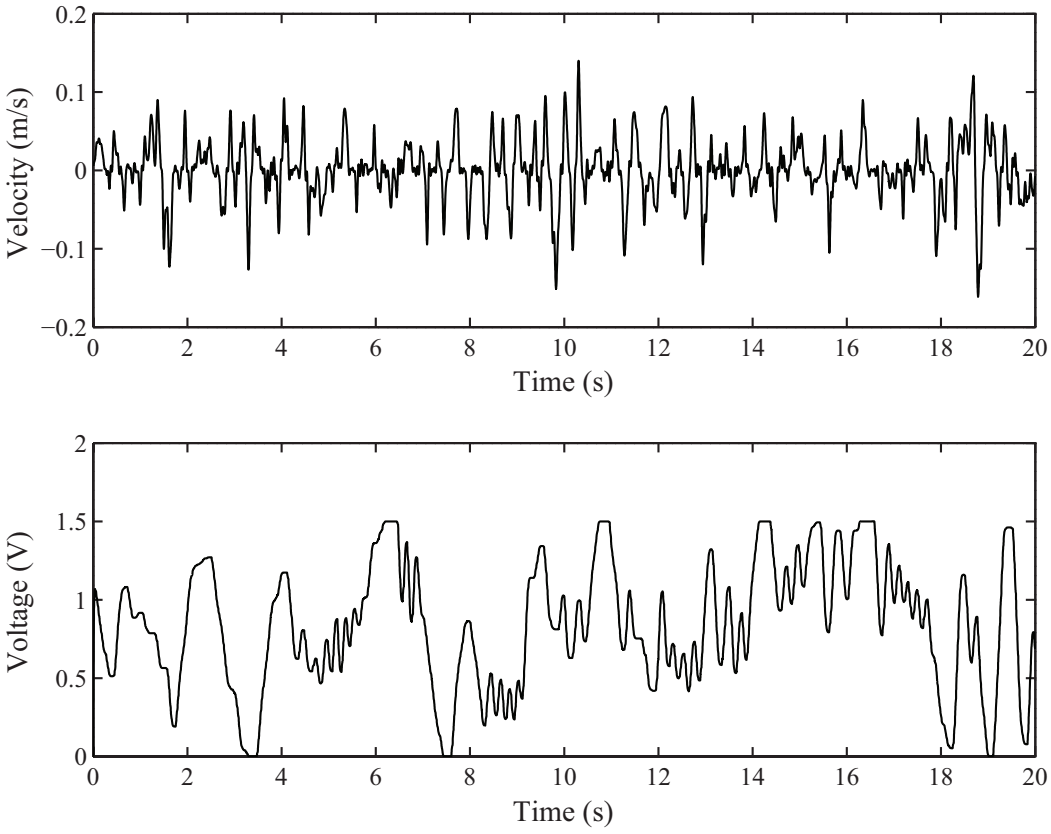

Figure 4.20: Two inputs: voltage and velocity in experiment.

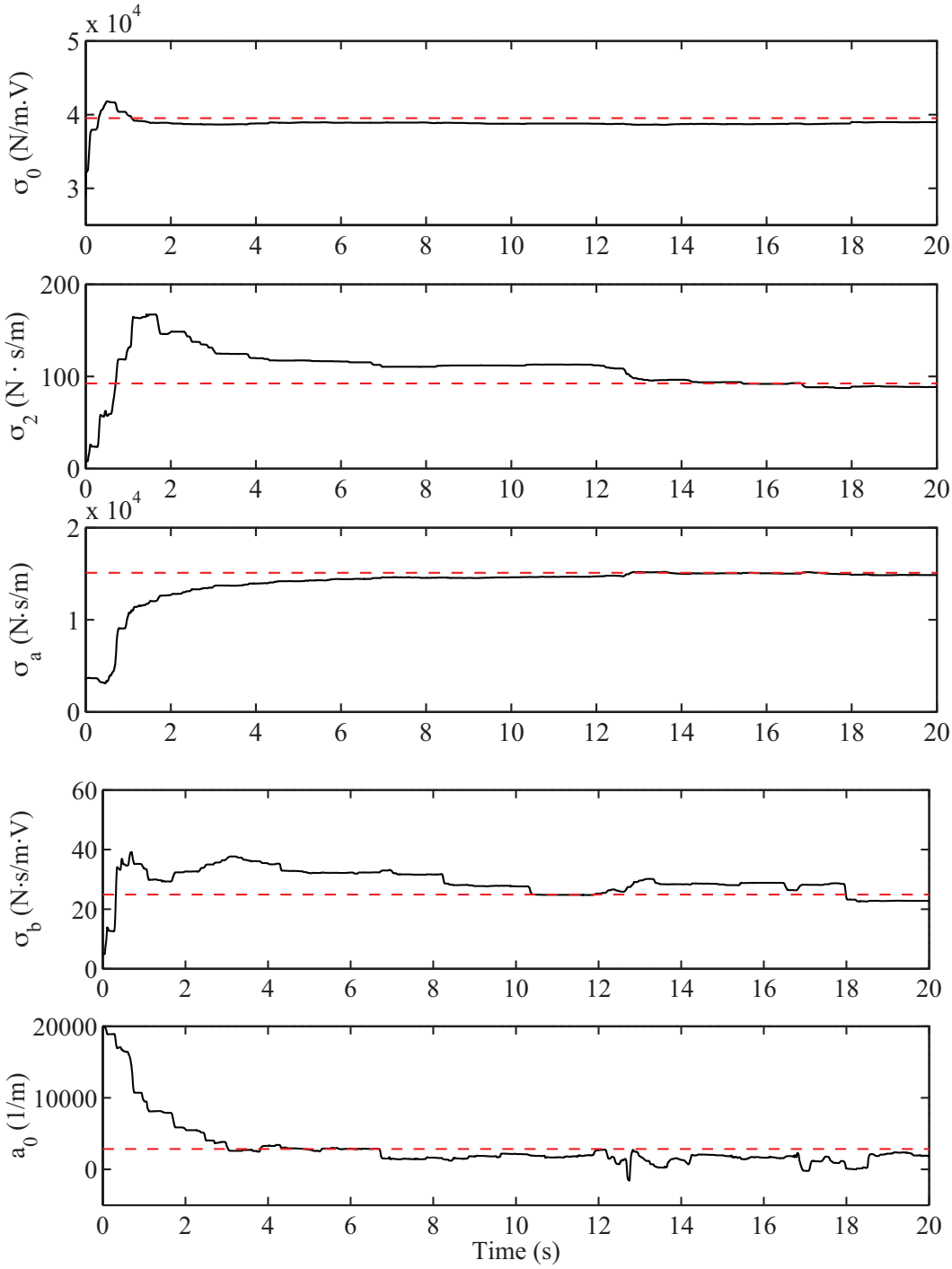

Figure 4.21: Identified forward model parameters.

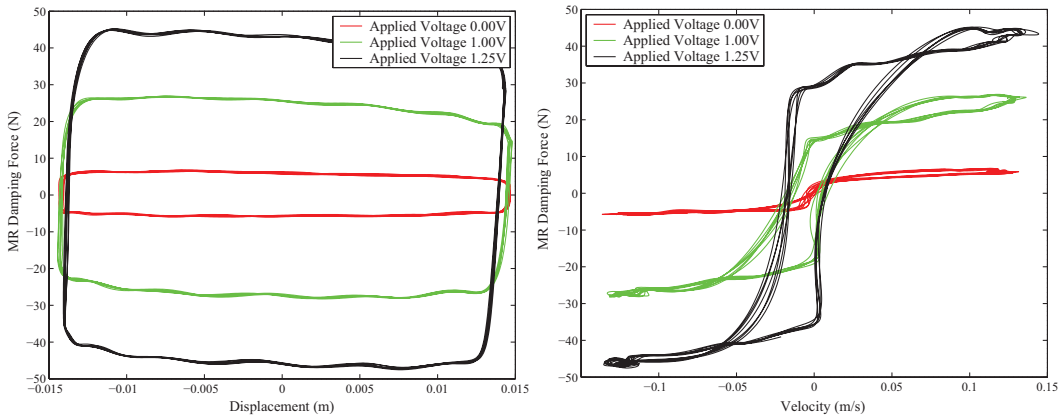

Figure 4.22: Measured hysteresis characteristics of MR damper

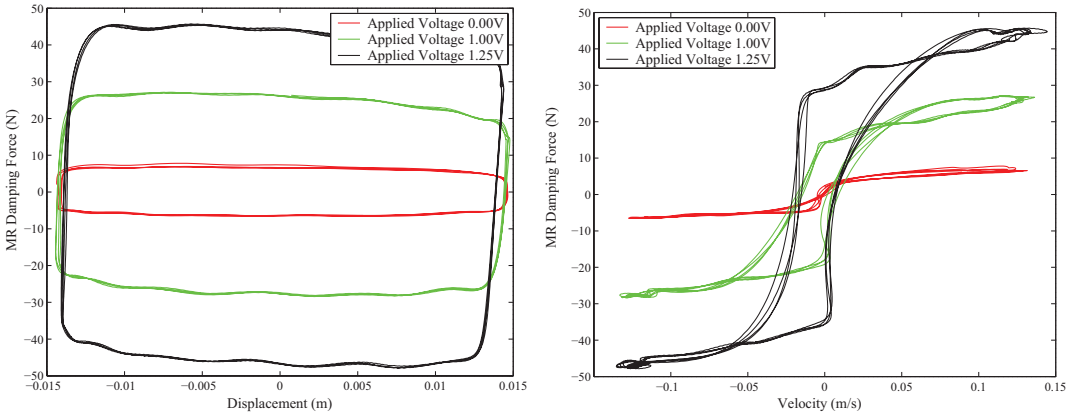

Figure 4.23: Estimated hysteresis characteristics of MR damper with always updated parameters obtained by the proposed adaptive identification method.

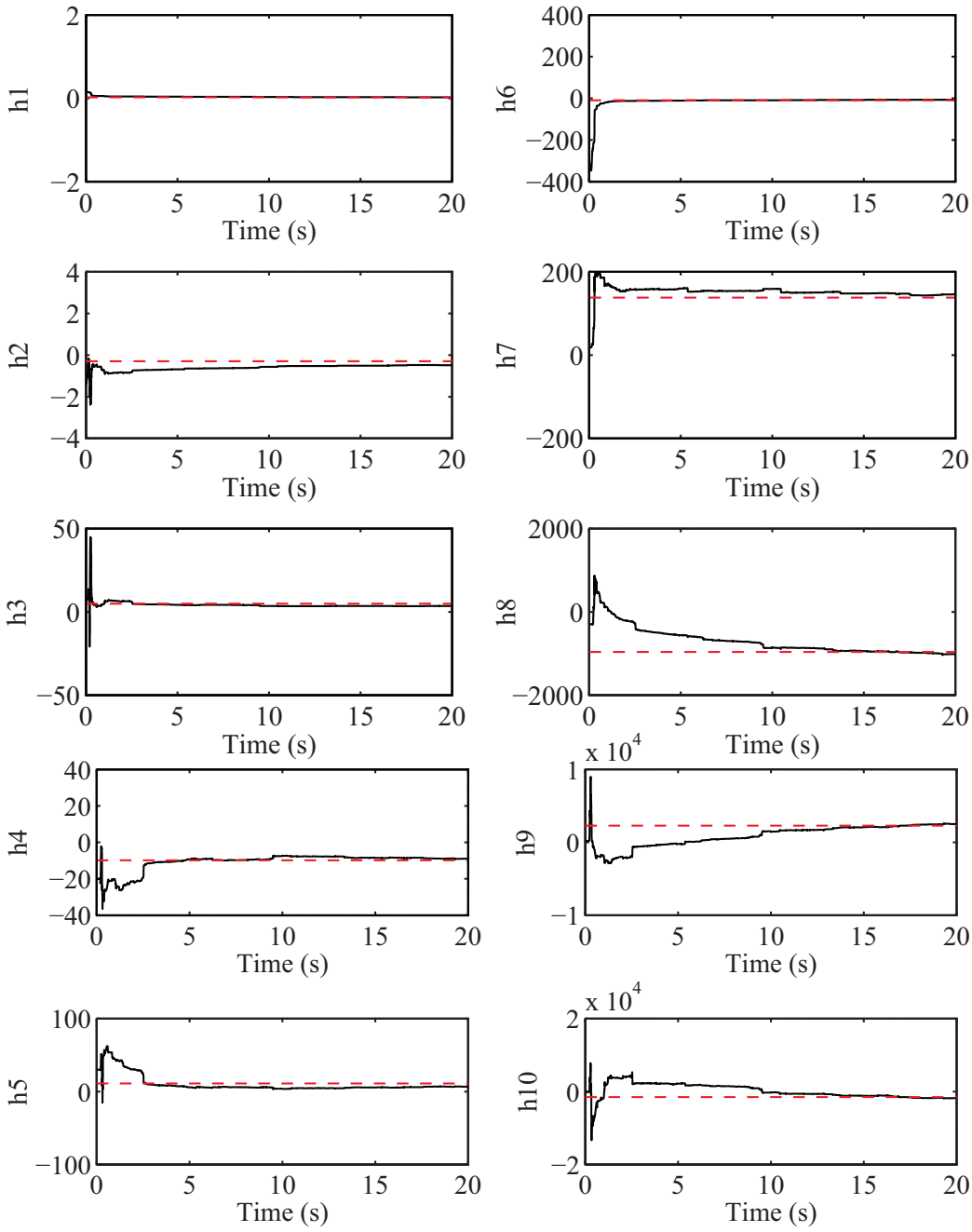

Figure 4.24: Parameter behavior of adaptive inverse controller for compensation of nonlinearity of MR damper.

Chapter 5

Adaptive Friction Compensation

This chapter develops an adaptive friction compensator using the generalized Maxwell-slip (GMS) friction model, with a new, linearly-parameterized Stribeck function. It employs a polynomial equation that is linear-in-the-parameter to approximate the nonlinear Stribeck effect in the GMS model, and simplifies the design of an adaptive friction compensator. The proposed compensator has a switching structure to accomodate for the hybrid nature of the GMS model, and contains a robustifying term to account for unmodelled dynamics. The validity and effectiveness of the proposed, linearly-parameterized friction compensator is verified by simulations for the velocity and position control of an inertia system under the influence of dynamic friction.

5.1 Introduction

It is widely recognized that most mechanical systems involving two or more contact surfaces with relative motion, would experience to varying degrees some form of frictional effects. The presence of dynamic friction in such industrial applications as robotic manipulators, hydraulic systems, precision engineering, and so forth, can lead to significant tracking error, or even instability. Passive friction compensation techniques, such as lubrication, present only a partial solution to the problem, and should be complemented by an effective control scheme [6]. However, the task of controller design is greatly complicated by nonlinearities of the surface contact mechanics, structural and parametric uncertainties.

The demand for an accurate and efficient friction compensation method has led to immense

research efforts from control engineers. Most notably, the works of Armstrong-Hélouvry [4,5], in which important contributions from tribology, lubrication, and physics literatures are restated in a control framework, have generated considerable interest in the friction problem. A comprehensive overview and survey of friction characteristics and classical compensation methods can be found in the references [4, 5, 39]. Traditionally, the friction process is characterized by two regimes: the so-called presliding or micro-slip regime; and the gross sliding regime. Important properties of friction that have been observed include the presliding hysteresis, stick-slip limit cycling, non-local memory, non-drifting property, viscosity, the nonlinear Stribeck effect, static and Coulomb friction. A generic friction model based upon these physical considerations and experimental data has been proposed [1]. Though the generic friction model is highly accurate and captures all the important properties of friction, its mathematical complexity renders it an invalid choice for controller design. However, the generic friction model remains a powerful tool for analyzing the fidelity and accuracy of other friction models, which are classified by their static and dynamic characteristics.

Currently, friction compensation schemes are divided into non-model and model-based methods. Studies have shown that simple PD or PID controllers suffer significant performance degradation due to the nonlinear characteristics of friction, which can lead to hunting behaviors and instability [5]. Several observer-based nonlinear friction compensation scheme have been proposed [20]. Black-box methods employing neural networks or fuzzy logic for friction compensation have also been widely researched [25, 26, 44]. In comparison, the potential of model-based adaptive friction compensation has been demonstrated by several researchers. These efforts include the modeling and compensation of Coulomb friction [3,16], a control scheme for dynamic, linear friction [30], and nonlinear static mapping of the Stribeck effect [31]. These methods provide powerful arguments for the use of adaptive control in friction compensation, but do not combine it with a sufficiently complex and accurate dynamic friction model.

To this end, several dynamic friction models have been developed [7,14], the most popular of which is the LuGre model [11]. Due to its relative simplicity, extensive literature exists regarding the use of the LuGre friction model in various compensation schemes [10, 32, 43]. However, it has been pointed out that the LuGre model compromises fidelity in favor of simplicity. Most notably, the LuGre model does not explicitly account for friction lag characteristics, and its hysteresis-like behavior fails to exhibit non-drifting and non-local memory properties [53].

Therefore, this chapter develops a robust adaptive compensation scheme using the general-

ized Maxwell-slip (GMS) friction model, which has been proposed as a more accurate representation of the friction phenomenon than the LuGre model [2, 29]. The GMS model consists of parallel elementary blocks and separates frictional mechanism into two regimes: sticking and slipping. This results in a hybrid system, with two separate models. Maxwell-slip functions are utilized to describe the hysteresis behavior in the sticking regime. For the slipping regime, a state rate law is employed that includes the Stribeck effect and an explicit term for describing frictional lag characteristics. The GMS model yields results that correspond to experimental observation, while maintaining a simpler structure than the generic friction model [1]. Offline identification algorithms of the GMS model using Nelder-Mead simplex [55] and particle swarm optimization (PSO) [23,24,37] have been presented. However, designing an adaptive controller using the GMS model can be difficult due to its switching nature and also the nonlinear Stribeck effect.

The main novelty of this paper is the proposal of a polynomial Stribeck function that is readily applicable to the GMS friction model. The validity of using a polynomial approximation function to describe the Stribeck effect has been investigated in previous works [8,21,35,36,56]. By using the polynomial approximation function, the development of adaptive control laws are simplified, as friction models can be linearly-parameterized. For the reasons outlined above, the GMS friction model is chosen for the model-based adaptive controller. Previous investigations [35,36] suggest that issues of robustness may occur due to unmodeled dynamics, which include dynamic perturbations, switching uncertainties, and the approximation error of the polynomial equation. Therefore, this study specifically addresses this problem by introducing a sliding-mode based smooth adaptive robustifying term into the control law [47]. Stability analysis is presented to show the robustness of the algorithm, provided that a bound on the unmodeled terms is known to exist. The validity of the proposed robust adaptive control algorithm based upon the GMS friction model is demonstrated by simulation results.

5.2 Problem Statement

The objective of this chapter is the control of a mass acting under the influence of friction forces. Consider the following state-space representation of a simple mass system:

$$m\dot{\boldsymbol{x}}_p = \boldsymbol{A}_p\boldsymbol{x}_p + \boldsymbol{b}_p^T\left(u - F_f\right) \tag{5.1}$$

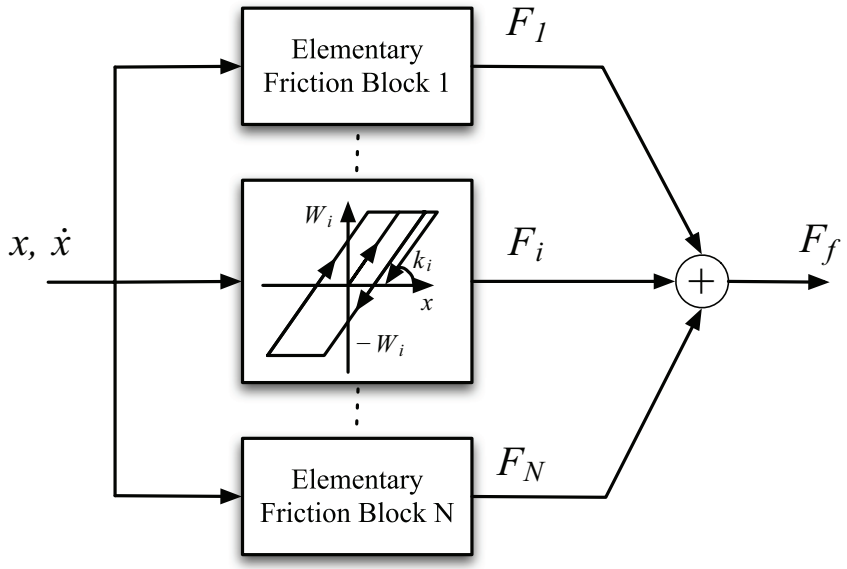

Figure 5.1: Parallel connection of N elementary blocks in the GMS model.

where:

$$\boldsymbol{x}_p = \begin{bmatrix} x & \dot{x} \end{bmatrix}^T, \quad \boldsymbol{A}_p = \begin{bmatrix} 0 & m \\ 0 & 0 \end{bmatrix}, \quad \boldsymbol{b}_p = \begin{bmatrix} 0 & 1 \end{bmatrix}^T$$

Here, m is the mass, while x and $\dot{x}$ are the mass position and velocity, respectively. u is the input force and F_f represents friction. To describe the effects of friction, this study employs the generalized Maxwell-slip (GMS) friction model [2, 29]. The GMS model is an asperity-based description of the friction phenomenon. It consists of parallel connections of elementary blocks, shown in Figure 5.1, and expressed by:

$$F_f = \sum_{i=1}^{N} F_i \tag{5.2}$$

Here, N represents the number of elementary blocks employed by the GMS model, and viscous friction is neglected. Each elementary block is governed by a set of two dynamical equations, depending on whether it is in a sticking or slipping state. The sticking state contains a Maxwell-slip equation to describe hysteresis and other presliding characteristcs. The slipping state equation results in frictional lag and the Stribeck effect. Mathematically, this is expressed as:

- If the elementary block is sticking, the differential equation is given by:

$$\dot{F}_i = k_i \dot{x} \tag{5.3}$$

and the elementary block remains sticking until $|F_i| > \alpha_i s(\dot{x}) = W_i$.

- If the elementary block is slipping, the differential equation is given by:

$$\dot{F}_i = C\left(\alpha_i sgn(\dot{x}) - \frac{F_i}{s(\dot{x})}\right) \tag{5.4}$$

and the elementary block remains slipping until the velocity goes through zero.

Here, C is a constant term introduced by the GMS model to directly account for frictional lag dynamics, and $\sum \alpha_i = 1$. $s(\dot{x})$ describes the Stribeck effect, which is generally expressed by the following function:

$$s(\dot{x}) = F_C + (F_S - F_C)\, e^{-\left(\frac{|\dot{x}|}{V_S}\right)^{\sigma_S}} \tag{5.5}$$

where F_C is the Coulomb friction parameter, F_S represents static friction, V_S is the Stribeck velocity, and σ_S is a shaping factor. Notice the hybrid structure of the GMS model; two separate models are used to represent the sticking and slipping states. From a control perspective, any controller constructed using the GMS model would have to account for this switching structure.

Considering only the slipping state of friction under constant velocity, the steady-state equation for each elementary block reduces to:

$$F_{i,ss} = \alpha_i s(\dot{x}) sgn(\dot{x}) \tag{5.6}$$

Defining $\delta_{i,D} = F_i - F_{i,ss}$, the frictional force equation in the slipping regime becomes:

$$\begin{aligned} F_i &= F_{i,ss} + \delta_{i,D} \\ &= \alpha_i s(\dot{x}) sgn(\dot{x}) + \delta_{i,D} \end{aligned} \tag{5.7}$$

Analysis of the above equation reveals that the friction force is comprised of two terms: a static term corresponding to the Stribeck effect; and a dynamic term $\delta_{i,D}$ that acts as a perturbation.

A Lyapunov argument can be used to show that, given bounds on the parameter values, then the dynamic term $\delta_{i,D}$ is bounded [11,32]. This is formally stated in Lemma 5.1. The stability of the adaptive control design makes use of the consequential property that the dynamic effects are bounded by a constant term.

LEMMA 5.1 *Assuming that the system parameters are bounded, the dynamic perturbations in the slipping state of each elementary block in the GMS friction model are also bounded.*

Proof: Define a candidate Lyapunov function as:

$$V_i = \frac{1}{2}F_i^2 \tag{5.8}$$

Then the derivative of (5.8) along the frictional dynamics is given as:

$$\begin{aligned}\dot{V}_i &= F_i\dot{F}_i \\ &= F_iC\left(\alpha_i sgn(\dot{x}) - \frac{F_i}{s(\dot{x})}\right) \\ &= C\left|F_i\right| sgn(F_i)sgn(\dot{x})\left(\alpha_i - \frac{|F_i|}{s(\dot{x})}\right)\end{aligned} \tag{5.9}$$

In the slipping state, it is noted that the sign of F_i and $\dot{x}$ are always the same and are different from zero. Therefore, $\dot{V}_i$ is negative definite if:

$$|F_i| \leq \alpha_i s(\dot{x}) = |F_{i,ss}| \leq \alpha_i F_S \tag{5.10}$$

From (5.7) and (5.10), it is clear that since F_i and $F_{i,ss}$ are bounded, the perturbation term $\delta_{i,D}$ must also be bounded. □

5.3 Identification of GMS Model

Several offline methods have been proposed to identify the parameters associated with the GMS model. Experimental identification procedures using the Nelder-Mead Simplex algorithm has been presented [55]. Another method is the use of particle swarm optimization (PSO), which is a global minimization technique designed for nonlinear problems that avoids being trapped by local minimums [23, 24]. It is therefore especially suited to the identification of the GMS friction model.

The PSO algorithm can be applied to identify the nonlinear GMS model by considering I particles uniformly distributed across the parameter space. Each particle has its own position, p, transfer vector, q, and the best position visited so far by the particle, p_{best}. All particles share g_{best}, or the best position visited by all the particles so far. In the $(r+1)^{\text{th}}$ transfer, the j^{th} coordinate component of the transfer vector of the i^{th} particle is manipulated according to the following equation:

$$q_{ij}^{r+1} = w \cdot q_{ij}^r + c_1 \cdot rand_1 \cdot \left(p_{best,ij} - p_{ij}^r\right) + c_2 \cdot rand_2 \cdot \left(g_{best,ij} - p_{ij}^r\right) \tag{5.11}$$

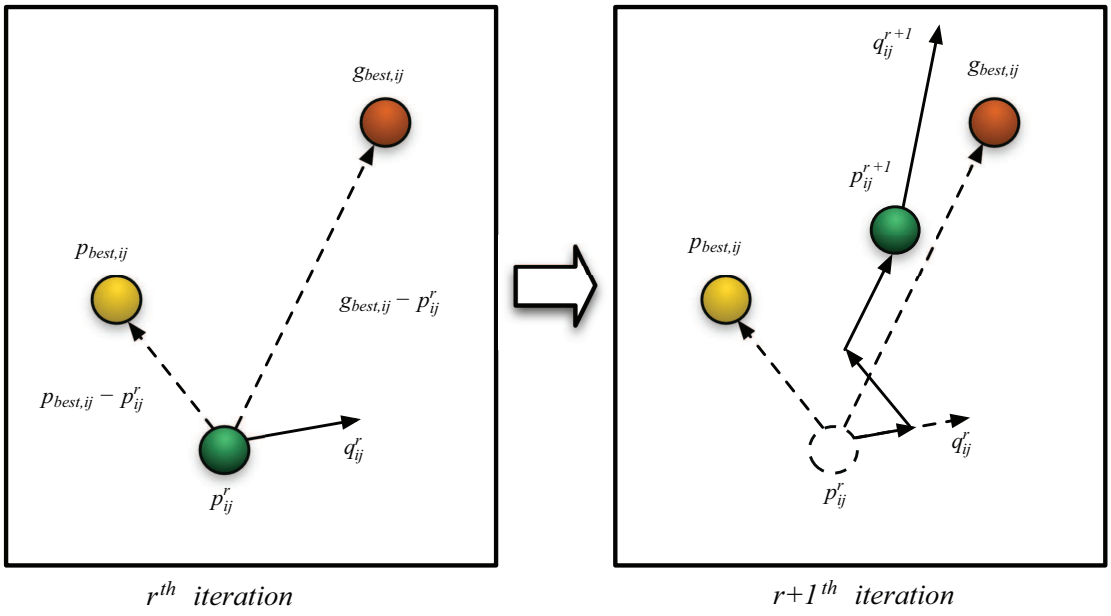

Figure 5.2: Example of particle movement per iteration.

where $i = 1, \cdots, I$, and I is the size of the swarm; $j = 1, \cdots, J$, and J is the size of the space of a given problem, which in this case corresponds to the number of parameters in the GMS model. c_1 and c_2 are positive constants; $rand_1$ and $rand_2$ are random numbers uniformly distributed in $[0, 1]$; and r determines the iteration number. The weighting function w is chosen as:

$$w = w_{\max} - \frac{w_{\max} - w_{\min}}{r_{\max}} \times r \tag{5.12}$$

where $w_{\max}$ and $w_{\min}$ are the initial and final weight, $r_{\max}$ is the maximum iteration number, and r is the current iteration. Then each particle moves according to the following equation:

$$p_{ij}^{r+1} = p_{ij}^r + q_{ij}^{r+1} \tag{5.13}$$

An example of particle movement determined by the PSO algorithm is shown in Figure 5.2. A general flow chart of the PSO is given in Figure 5.3. The identification of the GMS model using the PSO algorithm was explored and presented by the author [37]. It may also be used to determine the required number of elementary blocks to accurately describe the friction process.

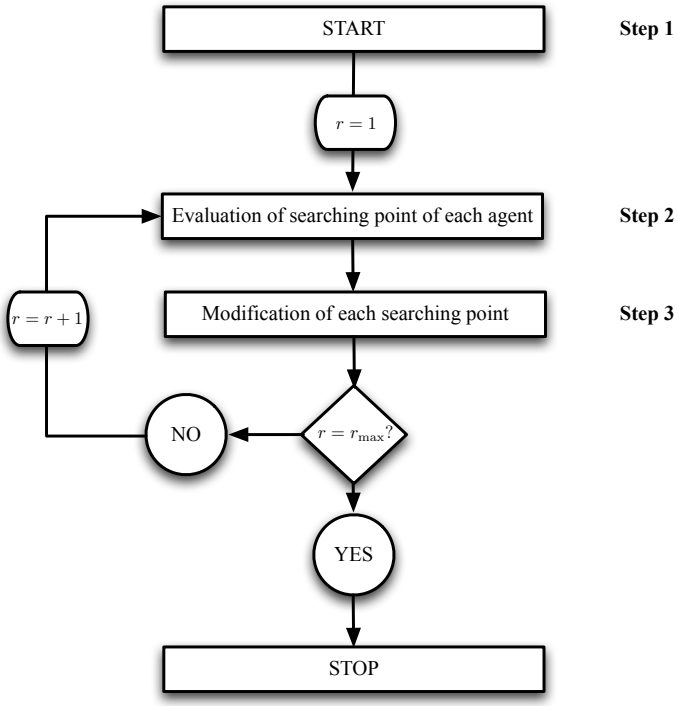

Figure 5.3: A general flow chart of PSO.

5.4 Linearly-Parameterized GMS Model

The GMS model described in the previous section employs a Stribeck function that contains nonlinear parameterization. While each term in (5.5) has a physical meaning, the task of designing an adaptive friction compensator for the resulting nonlinear friction model becomes complicated due to the presence of nonlinearity, which results in control issues such as stability, robustness and convergence. Therefore, this study proposes a new approximator function for the Stribeck effect that is linearly-parameterized and has a polynomial form:

$$s(\dot{x}) = s^*(\dot{x}, n) + \delta_S \tag{5.14}$$

where:

$$\begin{aligned} s^*(\dot{x}, n) &= \beta_1 + \beta_2 |\dot{x}| + \ldots + \beta_n |\dot{x}|^{n-1} \\ &= \sum_{i=1}^{n} \beta_i |\dot{x}|^{i-1} \end{aligned} \tag{5.15}$$

Here, $s^*(\dot{x}, n)$ is the proposed linearly-parameterized approximator function, δ_S is the approximation error, and n is the order of the approximator function. A bound on δ_S on any closed and bounded interval $\Omega_{\dot{x}} = [\dot{x}_{\min}, \dot{x}_{\max}]$ exists and can be expressed as:

$$\sup_{\Omega_{\dot{x}}} |\delta_S| \leq \Delta_S \tag{5.16}$$

The main contribution of this study is that, using this new Stribeck equation, the GMS friction model is linearly-parameterized, allowing for the applications of linear adaptive control theories for compensation.

Employing the linearly-parameterized Stribeck function, each elementary block of the GMS model becomes:

- In the sticking state, the friction force is given as:

$$F_i = \theta_{i,stick}\omega_{stick} \tag{5.17}$$

  where:

$$\begin{aligned} \theta_{i,stick} &= k_i \\ \omega_{stick} &= \int_{t_0}^{t} \dot{x}(\tau)d\tau \end{aligned}$$

  and remains sticking until $|F_i| > \alpha_i(s^*(\dot{x}, n) + \delta_S)$.

- In the slipping state, the friction force is described by:

$$F_i = \boldsymbol{\theta}_{i,slip}^T \boldsymbol{\omega}_{slip} + \alpha_i sgn(\dot{x})\delta_S + \delta_{i,D} \tag{5.18}$$

  where:

$$\begin{aligned} \boldsymbol{\theta}_{i,slip} &= \begin{bmatrix} \alpha_i\beta_1 & \alpha_i\beta_2 & \dots & \alpha_i\beta_n \end{bmatrix}^T \\ &= \begin{bmatrix} \theta_{i,1} & \theta_{i,2} & \dots & \theta_{i,n} \end{bmatrix}^T \\ \boldsymbol{\omega}_{slip} &= sgn(\dot{x}) \cdot \begin{bmatrix} 1 & |\dot{x}| & \dots & |\dot{x}|^{n-1} \end{bmatrix}^T \end{aligned}$$

  and remains slipping until the velocity goes through zero.

This linearly-parameterized friction model is used to construct a suitable adaptive controller for compensation.

To express the two regimes of the GMS model in a unified framework, define the indicator function $\chi[X]$ of the event X as:

$$\chi[X] = \begin{cases} 1 & \text{if } X \text{ is true} \\ 0 & \text{otherwise} \end{cases} \tag{5.19}$$

This allows the expression of the GMS model as:

$$F_f = \boldsymbol{\theta}^T \boldsymbol{\omega} + \sum_{i=1}^{N} \chi_{i,slip} \left(\alpha_i sgn(\dot{x}) \delta_S + \delta_{i,D} \right) \tag{5.20}$$

where:

$$\boldsymbol{\theta} = \begin{bmatrix} \theta_{1,stick} & \dots & \theta_{N,stick} & \boldsymbol{\theta}_{1,slip}^T & \dots & \boldsymbol{\theta}_{N,slip}^T \end{bmatrix}^T$$

$$\boldsymbol{\omega} = \begin{bmatrix} \chi_{1,stick}\omega_{stick} & \dots & \chi_{N,stick}\omega_{stick} & \chi_{1,slip}\boldsymbol{\omega}_{slip}^T & \dots & \chi_{N,slip}\boldsymbol{\omega}_{slip}^T \end{bmatrix}^T$$

$$\chi_{i,stick} = \chi\left[F_i \text{ is sticking}\right]$$

$$\chi_{i,slip} = \chi\left[F_i \text{ is slipping}\right]$$

Notice that $\chi_{i,stick}$ and $\chi_{i,slip}$ are mutually exclusive events that indicate the current state of each elementary block in the GMS model. That is, each elementary block must either be sticking or slipping, but cannot be both, at any given time.

5.5 Adaptive Friction Compensator

This section formulates an adaptive friction compensator that consists of a friction estimator and a linear controller. Using the proposed linearly-parameterized GMS model, a compensator is designed with adaptation for all the linearly-occurring parameters. Perturbations due to the dynamic friction effects, $\delta_{i,D}$, are considered as a disturbance. This study proposes two algorithms for velocity and positional control of a mass acting under the influence of friction as described by the GMS model.

5.5.1 Velocity Control

The structure of the adaptive friction compensator for velocity control is shown in Figure 5.4. The system is given as a mass acting under the influence of friction as described by the GMS

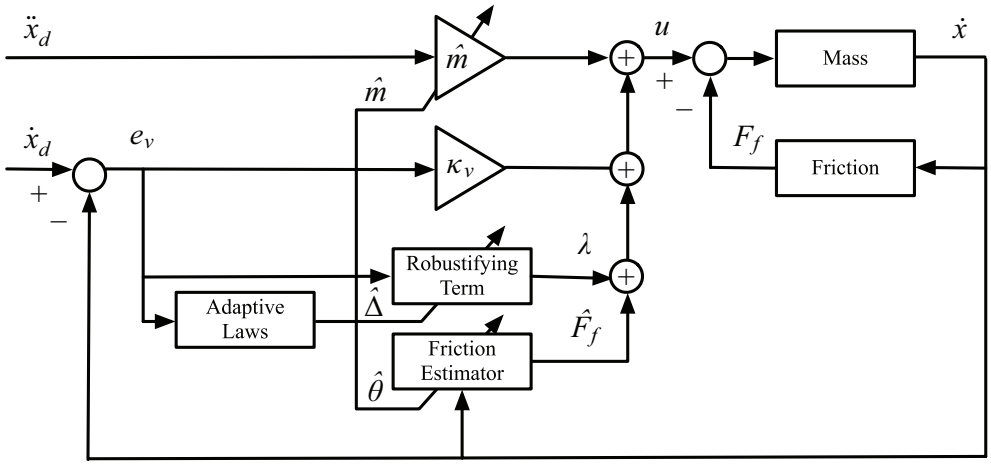

Figure 5.4: Adaptive friction compensator for velocity control.

model. The control objective is the velocity tracking of a desired trajectory defined by $\dot{x}_d$, that is assumed to be designed such that $\ddot{x}_d$ exists and is bounded. A velocity tracking error is stated as:

$$e_v = \dot{x}_d - \dot{x} \tag{5.21}$$

The proposed control law is give as:

$$u = \hat{m}\ddot{x}_d + \kappa_v e_v + \hat{F}_f + \lambda \tag{5.22}$$

where $\hat{m}$ is the estimated value of the mass, and λ is a robustifying term to be defined later. The friction force estimate, $\hat{F}_f$, is defined as:

$$\hat{F}_f = \hat{\boldsymbol{\theta}}^T \hat{\boldsymbol{\omega}} \tag{5.23}$$

where:

$$\hat{\boldsymbol{\theta}} = \left[\hat{\theta}_{1,stick} \quad \dots \quad \hat{\theta}_{N,stick} \quad \hat{\boldsymbol{\theta}}^T_{1,slip} \quad \dots \quad \hat{\boldsymbol{\theta}}^T_{N,slip}\right]^T$$

$$\hat{\boldsymbol{\omega}} = \left[\hat{\chi}_{1,stick}\omega_{stick} \quad \dots \quad \hat{\chi}_{N,stick}\omega_{stick} \quad \hat{\chi}_{1,slip}\boldsymbol{\omega}^T_{slip} \quad \dots \quad \hat{\chi}_{N,slip}\boldsymbol{\omega}^T_{slip}\right]^T$$

$$\hat{\chi}_{i,stick} = \chi\left[\hat{F}_i \text{ is sticking}\right]$$

$$\hat{\chi}_{i,slip} = \chi\left[\hat{F}_i \text{ is slipping}\right]$$

Here $\hat{\boldsymbol{\theta}}$ are the estimates of the parameters of the linearly-parameterized friction model. It is noted that the true GMS friction model can thus be expressed in terms of $\hat{\boldsymbol{\omega}}$ as:

$$F_f = \boldsymbol{\theta}^T \hat{\boldsymbol{\omega}} + \delta \tag{5.24}$$

where:

$$\begin{aligned} \delta &= \delta_{sw} + \sum_{i=1}^{N} \left[\chi_{i,slip} \left(\alpha_i sgn(\dot{x}) \delta_S + \delta_{i,D} \right) \right] \\ \delta_{sw} &= \boldsymbol{\theta}^T \left(\boldsymbol{\omega} - \hat{\boldsymbol{\omega}} \right) \end{aligned} \tag{5.25}$$

Here, δ is an uncertainty term that arises from the switching error between the true GMS model and friction compensator, δ_{sw}, the approximation error δ_S, and dynamic perturbation terms $\delta_{i,D}$. It can easily be shown that Δ is a bounded term. That is:

$$\sup_{\Omega_{\dot{x}}} |\delta| \leq \Delta \tag{5.26}$$

Setting the robustifying term λ as:

$$\lambda = \hat{\Delta} \eta_\Delta \tanh\left((a + bt) e_v \right) \tag{5.27}$$

where $\hat{\Delta}$ is the estimate of Δ, a and b are user-defined positive constants, $\kappa_\Delta > 1$. The parameter estimation errors are defined as:

$$\tilde{m} = \hat{m} - m \tag{5.28}$$

$$\tilde{\boldsymbol{\theta}} = \hat{\boldsymbol{\theta}} - \boldsymbol{\theta} \tag{5.29}$$

$$\tilde{\Delta} = \hat{\Delta} - \Delta \tag{5.30}$$

The adaptive laws are established according to:

$$\dot{\tilde{m}} = \dot{\hat{m}} = \gamma_m \ddot{x}_d e_2 - \sigma_m \gamma_m \hat{m} \tag{5.31}$$

$$\dot{\tilde{\boldsymbol{\theta}}} = \dot{\hat{\boldsymbol{\theta}}} = \boldsymbol{\Gamma}_\theta \hat{\boldsymbol{\omega}} e_v - \sigma_\theta \boldsymbol{\Gamma}_\theta \hat{\boldsymbol{\theta}} \tag{5.32}$$

$$\dot{\tilde{\Delta}} = \dot{\hat{\Delta}} = \gamma_\Delta |e_v| - \sigma_\Delta \gamma_\Delta \hat{\Delta} \tag{5.33}$$

where $\boldsymbol{\Gamma}_\theta$, γ_m, γ_Δ, σ_m, σ_θ and σ_Δ are positive. The main stability result of the proposed method is now presented.

THEOREM 5.1 *Consider the mass system acting under the influence of friction as given in (5.1) and assume that (5.26) holds, but is unknown. The control signal (5.22) together with the adaptive laws (5.31), (5.32), and (5.33), guarantees that Lyapunov function defined as:*

$$V = \frac{1}{2}me_v^2 + \frac{1}{2}\gamma_m^{-1}\tilde{m}^2 + \frac{1}{2}\tilde{\boldsymbol{\theta}}^T\boldsymbol{\Gamma}_\theta^{-1}\tilde{\boldsymbol{\theta}} + \frac{1}{2}\gamma_\Delta^{-1}\tilde{\Delta}^2 \tag{5.34}$$

is uniformly bounded and converges to a small neighborhood of the origin. The same property holds for the error signals e_v, $\tilde{m}$, $\tilde{\boldsymbol{\theta}}$, and $\tilde{\Delta}$.

Proof: Taking the derivative of the candidate Lyapunov function defined by (5.34) and using (5.1) and (5.22):

$$\begin{aligned}
\dot{V} &= me_v\dot{e}_v + \gamma_m^{-1}\tilde{m}\dot{\tilde{m}} + \tilde{\boldsymbol{\theta}}^T\ \boldsymbol{\Gamma}_\theta^{-1}\dot{\tilde{\boldsymbol{\theta}}} + \gamma_\Delta^{-1}\tilde{\Delta}\dot{\tilde{\Delta}} \\
&= e_v\left(m\ddot{x}_d - u + F_f\right) + \gamma_m^{-1}\tilde{m}\dot{\tilde{m}} + \tilde{\boldsymbol{\theta}}^T\ \boldsymbol{\Gamma}_\theta^{-1}\dot{\tilde{\boldsymbol{\theta}}} + \gamma_\Delta^{-1}\tilde{\Delta}\dot{\tilde{\Delta}} \\
&= -\kappa e_v^2 + \tilde{m}\left(\gamma_m^{-1}\dot{\tilde{m}} - \ddot{x}_d e_2\right) + \tilde{\boldsymbol{\theta}}^T\left(\boldsymbol{\Gamma}_\theta^{-1}\dot{\tilde{\boldsymbol{\theta}}} - \hat{\boldsymbol{\omega}}e_v\right) + \Lambda
\end{aligned} \tag{5.35}$$

where:

$$\Lambda = \gamma_\Delta^{-1}\tilde{\Delta}\dot{\tilde{\Delta}} + \delta e_v - \lambda e_v \tag{5.36}$$

Substituting the adaptive laws (5.31) and (5.32):

$$\begin{aligned}
\dot{V} &= -\kappa_v e_v^2 - \sigma_m\tilde{m}\hat{m} - \sigma_\theta\tilde{\boldsymbol{\theta}}^T\hat{\boldsymbol{\theta}} + \Lambda \\
&\leq -\kappa_v e_v^2 - \frac{\sigma_m}{2}\tilde{m}^2 - \frac{\sigma_\theta}{2}\tilde{\boldsymbol{\theta}}^T\tilde{\boldsymbol{\theta}} + \frac{\sigma_m}{2}m^2 + \frac{\sigma_\theta}{2}\boldsymbol{\theta}^T\boldsymbol{\theta} + \Lambda
\end{aligned} \tag{5.37}$$

Using (5.27) and the adaptive law (5.33):

$$\begin{aligned}
\Lambda &= \gamma_\Delta^{-1}\tilde{\Delta}\dot{\tilde{\Delta}} + \delta e_v - \hat{\Delta}\eta_\Delta\tanh\left((a+bt)e_v\right)e_v \\
&= \tilde{\Delta}|e_v| + \delta e_v - \hat{\Delta}\eta_\Delta\tanh\left((a+bt)|e_v|\right)|e_v| - \sigma_\Delta\tilde{\Delta}\hat{\Delta} \\
&\leq \tilde{\Delta}|e_v| + \Delta|e_v| - \hat{\Delta}\eta_\Delta\tanh\left((a+bt)|e_v|\right)|e_v| - \frac{\sigma_\Delta}{2}\tilde{\Delta}^2 + \frac{\sigma_\Delta}{2}\Delta^2 \\
&= \hat{\Delta}|e_v|\left(1 - \eta_\Delta\tanh\left((a+bt)|e_v|\right)\right) - \frac{\sigma_\Delta}{2}\tilde{\Delta}^2 + \frac{\sigma_\Delta}{2}\Delta^2
\end{aligned} \tag{5.38}$$

Note that:

$$1 - \eta_\Delta\tanh\left((a+bt)|e_v|\right) \leq 0 \tag{5.39}$$

if and only if:

$$|e_v| \geq \nu \tag{5.40}$$

where:

$$\nu = \frac{1}{a+bt} \ln\left(\frac{\eta_\Delta + 1}{\eta_\Delta - 1}\right) \tag{5.41}$$

By examining (5.41), it is clear that as $t \to \infty$, $\nu \to 0$ when $\eta_\Delta > 1$. Therefore, (5.40) is satisfied and:

$$\dot{V} \leq -cV + \lambda \tag{5.42}$$

where:

$$c = \min\left\{\frac{2\kappa_v}{m}, \sigma_m\gamma_m, \frac{\sigma_\theta}{\lambda_{\max}(\mathbf{\Gamma}_\theta^{-1})}, \sigma_\Delta\gamma_\Delta\right\} \tag{5.43}$$

$$\lambda = \frac{\sigma_m}{2}m^2 + \frac{\sigma_\theta}{2}\boldsymbol{\theta}^T\boldsymbol{\theta} + \frac{\sigma_\Delta}{2}\Delta^2 \tag{5.44}$$

As $\lambda/c > 0$, (5.42) results in:

$$0 \leq V(t) \leq \lambda/c + (V(0) - \lambda/c)\, e^{-ct} \tag{5.45}$$

Therefore all error signals e_v, $\tilde{m}$, $\tilde{\boldsymbol{\theta}}$ and $\tilde{\Delta}$ are uniformly bounded and converge to a small neighborhood of the origin. □

5.5.2 Positional Control

The structure of the adaptive friction compensator for positional control is shown in Figure 5.5. The system is given as a mass acting under the influence of friction as described by the GMS model. The control objective is the positional tracking of a desired trajectory defined by x_d, that is assumed to be designed such that $\dot{x}_d$ and $\ddot{x}_d$ exist and are bounded. A position tracking error is stated as:

$$e_1 = x_d - x \tag{5.46}$$

The following filtered tracking error is defined to facilitate the subsequent design and analysis:

$$e_2 = \dot{e}_1 + \kappa_1 e_1 \tag{5.47}$$

The proposed control law is give as:

$$u = \hat{m}\ddot{x}_d + \kappa_1 e_2 + e_1 + \hat{m}\kappa_1\dot{e}_1 + \hat{F}_f + \lambda \tag{5.48}$$

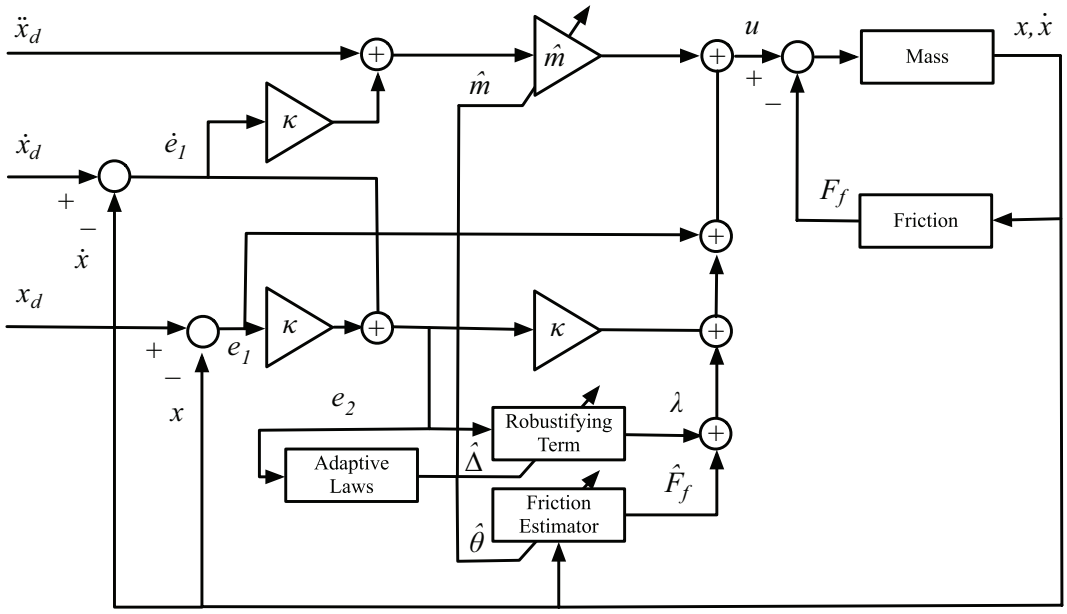

Figure 5.5: Adaptive friction compensator for position control.

where $\hat{m}$ is the estimated value of the mass, and λ is a robustifying term to be defined later. The friction force estimate, $\hat{F}_f$, is defined similar to the previous section as:

$$\hat{F}_f = \hat{\boldsymbol{\theta}}^T \hat{\boldsymbol{\omega}} \tag{5.49}$$

Here $\hat{\boldsymbol{\theta}}$ are the estimates of the parameters of the linearly-parameterized friction model. Define the robustifying term λ as:

$$\lambda = \hat{\Delta}\eta_\Delta \tanh\left((a+bt)e_2\right) \tag{5.50}$$

where $\hat{\Delta}$ is the estimate of Δ, a and b are user-defined positive constants, $\kappa_\Delta > 1$. The parameter estimation errors are defined as:

$$\tilde{m} = \hat{m} - m \tag{5.51}$$

$$\tilde{\boldsymbol{\theta}} = \hat{\boldsymbol{\theta}} - \boldsymbol{\theta} \tag{5.52}$$

$$\tilde{\Delta} = \hat{\Delta} - \Delta \tag{5.53}$$

The adaptive laws are established according to:

$$\dot{\tilde{m}} = \dot{\hat{m}} = \gamma_m \left(\ddot{x}_d + \kappa \dot{e}_1\right) e_2 - \sigma_m \gamma_m \hat{m} \tag{5.54}$$

$$\dot{\tilde{\boldsymbol{\theta}}} = \dot{\hat{\boldsymbol{\theta}}} = \boldsymbol{\Gamma}_\theta \hat{\boldsymbol{\omega}} e_2 - \sigma_\theta \boldsymbol{\Gamma}_\theta \hat{\boldsymbol{\theta}} \tag{5.55}$$

$$\dot{\tilde{\Delta}} = \dot{\hat{\Delta}} = \gamma_\Delta |e_2| - \sigma_\Delta \gamma_\Delta \hat{\Delta} \tag{5.56}$$

where $\mathbf{\Gamma}_\theta$, γ_m, γ_Δ, σ_m, σ_θ and σ_Δ are positive. The main stability result of the proposed method is now presented.

THEOREM 5.2 *Consider the mass system acting under the influence of friction as given in (5.1) and assume that (5.26) holds, but is unknown. The control signal (5.48) together with the adaptive laws (5.54), (5.55), and (5.56), guarantees that Lyapunov function defined as:*

$$V = \frac{1}{2}e_1^2 + \frac{1}{2}me_2^2 + \frac{1}{2}\gamma_m^{-1}\tilde{m}^2 + \frac{1}{2}\tilde{\boldsymbol{\theta}}^T\mathbf{\Gamma}_\theta^{-1}\tilde{\boldsymbol{\theta}} + \frac{1}{2}\gamma_\epsilon^{-1}\tilde{\Delta}^2 \tag{5.57}$$

is uniformly bounded and converges to a small neighborhood of the origin. The same property holds for the error signals e_1, e_2, $\tilde{m}$, $\tilde{\boldsymbol{\theta}}$, and $\tilde{\Delta}$.

Proof: By examining (5.46) and (5.47), it is noted that:

$$\dot{e}_1 = -\kappa e_1 + e_2 \tag{5.58}$$

$$\dot{e}_2 = \ddot{e}_1 + \kappa\dot{e}_1 \tag{5.59}$$

Taking the derivative of the candidate Lyapunov function defined by (5.57) and using (5.1) and (5.48):

$$\begin{aligned}
\dot{V} &= e_1\dot{e}_1 + me_2\dot{e}_2 + \gamma_m^{-1}\tilde{m}\dot{\tilde{m}} + \tilde{\boldsymbol{\theta}}^T\,\mathbf{\Gamma}_\theta^{-1}\dot{\tilde{\boldsymbol{\theta}}} + \gamma_\Delta^{-1}\tilde{\Delta}\dot{\tilde{\Delta}} \\
&= -\kappa e_1^2 + e_1e_2 + e_2\left(m\ddot{x}_d - u + F_f + m\kappa\dot{e}_1\right) + \gamma_m^{-1}\tilde{m}\dot{\tilde{m}} + \tilde{\boldsymbol{\theta}}^T\,\mathbf{\Gamma}_\theta^{-1}\dot{\tilde{\boldsymbol{\theta}}} + \gamma_\Delta^{-1}\tilde{\Delta}\dot{\tilde{\Delta}} \\
&= -\kappa e_1^2 - \kappa e_2^2 + \tilde{m}\left(\gamma_m^{-1}\dot{\tilde{m}} - \left(\ddot{x}_d + \kappa\dot{e}_1\right)e_2\right) + \tilde{\boldsymbol{\theta}}^T\left(\mathbf{\Gamma}_\theta^{-1}\dot{\tilde{\boldsymbol{\theta}}} - \hat{\boldsymbol{\omega}}e_2\right) + \Lambda
\end{aligned} \tag{5.60}$$

where:

$$\Lambda = \gamma_\Delta^{-1}\tilde{\Delta}\dot{\tilde{\Delta}} + \delta e_2 - \lambda e_2 \tag{5.61}$$

Substituting the adaptive laws (5.54) and (5.55):

$$\begin{aligned}
\dot{V} &= -\kappa e_1^2 - \kappa e_2^2 - \sigma_m\tilde{m}\hat{m} - \sigma_\theta\tilde{\boldsymbol{\theta}}^T\hat{\boldsymbol{\theta}} + \Lambda \\
&\leq -\kappa e_1^2 - \kappa e_2^2 - \frac{\sigma_m}{2}\tilde{m}^2 - \frac{\sigma_\theta}{2}\tilde{\boldsymbol{\theta}}^T\tilde{\boldsymbol{\theta}} + \frac{\sigma_m}{2}m^2 + \frac{\sigma_\theta}{2}\boldsymbol{\theta}^T\boldsymbol{\theta} + \Lambda
\end{aligned} \tag{5.62}$$

Using (5.50) and the adaptive law (5.56):

$$\begin{aligned}
\Lambda &= \gamma_\Delta^{-1}\tilde{\Delta}\dot{\tilde{\Delta}} + \delta e_2 - \hat{\Delta}\eta_\Delta\tanh\left((a+bt)e_2\right)e_2 \\
&= \tilde{\Delta}|e_2| + \delta e_2 - \hat{\Delta}\eta_\Delta\tanh\left((a+bt)|e_2|\right)|e_2| - \sigma_\Delta\tilde{\Delta}\hat{\Delta} \\
&\leq \tilde{\Delta}|e_2| + \Delta|e_2| - \hat{\Delta}\eta_\Delta\tanh\left((a+bt)|e_2|\right)|e_2| - \frac{\sigma_\Delta}{2}\tilde{\Delta}^2 + \frac{\sigma_\Delta}{2}\Delta^2 \\
&= \hat{\Delta}|e_2|\left(1 - \eta_\Delta\tanh\left((a+bt)|e_2|\right)\right) - \frac{\sigma_\Delta}{2}\tilde{\Delta}^2 + \frac{\sigma_\Delta}{2}\Delta^2
\end{aligned} \tag{5.63}$$

Note that:

$$1 - \eta_\Delta \tanh\left((a+bt)|e_2|\right) \leq 0 \tag{5.64}$$

if and only if:

$$|e_2| \geq \nu \tag{5.65}$$

where:

$$\nu = \frac{1}{a+bt} \ln\left(\frac{\eta_\Delta + 1}{\eta_\Delta - 1}\right) \tag{5.66}$$

By examining (5.66), it is clear that as $t \to \infty$, $\nu \to 0$ when $\kappa_\Delta > 1$. Therefore, (5.65) is satisfied and:

$$\dot{V} \leq -cV + \lambda \tag{5.67}$$

where:

$$c = \min\left\{2\kappa, \frac{2\kappa}{m}, \sigma_m\gamma_m, \frac{\sigma_\theta}{\lambda_{\max}(\boldsymbol{\Gamma}_\theta^{-1})}, \sigma_\Delta\gamma_\Delta\right\} \tag{5.68}$$

$$\lambda = \frac{\sigma_m}{2}m^2 + \frac{\sigma_\theta}{2}\boldsymbol{\theta}^T\boldsymbol{\theta} + \frac{\sigma_\Delta}{2}\Delta^2 \tag{5.69}$$

As $\lambda/c > 0$, (5.67) results in:

$$0 \leq V(t) \leq \lambda/c + \left(V(0) - \lambda/c\right)e^{-ct} \tag{5.70}$$

Therefore all error signals e_1, e_2, $\tilde{m}$, $\tilde{\boldsymbol{\theta}}$ and $\tilde{\Delta}$ are uniformly bounded and converge to a small neighborhood of the origin. □

5.6 Simulation Results

Simulation results are presented to illustrate the validity of the proposed linearly-parameterized GMS model in compensating for frictional dynamics. First, procedures for identifying and determining the appropriate number of elementary blocks in the GMS model using PSO is discussed. An analysis is conducted on the accuracy of the polynomial Stribeck function in describing the Stribeck effect. The effectiveness of the proposed adaptive friction compensator is then demonstrated by examining the tracking performance for velocity and position trajectories.

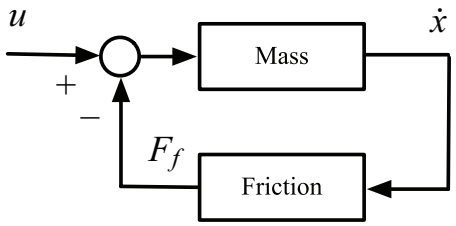

Figure 5.6: Data acquisition for PSO identification process.

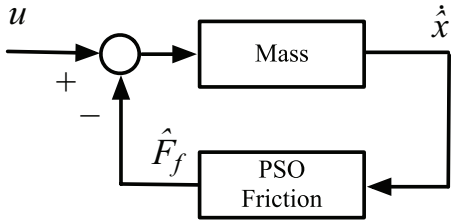

Figure 5.7: Evaluation of each particle in the swarm.

5.6.1 Identification of GMS Model Parameters

A vital component of constructing the adaptive friction compensator is determining initial parameter estimates and the required number of elementary blocks in the GMS model that accurately captures frictional characteristics. Using offline optimization methods and available measurements, the number of elementary blocks can be chosen to provide accuracy while minimizing the number of parameters. One possible method is the PSO algorithm, which has been explored for identifying the GMS model [37].

A data acquisition experiment is performed by subjecting the mass-friction system to a random force input, u, and measuring the resulting velocity, $\dot{x}$. The same input u is then injected into a simulation consisting of the estimated system candidates, whose parameters are defined by the position of each particle in the PSO swarm. This yields a velocity profile $\dot{\hat{x}}_i$ for particles $i = 1, \ldots, I$. This process is illustrated in Figures 5.6 and 5.7. The PSO algorithm as outlined in the previous section is used to minimize the following mean-square performance index when only the velocity is measurable:

$$J_i = \frac{1}{T} \sum_{t=0}^{T} \left(\dot{x}(t) - \dot{\hat{x}}_i(t) \right)^2 \tag{5.71}$$

where T is the total number of data samples. The random force input and resulting measured velocity used for PSO identification in this study is shown in Figure 5.8. The true GMS friction

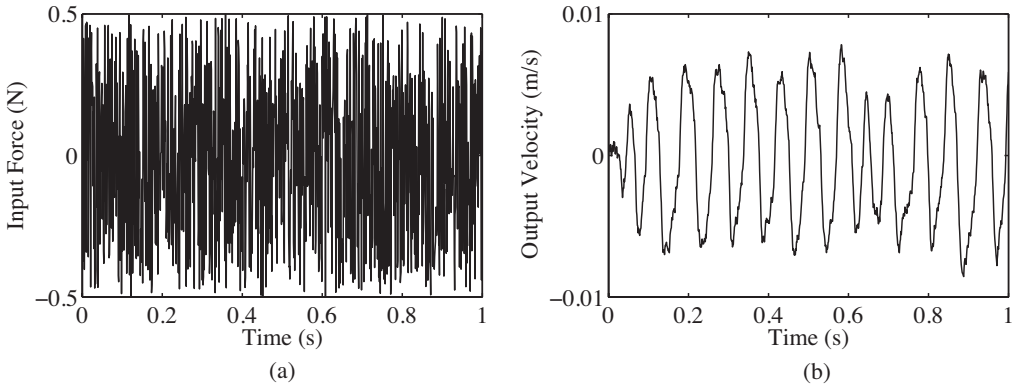

Figure 5.8: (a) Random force input u and (b) resulting velocity profile for PSO identification.

model is comprised of four elementary blocks with the parameters as given in Table 5.1. Using the PSO algorithm with a population size of $I = 50$, and a maximum number of iteration as $r_{\max} = 50$, the other PSO parameters are set as:

$$w_{\max} = 0.9, \quad w_{\min} = 0.4, \quad c_1 = 1, \quad c_2 = 1 \tag{5.72}$$

It is assumed that the true number of elementary blocks is unknown. Therefore, PSO identification is conducted for various numbers of elementary blocks, ranging from one to six, and a comparison of the best achievable performance index after 50 iterations is shown in Figure 5.9. It is noted that the PSO algorithm accurately determined the number of elementary blocks of the GMS model to be four. The identified GMS model parameters are compared to the true values in Table 5.1.

5.6.2 Determination of Stribeck Approximation Function

This section deals with the determination of the linearly-parameterized Stribeck function and analysis of its accuracy in describing the Stribeck effect. The nonlinear Stribeck function is assumed to be described by (5.5), with the following parameters:

$$\begin{aligned} &F_S = 1.05 \text{ [N]}, \;\; \mathrm{F_C} = 0.2 \text{ [N]} \\ &V_S = 98 \times 10^{-5} \text{ [m/s]}, \;\; \sigma_{\mathrm{S}} = 0.78 \end{aligned} \tag{5.73}$$

The approximation of this function by the proposed polynomial Stribeck equation is accomplished by using off-line, least-square, curve fitting technique. The identification process was

Table 5.1: True and identified parameter values of GMS model

Parameter	Identified	True	Parameter	Identified	True
C	26	24	α_1	0.30	0.25
F_S [N]	1.04	1.05	α_2	0.22	0.25
F_C [N]	0.20	0.20	α_3	0.27	0.25
V_S [m/s]	0.99×10^{-5}	0.98×10^{-5}	α_4	0.21	0.25
σ_S	0.80	0.78	k_1 [N/m]	1.16×10^4	1.00×10^4
			k_2 [N/m]	0.61×10^4	0.70×10^4
			k_3 [N/m]	0.44×10^4	0.50×10^4
			k_4 [N/m]	0.21×10^4	0.30×10^4

conducted for various orders of the linearly-parameterized Stribeck function to determine a model order that provides good trade-off between modeling accuracy and minimal parameters. This will be used to construct the adaptive friction compensator. The mapping of the nonlinear Stribeck function is conducted for all the velocity corresponding to the desired operational range.

Figure 5.10(a) illustrates the Stribeck effect. The model order for the linearly-parameterized function is varied from 1 to 10. The resulting modeling error is shown in Figure 5.10(b). Based upon these results, it is determined that $n = 4$ provides a good approximation of the nonlinear Stribeck function while maintaining a small amount of parameters. From this observation, the friction compensator proposed in this reserach is constructed using a linearly-parameterized Stribeck function of order 4.

5.6.3 Performance of Adaptive Controller

The effectiveness of the proposed adaptive controllers is illustrated for velocity and position trajectory signals. The frictional dynamics are chosen to be governed by four elementary blocks. Experimental investigations have determined that a GMS model constructed with four elementary blocks is sufficient to accurately capture frictional characteristics under realistic conditions [2,55]. The results indicate that increasing the number of elementary block does not

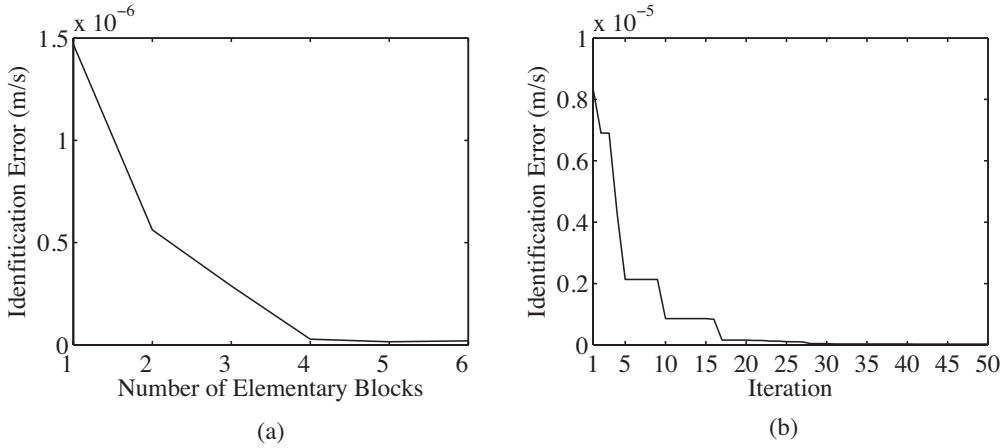

Figure 5.9: (a) Best achievable performance index for various elementary blocks after 50 iterations; and (b) evolution of the performance index for four elementary blocks using PSO.

serve to improve the modeling accuracy. The system parameters are given as:

$$\begin{aligned} &m = 1\ [\text{kg}],\ \ \text{C} = 24\ [\text{N/s}] \\ &k_1 = 1.0\times 10^4\ [\text{N/m}],\ \ \text{k}_2 = 0.7\times 10^4\ [\text{N/m}] \\ &k_3 = 0.5\times 10^4\ [\text{N/m}],\ \ \text{k}_4 = 0.3\times 10^4\ [\text{N/m}] \\ &\alpha_1 = \alpha_2 = \alpha_3 = \alpha_4 = 0.25 \end{aligned} \tag{5.74}$$

For the Stribeck effect described by the parameters given in (5.73), the coefficients of the proposed polynomial Stribeck function with a model order of four is determined as outlined above, and is given in Table 5.2.

Velocity Control

In this section, simulation results for velocity control using the proposed adaptive friction compensator is presented. The gains κ_v and κ_Δ are chosen as:

$$\kappa_v = 200,\ \ \kappa_\Delta = 2000 \tag{5.75}$$

The performance of the proposed adaptive controller is evaluated for the trajectory tracking of a random step velocity signal, and is compared to a PD controller with the following gains:

$$k_P = 40000,\ \ k_D = 200 \tag{5.76}$$

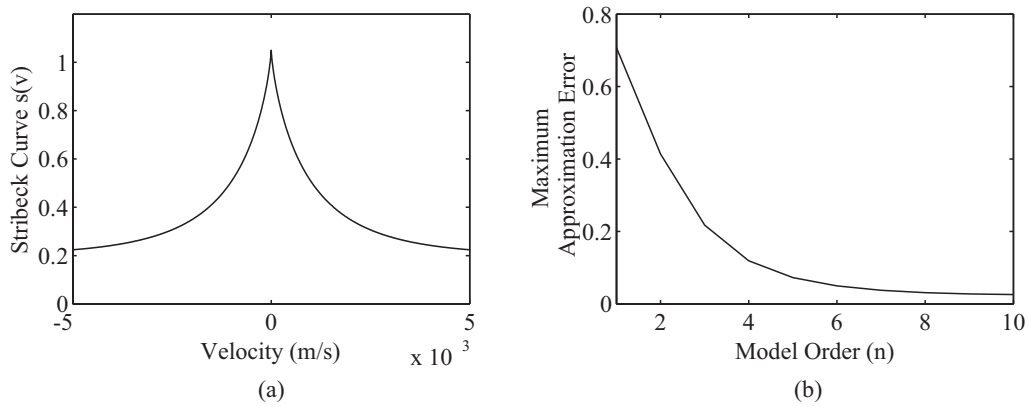

Figure 5.10: (a) The Stribeck curve; and (b) approximation error of the Stribeck curve for various model order.

The convergence of the polynomial Stribeck parameters and the Maxwell-slip parameters, when the reference trajectory satisfies the persistently exciting condition, are shown in Figures 5.11 and 5.12 respectively. This is compared to the true values in Table 5.2. The robustifying term $\hat{\Delta}$ is also shown in Figure 5.12. Using these converged estimates, trajectory tracking performances of the proposed adaptive controller and the PD controller are compared in Figure 5.13 for a random step velocity trajectory. It is noted that Figure 5.13 shows the effectiveness of the proposed adaptive algorithm after convergence in achieving trajectory tracking. The PD controller also provides acceptable tracking, but exhibits steady-state error in the low-velocity region, where the Stribeck effect results in a high frictional force. This suggests that the PD controller may not be suitable for position tracking, as random step position signals would operate mainly in the zero velocity region. This observation is confirmed in the following section that deals with positional control. The improvement in tracking performances offered by the proposed adaptive friction compensation scheme over conventional PD controllers can also be shown by comparing the RMS error. The RMS tracking error for the conventional PD controller during the entire simulation is 1.27×10^{-4} m/s, while the RMS tracking error for the proposed adaptive algorithm is merely 0.24×10^{-4} m/s. The ability of the proposed algorithm to estimate and compensate for friction forces is further illustrated in Figure 5.14, which shows the true and estimated friction force for the random step trajectory. The results clearly show the effectiveness of the proposed adaptive friction compensator in achieving velocity trajectory tracking and friction estimation despite modeling uncertainties.

Table 5.2: Initial, converged and LS/True parameter values.

Parameter	Initial	Converged	LS/True
β_1	0.3	0.8845	0.9200
β_2	0	-482.2020	-516.1794
β_3	0	1.31×10^5	1.37×10^5
β_4	0	-1.24×10^7	-1.24×10^7
k_1 [N/m]	1.50×10^4	0.86×10^4	1.00×10^4
k_2 [N/m]	1.05×10^4	0.66×10^4	0.70×10^4
k_3 [N/m]	0.75×10^4	0.45×10^4	0.50×10^4
k_4 [N/m]	0.45×10^4	0.32×10^4	0.30×10^4

Positional Control

This section presents the simulation results of the proposed adaptive friction compensator for position control. The gains κ_1 and κ_Δ are chosen as:

$$\kappa_1 = 200, \;\; \kappa_\Delta = 2000 \tag{5.77}$$

Similar to the previous section, the results of the proposed adaptive controller is compared to a PD controller with the following gains:

$$k_P = 40000, \;\; k_D = 200 \tag{5.78}$$

Another result using a conventional PID controller is also presented, with the gains set as:

$$k_P = 40000, \;\; k_I = 400000, \;\; k_D = 200 \tag{5.79}$$

The convergence of the polynomial Stribeck parameters and the Maxwell-slip parameters, when the reference trajectory satisfies the persistently exciting condition, are similar to those shown in Figures 5.11 and 5.12. In this section, the performance of the proposed adaptive controller is evaluated for the trajectory tracking of a random step and ramp position signal. Using the converged estimates, trajectory tracking performances of the proposed adaptive controller, conventional PD and PID controllers are compared in Figures 5.15 and 5.16. It is noted that Figure 5.15 shows the effectiveness of the proposed adaptive algorithm after convergence in achieving

trajectory tracking of a random step signal. The PD controller, however, exhibits considerable steady-state tracking error. The PID controller eliminates this steady-state error for a step signal. However, by examining Figure 5.16, it is seen that both the PD and PID controllers yield unacceptable tracking results for a ramp trajectory. In particular, the tendencies of these controllers to cause limit-cycling due to the stick-slip effect and integral wind-up is evident. This is compared to the proposed adaptive friction compensator, which effectively achieves position tracking for both random step and ramp trajectories despite modeling uncertainties.

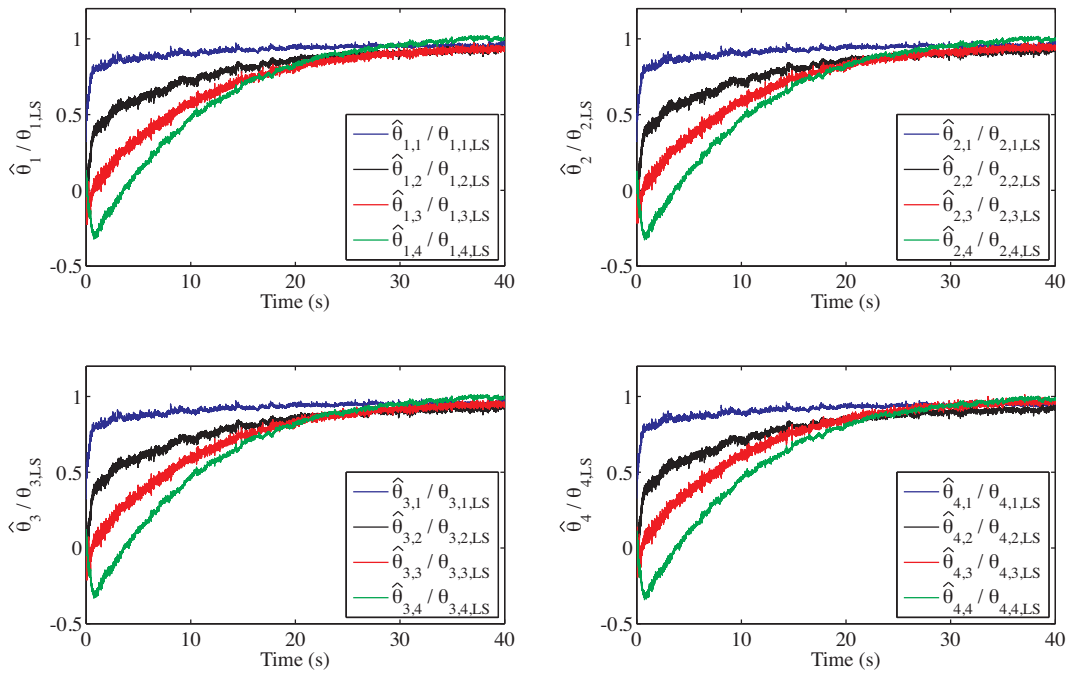

Figure 5.11: Convergence of linearly-parameterized Stribeck function coefficients.

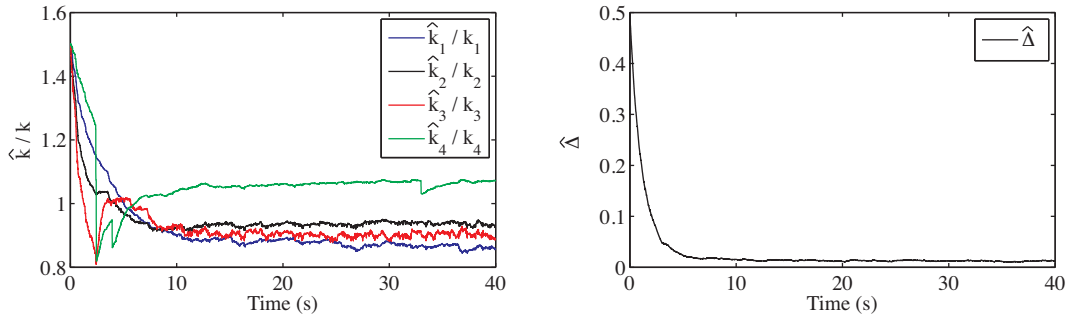

Figure 5.12: Convergence of Maxwell-slip parameters and $\hat{\Delta}$.

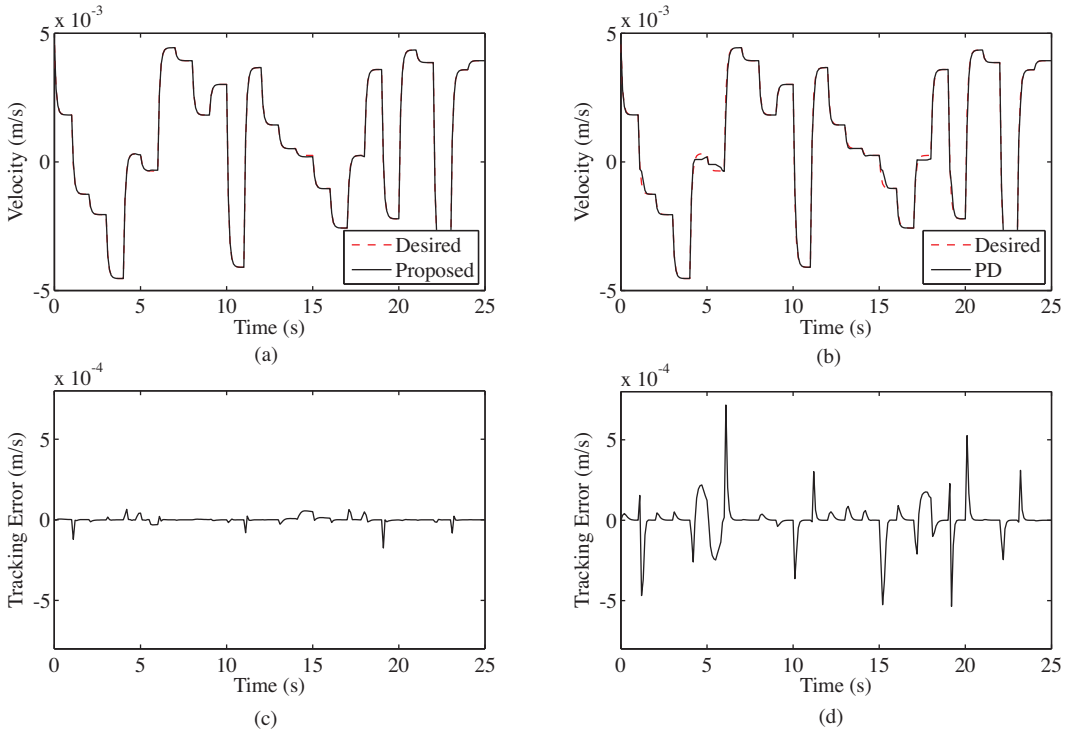

Figure 5.13: Comparison for velocity tracking performance of proposed controller after convergence and PD controller.

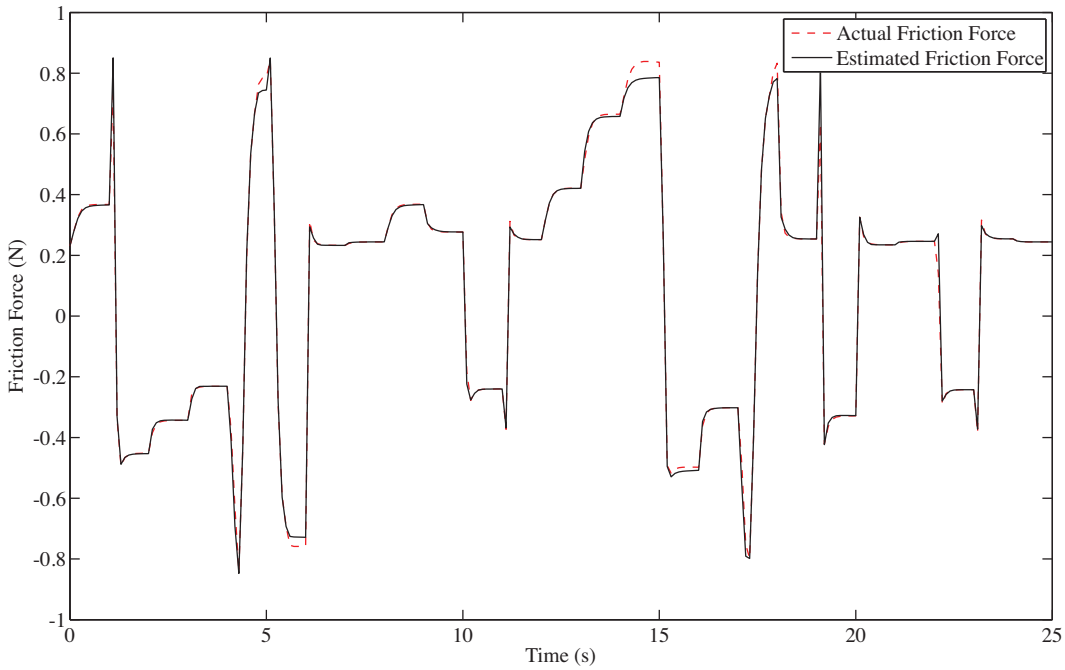

Figure 5.14: Friction estimation for random step signal. True friction force is given by the thin line, while estimated force is shown by the thick line.

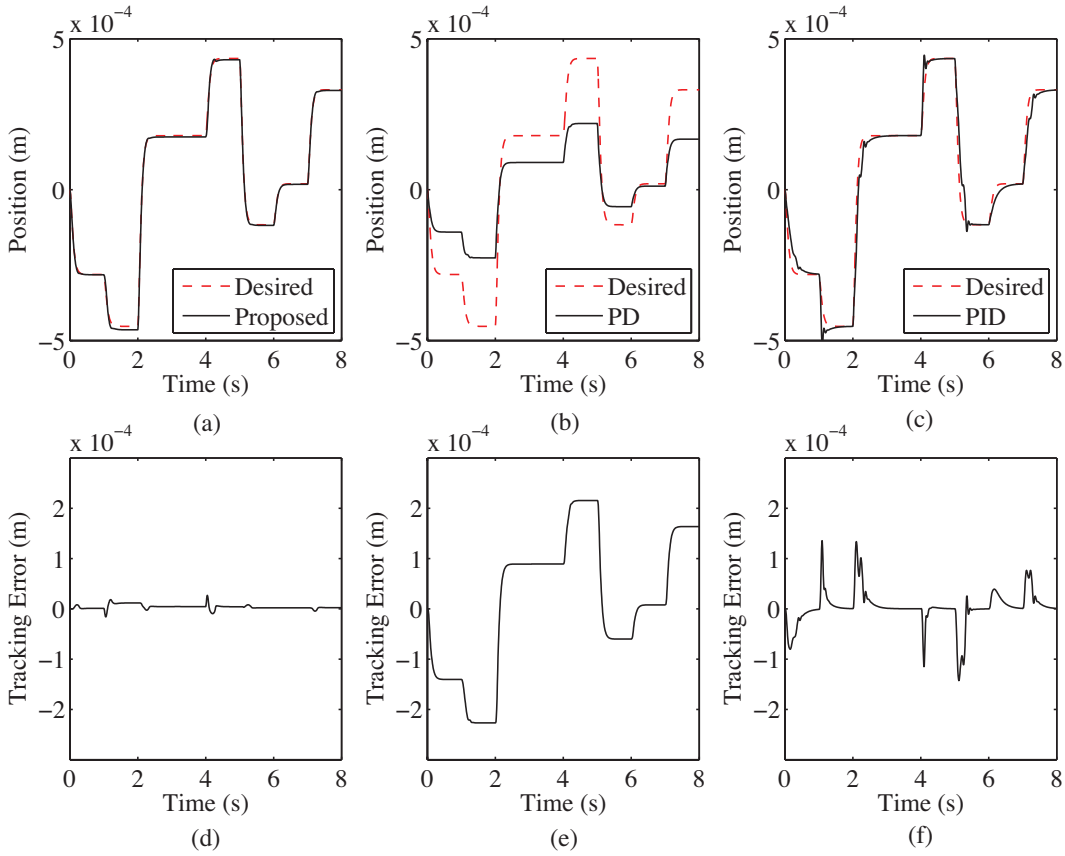

Figure 5.15: Comparison of position tracking performance for random step trajectory of proposed controller after convergence, PD and PID controllers.

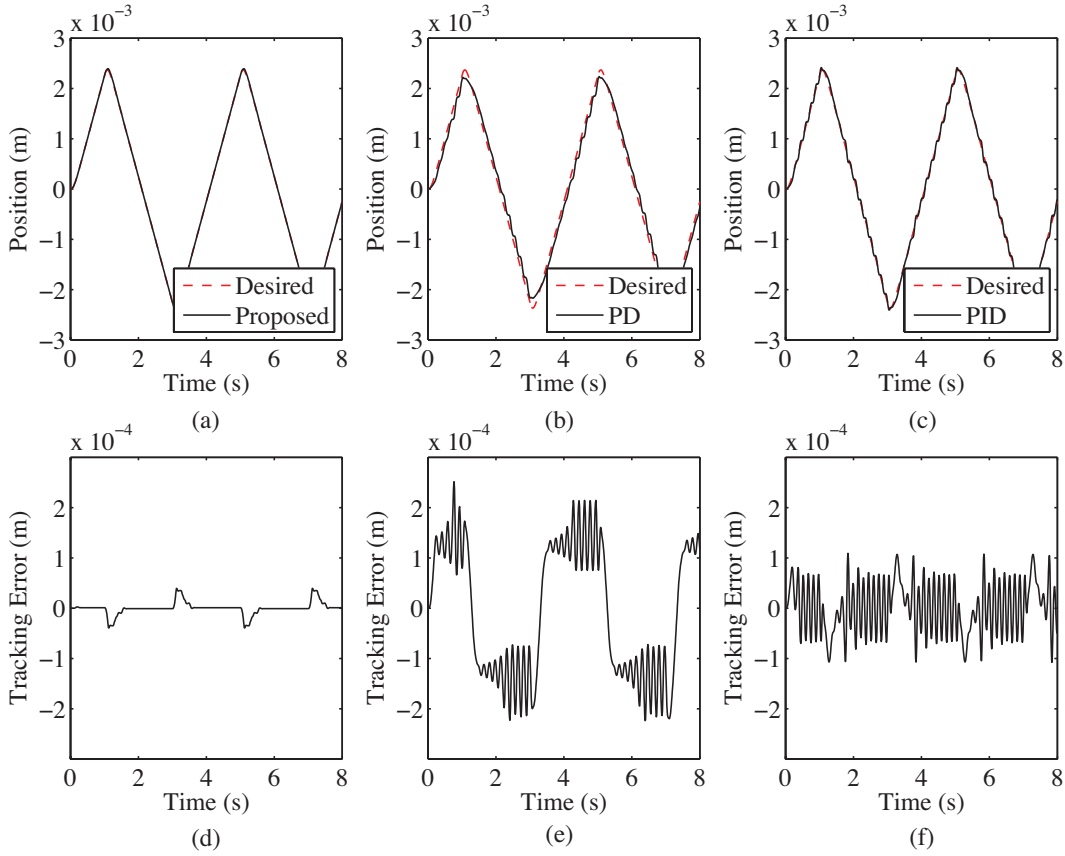

Figure 5.16: Comparison of position tracking performance for ramp trajectory of proposed controller after convergence, PD and PID controllers.

5.7 Summary

An adaptive friction compensator is proposed using polynomial approximation of the Stribeck effect. The structure is based upon the GMS friction model, which becomes linearly-parameterized, allowing for the straight-forward design of adaptive laws. Stability and robustness conditions with respect to unmodeled dynamics is guaranteed by introducing a robustifying term into the control signal. The friction force is accurately estimated and compensated for by the adaptive controller, and allows for trajectory tracking of velocity and position signals.

Chapter 6

Conclusion

The main objective of this thesis was the exploration of adaptive and iterative control methods for mechanical systems with parametric uncertainties. Three different systems were considered that represent varying aspects of the general control problem.

The first topic dealt with by this thesis was the iterative control of a two-mass torsional motor system with unknown parameters. The high order of the system, in addition to the interconnection between the different parameters, made this a very interesting control problem. By including a suitable reference model into the feedforward path of a 2DOF controller, this research was able to use CGT theory to establish a clear relationship between controller parameters and the physical model parameters. This was then used in conjunction with IFT method to tune the controller parameters. As the controller parameters is optimized, the proposed algorithm also resulted in the identification of the physical model parameters. The result is a comprehensive control algorithm suitable for the repetitive tasks usually performed by torsional motor systems, which provides excellent trajectory tracking while simultaneously identifying all the parameters of the two-mass motor system. As of the date of this publication, the proposed method remains the only viable scheme for achieving both objectives in an online manner. The algorithm presented in this thesis was successfully tested on an experimental system.

The scope of the study was then expanded to include nonlinear mechanical systems with parametric uncertainties. The second system considered by this research was vibration suppression of a wheel-chassis assembly with semi-active damping via a magnetorheological damper. Several different methods was proposed by this research, depending on the available knowledge of the system. The general concept employed by this study is the combination of a refer-

ence feedback controller with an adaptive inverse controller to achieve linearization of the MR damper. When the suspension parameters are known, the reference feedback was developed using robust LQ controller design. An examination was conducted to determine the benefits of including dissipativity into the performance function. The robust LQ controller was then used in conjunction with the proposed adaptive inverse controller, which can be adapted via forward or inverse modeling, yielding considerable performance improvements while requiring less power than an active actuator. The adaptive skyhook method was then proposed for the case of unknown suspension parameters. Due to discrepancies between the desired damping force and the achievable damping force with the semi-active MR damper, an auxiliary error signal was developed which guarantees the stability of the adaptive skyhook method despite this uncertainty. This was again combined with the adaptive inverse controller using forward or inverse modeling to achieve total adaptive control of an entirely unknown suspension system with semi-active MR damper.

The last issue considered by this study was the friction compensation problem. Friction compensation is a highly complicated task that depends greatly upon the accuracy of the friction model. This thesis developed an adaptive friction compensation scheme using the recently proposed GMS model. It is the first such method to be developed and displays promising results. In particular, a polynomial approximation function was proposed by this thesis to describe the Stribeck effect. This allowed for the utilization of well-established linear control theories. A smooth sliding mode-based control scheme was included to ensure robustness with respect to approximation error. The result is an effective compensation scheme that is able to identify all system parameters as well as the GMS model in an online, adaptive manner. In addition, the algorithm is highly robust to unmodelled dynamics, such switching error, dynamic perturbations and approximation error due to the inclusion of the smooth sliding-mode based control signal.

6.1 Suggestions for Future Work

Despite the impressive results obtained during the course of this research, there are always room for improvements. Limited by time and resources, the author was not able to complete every aspect of his research plans. Certain issues remained to be addressed, while the results also introduced new and fascinating problems. It is therefore the wish of the author to recommend

some ideas for future work.

The algorithm proposed for the IFT of the unknown two-mass torsional motor system was finalized by this thesis. Simulation and experimental results both verify the validity and effectiveness of the proposed approach in achieving simultaneous trajectory tracking and parameter identification. However, the author recommends that further research be conducted on how to extend this method to higher order systems, for example, a three-mass motor system, and if possible the development of an adaptive method to complement the proposed iterative tuning algorithm.

Suspension control is a highly complex problem with many obstacles to be taken into consideration. While this research successfully developed several algorithms for the the adaptive, semi-active control of an unknown suspension system, the author feels that a deeper integration can be achieved between the adaptive inverse controller and adaptive reference controller so as to minimized the differences between the desired damping force and the semi-active MR force. By taking into account the semi-active constraints of the MR damper when designing the adaptive feedback control, overall performance and robustness of the algorithm should be increased. Experimental verification should likewise be conducted.

Lastly, the issue of adaptive friction compensation remains the most interesting problem from a control perspective. The GMS friction model is relatively new, and the adaptive compensation scheme proposed in this research is the first of its kind. However, the GMS model introduces several complications such as switching and nonlinearities that should be studied in more detail. It is the opinion of this author that adaptive friction compensation schemes based upon the GMS model remains an extremely open and fascinating topic.

Bibliography

[1] F. Al-Bender, V. Lampaert, and J. Swevers. "A novel generic model at asperity level for dry friction force dynamics." *Tribology Letters*, vol. 16, no. 1, pp. 81–93 (2004).

[2] F. Al-Bender, V. Lampaert, and J. Swevers. "The generalized maxwell-slip model: a novel model for friction simulation and compensation." *IEEE Transactions on Automatic Control*, vol. 50, no. 11, pp. 1883–1887 (2005).

[3] J. Amin, B. Friedland, and A. Harnoy. "Implementation of a friction estimation and compensation technique." *IEEE Control Systems Magazine*, vol. 17, pp. 71–76 (1997).

[4] B. Armstrong-Hélouvry. *Control of Machines with Friction*. Kluwer Academic Publishers, Boston (1991).

[5] B. Armstrong-Hélouvry, P. Dupont, and C. Canudas de Wit. "A survey of models, analysis tools and compensation methods for the control of machines with friction." *Automatica*, vol. 30, no. 7, pp. 1083–1138 (1994).

[6] R. Arnell, P. Davies, J. Halling, and T. Whomes. *Tribology*. Macmillan, London, UK (1991).

[7] P. A. Bliman and M. Sorine. "Easy-to-use realistic dry friction models for automatic control." *European Control Conference*. Rome, Italy (1995).

[8] B. Bona, M. Indri, and N. Smaldone. "Nonlinar friction estimation for digital control of direct-drive manipulators." *European Control Conference*. Cambridge, UK (2003).

[9] J. R. Broussard and M. J. O'Brien. "Feedforward control to track the output of a forced model." *IEEE Transactions on Automatic Control*, vol. 25, no. 4, pp. 851–853 (1980).

[10] C. Canudas de Wit and P. Lischinsky. "Adaptive friction compensation with partially known dynamic friction model." *International Journal of Adaptive Control and Signal Processing*, vol. 11, pp. 65–80 (1997).

[11] C. Canudas de Wit, H. Olssen, K. J. Astrom, and P. Lischinsky. "A new model for control of systems with friction." *IEEE Transactions on Automatic Control*, vol. 40, pp. 419–425 (1995).

[12] C. C. Chang and L. Zhou. "Neural network emulation of inverse dynamics for a magnetorheological damper." *ASCE Journal of Structural Engineering*, vol. 128, no. 2, pp. 231–239 (2002).

[13] S. B. Choi and S. K. Lee. "A hysteresis model for the field-dependent damping force of a magnetorheological damper." *Journal of Sound and Vibration*, vol. 245, no. 2, pp. 375–383 (2001).

[14] P. R. Dahl. *A Solid Friction Model*. The Aerospace Corporation, USA (1968).

[15] S. J. Dyke, B. F. Spencer Jr., M. K. Sain, and J. D. Carison. "Modeling and control of magnetorheological dampers for seismic response reduction." *Smart Materials and Structures*, vol. 5, pp. 565–575 (1996).

[16] B. Friedland and Y. J. Par. "On adaptive friction compensation." *IEEE Transactions on Automatic Control*, vol. 10, pp. 1609–1612 (1992).

[17] T. Higashiyama, M. Mine, H. Ohmori, A. Sano, H. Nishida, and Y. Todoka. "Autotuning of motor drive system by simple adaptive control approach." *IEEE International Conference on Control Applications*, pp. 868–873 (2000).

[18] H. Hjalmarsson. "Iterative feedback tuning - an overview." *International Journal of Adaptive Control and Signal Processing*, vol. 16, pp. 373–395 (2002).

[19] H. Hjalmarsson, M. Gevers, S. Gunnarsson, and O. Lequin. "Iterative feedback tuning: theory and applications." *IEEE Control Systems Magazine*, pp. 26–41 (1998).

[20] M. Iwasaki, T. Shibata, and N. Matsui. "Disturbance-observer-based nonlinear friction compensation in table drive system." *IEEE/ASME Transactions on Mechatronics*, vol. 4, no. 1, pp. 3–8 (1999).

[21] F. Jatta, G. Legnani, and A. Visioli. "Friction compensation in hybrid force/velocity control of industrial manipulators." *IEEE Transactions on Industrial Electronics*, vol. 53, no. 2, pp. 604–613 (2006).

[22] H. Kaufman, I. Bar-kana, and K. Sobel. *Direct Adaptive Control Algorithms*. Springer-Verlag (1994).

[23] J. Kennedy and R. Eberhart. "Particle swarm optimization." *IEEE International Conference on Neural Networks*. Perth, Australia (1995).

[24] J. Kennedy and R. Eberhart. *Swarm Intelligence*. Morgan Kaufmann Publishers (2001).

[25] K. Kiguchi and T. Fukuda. "Fuzzy neural friction compensation method of robot manipulation during position/force control." *IEEE International Conference on Robotics and Automation*. Minneapolis, USA (1996).

[26] Y. H. Kim and F. L. Lewis. "Reinforcement adaptive learning neural network based friction compensation for high speed and compensation." *IEEE Conference on Decision and Control*. Tampa, FL (1998).

[27] T. Kitade, H. Ohmori, A. Sano, T. Miyashita, H. Nishida, and Y. Todoka. "Adaptive forward identification and auto-tuning for motor velocity control." *European Control Conference*. Cambridge, UK (2003).

[28] C. Y. Lai and W. H. Liao. "Vibration control of a suspension systems via a magnetorheological fluid damper." *Journal of Vibration and Control*, vol. 8, no. 4, pp. 525–547 (2002).

[29] V. Lampaert, F. Al-Bender, and J. Swevers. "A generalized maxwell-slip friction model appropriate for control purposes." *IEEE International Conference on Physics and Control*. St. Petersburg, Russia (2003).

[30] N. E. Leonard and P. S. Krishnaprasad. "Adaptive friction compensation for bi-directional low-velocity position tracking." *IEEE Conference on Decision and Control*. Tuscan, AZ (1992).

[31] W. Li and X. Cheng. "Adaptive high-precision control of positioning tables - theories and experiments." *IEEE Transactions on Control System Technology*, vol. 2, pp. 265–270 (1994).

[32] K. Misovec and A. Annaswamy. "Friction compensation using adaptive non-linear control with persistent excitation." *International Journal of Control*, vol. 72, pp. 457–459 (1999).

[33] I. Nilkhamhang and A. Sano. "Feedforward parameter identification by output oversampling iterative tuning." *IFAC Workshop on Adaptive Learning Control and Signal Processing*. Yokohama, Japan (2004).

[34] I. Nilkhamhang and A. Sano. "Iterative tuning algorithm for feedforward parameter identification of a two-mass motor system." *Asian Control Conference*. Melbourne, Australia (2004).

[35] I. Nilkhamhang and A. Sano. "Adaptive compensation of a linearly-parameterized gms friction model with parameter projection." *IEEE Conference on Decision and Control*. San Diego, USA (2006).

[36] I. Nilkhamhang and A. Sano. "Adaptive friction compensation using the gms model with polynomial stribeck function." *IEEE Conference on Control Application*. Munich, Germany (2006).

[37] I. Nilkhamhang and A. Sano. "Particle swarm optimization for identification of gms friction model." *SICE-ICCAS Annual Conference*. Pusan, Korea (2006).

[38] H. Nishimura and R. Kayama. "Gain-scheduled control of a semi-active suspension using an MR damper." *Transanctions of Japanese Society of Mechanical Engineers*, vol. 68, no. 676, pp. 3644–3651 (2002).

[39] H. Olsson, K. J. Astrom, C. Canudas de Wit, M. Gafwert, and P. Lischinsky. "Friction models and friction compensation." *European Journal of Control*, vol. 4, pp. 176–195 (1998).

[40] G. Pan, H. Matshushita, and Y. Honda. "Analytical model of a magnetorheological damper and its application to the vibration control." *IECON Annual Conference*, pp. 1850–1855 (2000).

[41] J. René and L. Alvarez. "Real time identification of structures with magnetorheological dampers." *IEEE Conference on Decision and Control*. Las Vegas, USA (2002).

[42] C. Sakai, H. Ohmori, and A. Sano. "Modeling of MR damper with hysteresis for adaptive vibration control." *IEEE Conference on Decision and Control*. Hawaii, USA (2003).

[43] K. Sato, K. Tsuruta, and A. Shoji. "Adaptive friction compensation for linear slider using projection adaptive laws." *SICE Annual Conference*. Okayama, Japan (2005).

[44] R. R. Selmic and F. L. Lewis. "Neural network approximation of piecewise continuous functions: application to friction compensation." *IEEE Transactions on Neural Networks*, vol. 13, no. 3, pp. 745–751 (2002).

[45] I. H. Shames and F. A. Cozzarelli. *Elastic and Inelastic Stress Analysis*. Prentice Hall, New Jersey, USA (1992).

[46] E. Shimizu, K. Kubota, M. Sampei, and M. Koga. "A design of a nonlinear h_∞ state feedback controller for bilinear systems." *SICE Transaction*, vol. 35, no. 9, pp. 1155–1161 (1999).

[47] G. Song, Y. Wang, L. Cai, and R. W. Longman. "A sliding-mode based smooth adaptive robust controller for friction compensation." *IEEE Conference on Decision and Control*. Seattle, USA (1995).

[48] X. Song, M. Ahmadian, S. Southward, and L. R. Miller. "An adaptive semiactive control algorithm for magnetorheological suspension systems." *ASME Journal of Vibration and Acoustics*, vol. 127, pp. 493–502 (2005).

[49] B. F. Spencer Jr., S. J. Dyke, M. K. Sain, and J. D. Carlson. "Phenomenological model of a magnetorheological damper." *ASCE Journal of Engineering Mechanics*, vol. 123, no. 3, pp. 230–238 (1997).

[50] R. Stanway, J. L. Sproston, and N. G. Stevens. "Nonlinear identification of an electro-rheological vibration damper." *IFAC Identification and System Parameter Estimation*, pp. 195–200 (1985).

[51] R. Stanway, J. L. Sproston, and N. G. Stevens. "Nonlinear modeling of an electro-rheological vibration damper." *Journal of Electrostatics*, vol. 20, no. 2, pp. 167–184 (1987).

[52] L. Sun, H. Ohmori, and A. Sano. "Output intersampling approach to direct closed-loop identification." *IEEE Transanction on Automatic Control*, vol. 46, no. 12, pp. 1936–1940 (2002).

[53] J. Swevers, F. Al-Bender, C. G. Ganseman, and T. Prajogo. "An integrated friction model structure with improved presliding behavior for accurate friction compensation." *IEEE Transactions on Automatic Control*, vol. 45, no. 4, pp. 675–686 (2000).

[54] T. Terasawa, C. Sakai, H. Ohmori, and A. Sano. "Adaptive identification of MR damper for vibration control." *IEEE Conference on Decision and Control*. Bahama (2004).

[55] T. Tjahjowidodo, F. Al-Bender, and H. V. Brussel. "Friction identification and compensation in a dc motor." *16th IFAC World Congress*. Prague, Czech Republic (2005).

[56] A. Visioli, R. Adamini, and G. Legnani. "Adaptive friction compensation for industrial robot control." *IEEE/ASME International Conference on Advanced Intelligent Mechatronics*. Como, Italy (2001).

[57] Y. K. Wen. "Method of random vibration of hysteretic systems." *ASCE Journal of Engineering Mechanics Division*, vol. 102, no. 2, pp. 246–263 (1976).

[58] G. Yang. *Large-scale Magnetorheological Fluid Damper for Vibration Mitigation: Modeling, Testing and Control*. Ph.D. thesis, The University of Notre Dame, Indiana, USA (2001).

[59] C. T. Zhang, J. P. Ou, and J. Q. Zhang. "Parameter optimization and analysis of a vehicle suspension system controlled by magnetorheological fluid damper." *Structural Control and Health Monitoring*, vol. 13, no. 5, pp. 885–896 (2006).

[60] L. Zuo, J. E. Slotine, and S. A. Nayfeh. "Experimental study of a novel adaptive controller for active vibration isolation." *American Control Conference*. Boston,USA (2004).